MODELING HYBRID-ELECTRIC AIRCRAFT AND THEIR FLEET-LEVEL CO_2 EMISSION IMPACTS

by

Samarth Jain

A Dissertation

Submitted to the Faculty of Purdue University

In Partial Fulfillment of the Requirements for the degree of

Doctor of Philosophy

School of Aeronautics and Astronautics

West Lafayette, Indiana

December 2022

THE PURDUE UNIVERSITY GRADUATE SCHOOL
STATEMENT OF COMMITTEE APPROVAL

Dr. William A. Crossley, Chair

School of Aeronautics and Astronautics

Dr. Daniel A. DeLaurentis

School of Aeronautics and Astronautics

Dr. Dengfeng Sun

School of Aeronautics and Astronautics

Dr. Jitesh Panchal

School of Mechanical Engineering

Approved by:

Dr. Gregory A. Blaisdell

To my parents and my wife

ACKNOWLEDGMENTS

I would like to thank my academic advisor, Dr. William Crossley, for his constant support and guidance throughout my graduate life at Purdue and for giving me the opportunity to work on several projects along with my dissertation work which helped me learn a wide array of subjects. I am grateful for his tremendous contributions to my professional and personal development. I am incredibly fortunate to have him as my mentor on my PhD journey.

I would also like to thank the members of my dissertation committee – Dr. Daniel DeLaurentis, Dr. Jitesh Panchal, and Dr. Dengfeng Sun – for their guidance and valuable feedback throughout my work. I am very grateful to Dr. DeLaurentis for all his advice related to my professional development.

I would also like to thank all the former and current members of the Aerospace Systems Design Analysis & Optimization Lab – I learned a lot from everyone in the group. Thank you, Dr. Apoorv Maheshwari, Dr. Jakob Hartl, Takashi Kanno, Brandon Sells, Dr. Hsun Chao, Dr. Kshitij Mall, and Purdue Cricket Club for making this a memorable journey.

I would also like to thank my friends, Soumya Roy, Swapnil Rai, Vivek Singla, Divya Agarwal, Dr. Aakriti Jain, and Lydia Hartl, for encouraging me throughout my PhD journey.

A special thanks goes to my family – my parents, Shanu and Kapil Jain, my wife, Dr. Vidushi Adlakha, and my brother, Samyak Jain – for their unconditional love and support throughout my graduate life.

Thank you, Vidushi, for always motivating me and supporting me.

TABLE OF CONTENTS

LIST OF TABLES

LIST OF FIGURES

ABBREVIATIONS

BCM/BCA	Best cruise Mach number / best cruise altitude
CAD	Computer-aided design
CTBG	Current trends best guess
DOC	Direct operating cost
EI	Emission intensity
EIS	Entry-into-service
FLEET	Fleet-level environmental evaluation tool
IOC	Indirect operating cost
IAS	Indicated air speed
LPT	Low pressure turbine
MDO	Multidisciplinary design optimization
NPSS	Numerical propulsion system simulation
PC	Power code or throttle setting
PMAD	Power management and distribution
SAND	Simultaneous analysis and design
TAS	True air speed

ABSTRACT

With rising concerns over commercial aviation's contribution to global carbon emissions, there exists a tremendous pressure on the aviation industry to find advanced technological solutions to reduce its share of CO_2 emissions. Single-aisle (or narrowbody) aircraft are the biggest contributors to CO_2 emissions by number of operations, insisting a need to reduce / eliminate their aircraft-level fuel consumption as soon as possible. A potential solution for this is to operate fully-electric single-aisle aircraft; however, the limitations of the current (and predicted future) battery technology is forcing the industry to explore hybrid-electric aircraft as a possible mid-term solution.

Modeling hybrid-electric aircraft comes with its own challenges due to the presence of two different propulsion sources – gas turbine engines (powered by Jet-A fuel) and electric motors (powered by batteries). Since traditional sizing approaches and legacy sizing tools do not seem to work well for hybrid-electric aircraft, this work presents a "flight-mechanics-based" conceptual sizing tool for hybrid-electric aircraft, set up as a Multidisciplinary Design Optimization (MDO) toolbox. Some of the key features of the sizing tool include concurrently sizing the electric motors and downsizing the gas turbine engines while meeting the one-engine-inoperative (OEI) and top-of-climb constraints, and re-sizing the fuselage to account for the volumetric constraints associated with required batteries. Current work considers a parallel hybrid-electric single-aisle aircraft with a 900 nmi design range, with electric power augmentation (with electric motors operating at full throttle) available only for the takeoff and climb segments when sizing the aircraft. Four hybrid-electric propulsion technology cases are considered, and the resulting hybrid-electric aircraft show 15.0% to 22.5% reduction in fuel burn compared to a Boeing 737-800 aircraft.

Another challenge with modeling hybrid-electric aircraft is determining their off-design performance characteristics (considering a different payload or mission range, or both). This work presents an energy management tool – set up as a nonlinear programming optimization problem – to minimize the fuel burn for a payload-range combination by identifying the optimal combination of throttle settings for the gas turbine engines and the electric motors during takeoff, climb, and cruise, along with identifying an optimal flight path. The energy

management tool enables fuel savings of at least of 2%, with actual savings ranging from 142.1 lbs to 276.1 lbs per trip for a sample route (LGA–ORD) at a 80% load factor.

Although the hybrid-electric aircraft sizing and performance analysis studies show encouraging results about the potential reduction in carbon emissions at an aircraft level, the future fleet-level carbon emissions are not expected to reduce proportionally to these aircraft level emission reductions. This work predicts the fleet-level environmental impacts of future single-aisle parallel hybrid-electric aircraft by modeling the behavior of a profit-seeking airline (with a mixture of conventional all Jet-A fuel burning and hybrid electric aircraft in its fleet) using the Fleet-Level Environmental Evaluation Tool (FLEET). FLEET's model-based predictions rely upon historically-based information about US-touching airline routes and passenger demand served by US flag-carrier airlines from the Bureau of Transportation Statistics to initiate model-based predictions of future demand, aircraft fleet mix, and aircraft operations. Using the aircraft performance coefficients from the energy management tool to represent the behavior of a single-aisle parallel hybrid-electric aircraft, the FLEET simulation predicts the changes in the fleet-wide carbon emissions due to the introduction of this new aircraft in an airline fleet in the year 2035. By 2055, FLEET results predict that the fleet-wide CO_2 emissions with hybrid-electric aircraft in the fleet mix are at least 1.2% lower than the fleet-wide CO_2 emissions of a conventional (all Jet-A fuel burning) aircraft-only airline. The rather limited reduction in emissions is an attribute of the reduced range capability and higher operating cost of the hybrid-electric aircraft (relative to a conventional aircraft of similar size). This causes the airline to change the usage, acquisition and retirement of its conventional aircraft when hybrid-electric aircraft are available; this is most notable to serve passenger demand on certain predominantly single-aisle service routes that cannot be flown by the future single-aisle hybrid-electric aircraft.

1. INTRODUCTION

The transportation sector is one of the largest contributors to U.S. greenhouse gas (GHG) emissions, with the commercial aviation industry acting as a significant contributor to the overall emissions from the sector. In 2018, CO_2 emissions from all commercial aircraft operations totaled 918 million metric tons, accounting for 2.4% of global CO_2 emissions from fossil fuel use [1]. In the last two decades (1990s and 2000s), carbon emissions from commercial aviation worldwide grew at a slower pace than the growth of the industry. However, emissions from commercial aviation between 2013 and 2019 have increased by 33% [1] due to increased commercial air traffic, raising the industry's contribution to global emissions. Although there seems to be a respite in aviation emissions for the past two years because of the COVID-19 pandemic-related travel restrictions, there are still high concerns over the future contribution of commercial aviation to global CO_2 emissions. These concerns – combined with the rising interest among fliers to reduce their carbon footprint – are responsible for the tremendous pressure that exists on the aviation industry to reduce (and eventually eliminate) its share of CO_2 emissions.

Organizations such as the International Air Transport Association (IATA) and the International Civil Aviation Organization (ICAO) have set goals for reducing CO_2 emissions from air transportation by 50% in 2050, relative to 2005 levels, and reducing individual aircraft fuel consumption by 1.5% to 2.0% per year from 2009 to 2020 [2], [3]. NASA's Subsonic Fixed Wing (SFW) project set up its own emission reduction goals for individual aircraft [4], [5]. In the SFW project, NASA used 2005 as the base or current year, with "N" denoting the current generation of aircraft, i.e., aircraft in-production in 2005. N+1 denotes the next major generation of aircraft with an expected Entry-In-Service (EIS) date of 2015. According to NASA's goals for the N+1 generation, individual aircraft fuel burn should reduce by 33% compared to the current N generation of aircraft. With the next generation of aircraft – N+2 (with an initial operating capability by 2020) – NASA seeks to reduce individual aircraft fuel burn by 40% with respect to the current N generation aircraft. The latest generation studied in the SFW project is N+3, with an expected EIS between 2030 and 2035. NASA hopes to reduce individual aircraft fuel burn by 70% for the N+3 generation compared to the

current N generation aircraft. To meet this fuel burn reduction goal for individual aircraft in the N+3 generation, NASA (along with other partners) is proposing / developing a range of new technologies, including high aspect ratio laminar wing, electrified propulsion systems (hybrid-electric, turbo-electric, and all-electric), boundary layer ingestion, hybrid-wing body, and use of advanced structural materials [6]. The combination of these technologies is essential to develop future fuel-efficient commercial aircraft, with electrified propulsion systems acting as the key to minimizing CO_2 emissions from commercial aircraft.

The ultimate solution to minimizing / eliminating aircraft-level CO_2 emissions would be to operate fully-electric aircraft (with batteries charged using as much green electricity as possible). Fully-electric small regional jets could become available as early as the end of the current decade, followed by fully-electric regional jets by early/mid-2030s. Single-aisle (or narrowbody) aircraft are the biggest contributors to CO_2 emissions by number of operations [1], insisting a need to electrify them as soon as possible. However, the limitations of the current (and predicted future) battery technology dictates that a fully-electric commercial subsonic aircraft – single-aisle size or bigger – might not take to the skies until at least the next two decades. Until fully-electric single-aisle (or bigger) commercial subsonic aircraft become viable, the mid-term solution to the rising aviation emissions problem could be to opt for some hybrid propulsion architectures that combine propulsion power from conventional Jet-A fuel and batteries. These aircraft with partially electrified propulsion technologies could serve as a stepping stone for developing sustainable fully-electric single-aisle (or bigger) commercial aircraft in the future, contributing to the momentum of electrification of commercial aviation.

Modeling a hybrid-electric aircraft comes with its own challenges. The conceptual sizing of a hybrid-electric aircraft requires information about the power and energy requirements for each segment of the flight, which is essential for determining and implementing the power split between the gas turbine engine (powered by Jet-A fuel) and the electric motor (powered by batteries). This power split information drives the size of the batteries (or fuel cells) and the amount of Jet-A fuel needed for the design mission. Traditional sizing approaches and legacy sizing tools are unable to provide this information because most of them were developed assuming a single energy source for aircraft propulsion. Hence, there

is a need to develop new sizing approaches / tools that enable the sizing and analysis of aircraft that utilize at least two sources of energy.

This work presents one such tool to model and analyze hybrid-electric aircraft — a "flight-mechanics-based" sizing tool. The tool is set up as a Multidisciplinary Design Optimization (MDO) toolbox that addresses multiple disciplines (including aerodynamics, propulsion, performance, weights) using a single aircraft sizing code. The tool simulates an aircraft's trajectory in two-dimensions and generates detailed information about the aircraft's power / energy requirements for discrete time steps, allowing to size the electric motor and battery system and re-size the gas turbine engines for an optimum design. Some of the key features of the sizing tool include re-sizing the gas turbine engines while considering the one-engine-inoperative (OEI) condition during takeoff, re-sizing the fuselage to consider the volumetric constraints associated with the required batteries without sacrificing the aircraft's cargo volume, and implementing a Simultaneous Analysis and Design (SAND) approach to avoid the traditional iteration-based sizing loop (while enabling fuselage re-sizing). Current work considers a parallel hybrid-electric single-aisle aircraft with a 900 nmi design range, with electric power augmentation (with electric motors operating at full throttle) available only for the takeoff and climb segments when sizing the aircraft. The tool can be expanded to include other types of aircraft, like business, regional, or twin-aisle size hybrid-electric aircraft; the tool can also be easily modified to include all-electric aircraft.

Another challenge with modeling hybrid-electric aircraft is determining their off-design performance characteristics. When the sized hybrid-electric aircraft is flown at a lower payload, or for a lower range than the design / maximum range of 900 nmi, or both, the battery energy required to takeoff and climb to the cruising altitude could be lower than the total battery energy onboard the sized aircraft (because the aircraft is lighter due to a combination of lower payload and lower amount of fuel in the fuel tanks considering a shorter mission). In this case, it would be beneficial to identify the optimal power split between the two energy sources to minimize the fuel burn for payload-range combination in consideration, and to utilize the remaining battery energy (if any) during cruise.

This work presents an energy management tool – derived from the "flight-mechanics-based" sizing tool – to minimize the fuel burn during a flight by identifying the optimal

combination of throttle settings for the gas turbine engine and the electric motor during takeoff, climb, and cruise. The tool is set up with an optimization problem at its core that minimizes the overall mission fuel burn and forces the aircraft to completely discharge the batteries (to their safety limit) during the mission to gain maximum fuel burn benefit. The final output helps to identify an optimal energy management scheme that resonates with how the airlines might end up using these aircraft in their daily operations (focusing on profitability in operation for every mission).

The existing literature focuses on the carbon emissions / block fuel burn reduction benefits possible from individual aircraft concepts with electrified propulsion. The literature indicates that future hybrid-electric aircraft are promising in terms of their aircraft-level emission reductions, but there is lack of knowledge about the future fleet-wide CO_2 emissions reductions possible due to the introduction of these aircraft. The future fleet-level carbon emissions are not expected to reduce proportionally to the individual carbon emissions benefits possible from hybrid-electric aircraft, once these aircraft are introduced for fleet-wide operations in the mid-2030's (which matches the targeted EIS date for most single-aisle hybrid-electric aircraft in literature). There are a number of obvious reasons for this most-likely-possible scenario – 1) there will be a limit to aircraft production and delivery based on materials, logistics, and supply chain limits, 2) airlines will not be able to suddenly retire their existing single-aisle aircraft (forced early aircraft retirement) to operate an all hybrid-electric single-aisle aircraft fleet, and, 3) hybrid-electric aircraft will have a shorter range compared to conventional (all Jet-A fuel burning) aircraft, limiting the direct replacement of the conventional single-aisle aircraft with lesser carbon emitting hybrid-electric aircraft in an airline fleet. These points signify the importance of looking at the fleet-level environmental impact of the introduction of the single-aisle hybrid-electric aircraft in year 2035 and beyond, so that the aviation industry can be realistic on its ability to meet the global carbon emissions goals even with the introduction of these aircraft (assuming no change in the continual demand growth and government policy). As per the author's knowledge, there exists no such study that discusses the environmental impacts and fleet-level carbon emission reductions possible from the introduction of range-limited single-aisle hybrid-electric aircraft in an airline fleet.

This work describes an attempt to simulate a profit-seeking "U.S.-flag carrier" airline's behavior when hybrid-electric aircraft are made available to its fleet in 2035, and to predict the subsequent total fleet carbon emissions, using the Fleet-Level Environmental Evaluation Tool (FLEET) [7]. The energy management tool provides the hybrid-electric aircraft performance coefficients to FLEET. The fleet-level results assess the contribution of single-aisle hybrid-electric aircraft in driving down future fleet-level CO_2 emissions. Additionally, this work comments on whether the fleet-level CO_2 emissions from commercial aviation will be able to meet the CO_2 emission targets set by organizations, such as IATA and ICAO.

The objective of this work is to appropriately model hybrid-electric aircraft, identify the optimal energy management scheme for minimizing hybrid-electric aircraft fuel burn on potential routes, and investigate if there is a significant reduction in the fleet-level CO_2 emissions from the introduction of these range-limited hybrid electric aircraft (that show significant block fuel burn reduction at an aircraft level). Chapter 2 talks about the existing literature concerning hybrid-electric aircraft modeling, proposed energy management approaches, and existing fleet-level studies. Chapter 3 describes in detail the hybrid-electric aircraft sizing tool developed in this work, hybrid-electric aircraft sizing results, the energy management tool, and sample energy-optimal route results. Chapter 4 provides details about the modeling tool FLEET and the setup for introducing hybrid-electric aircraft in FLEET. Chapter 5 discusses the fleet-level results considering several aircraft technology-related, future demand-related, and cost-related scenarios. Chapter 6 throws light on the limitations of this work along with recommendations for future work, while Chapter 7 concludes the findings of this work.

2. LITERATURE REVIEW

2.1 Carbon Emissions from Aviation

There has been a rising concern about the global CO_2 emissions from commercial aviation, with the 2015 Paris Agreement's goal of keeping the global average temperature rise to below 2°C (while pursuing efforts to limit the rise to 1.5°C) drawing extra attention to the aviation industry.

According to reference [8], the global CO_2 emissions in the atmosphere should be less than 420 gigatonnes (Gt) to stay below the 1.5°C threshold, calculated from end-2017. However, since around 42 Gt of CO_2 is emitted globally every year, this budget is expected to be used up in just over nine years. The carbon budget for staying below the 2°C threshold, (approximately 1,170 Gt) will be exhausted in about 26 years (counting from end-2017). According to another study [9], the world can now only emit 770 Gt of CO_2 to have a medium chance of limiting warming to 1.5°C, with estimates showing that we will blow through the entirety of this remaining carbon budget by 2030. The remaining carbon budget for 2°C global temperature rise is 1,690 Gt for a 50% chance, or 1,320 Gt for a 67% chance. Even in an overly optimistic scenario with the current levels of CO_2 emissions being held constant, this budget will be exhausted by 2049. All these estimates are based on the 2018 report by the Intergovernmental Panel on Climate Change (IPCC) [10]. Reference [11] details the various carbon budget estimates for 1.5°C using many different models.

Commercial aviation produced about 918 million tonnes and 915 million tonnes of CO_2 globally in 2018 and 2019, respectively, amounting to about 2.4% and 2% of all human-induced CO_2 emissions in the respective years [12], [13]. While this may seem like a relatively small amount, in a hypothetical scenario, considering global commercial aviation to be a country in the national CO_2 emissions standings, the industry would rank number six in the world between Japan and Germany. Non-CO_2 effects, such as warming induced by aircraft contrails and other pollutants, bring the combined total contribution of commercial aviation to approximately 5 percent of the world's climate-warming problem [14]. Breaking down the global CO_2 emissions from commercial aviation by aircraft type, in 2018, 43% of the emissions were linked to passenger movement in single-aisle – narrowbody aircraft, followed

by twin-aisle – widebody jets (33%), and regional aircraft (5%). The remaining aviation emissions were driven by freight carriage. Flights departing airports in the United States (U.S.) and its territories, with the world's largest commercial air traffic system, contributed to about one-quarter (24%) of global CO_2 emissions from commercial aviation, two-thirds of which came from U.S. domestic flights [12].

Many articles discuss the projected share of commercial aviation in the global carbon emissions by 2050. According to reference [15], between 2016 and 2050 global aviation will generate an estimated 43 Gt of CO_2 emissions if left unchecked (business as usual scenario, where the aviation industry grows by 5% per year, but there are no major changes to technology or infrastructure), which amounts to more than 4% of the world's entire remaining carbon budget (the maximum amount of CO_2 that can be emitted before catastrophic global warming becomes virtually certain). The article also mentions that under the business as usual scenario, the U.S. aviation alone is estimated to release 9 Gt of CO_2 from 2016 through 2050. Another article [16] states that even if the aviation industry is able to meet all its targets, global aviation will still have consumed 12% of the global carbon budget for 1.5°C by 2050. In case the industry is unable to meet its target, its share of the carbon budget could rise to as much as 27%. Moreover, the article states that the total CO_2 emissions from 2015 to 2050 are projected to reach approximately 56 gigatonnes when considering a business-as-usual projection. References [14], [17]–[22] include various articles that discuss the contribution of aviation to climate change and some necessary steps / approaches that could help to tackle this issue.

2.2 Aircraft With Electrified Propulsion

Aircraft with electrified propulsion integrate an electrical powertrain with the aircraft; different integration strategies lead to six different propulsion architectures – three hybrid-electric, two turbo-electric, and one all-electric [23], [24]. Figure 2.1 depicts all the electrified propulsion architectures. A hybrid-electric architecture combines a fuel-burning gas turbine engine with battery-/generator-(or both)-powered electric motor(s). A parallel hybrid-electric architecture mounts a fuel-burning gas turbine engine and battery-powered electric

motor(s) on the same fan shaft such that both the sources can power the fan independently. This architecture seems suitable for reducing the fuel consumption of the power intensive segments of the mission, like takeoff and climb, and behaves like a power augmentation mechanism for the gas turbine engine. In a series hybrid-electric architecture, a gas turbine engine powers the electric motors or charges the batteries that in turn power the electric motors, or a combination of both. This architecture seems suitable for aircraft with multiple distributed fans. The series/parallel partial hybrid-electric architecture combines features of a pure series and pure parallel hybrid-electric architecture. Turbo-electric architectures do not use electro-chemical energy storage (like batteries), rather they use onboard generators to completely convert the power from a fuel-burning gas turbine engine to electrical power to run the electric motors. An all-electric architecture uses power from electro-chemical energy storage (like batteries) for propulsion. There exist several studies in literature that perform conceptual design of aircraft with electrified propulsion [23]–[33]; Brejle and Martins [34] provide a summary of all the hybrid-electric, turbo-electric, and all-electric aircraft concepts studied until 2019. Given the current outlook on battery energy density growth in the next decade or so, a parallel hybrid-electric propulsion system seems to be the most plausible option for aircraft partial electrification in the near future, followed by turbo-electric, series hybrid, and all-electric propulsion systems. Many studies have explored the conceptual design of single-aisle parallel hybrid-electric aircraft in detail. A few of the main efforts include Boeing's SUGAR Volt, United Technologies Research Center (UTRC) parallel hybrid-electric aircraft, and Bauhaus Luftfahrt's hybrid retrofit concept. These studies predict a reduction in aircraft-level carbon emissions from hybrid-electric powertrains due to reduced fuel burn compared to their conventional (all fuel-burning) counterparts.

The Boeing SUGAR (Subsonic Ultra-Green Aircraft) studies [25], [26] presented a parallel hybrid-electric single-aisle aircraft – SUGAR Volt – with an entry into service (EIS) of 2030-2035. The aircraft is sized for a 900 nmi economic mission, with a seating capacity of 154 passengers. The study uses a battery energy density of 750 Wh/kg. Compared to the SUGAR Free aircraft (modeled as 2008 baseline configuration), the SUGAR Volt Balanced (Ref Hp 1,380) shows a block fuel burn reduction of 58.7%, the SUGAR Volt Balanced (Ref Hp 1,750) shows a block fuel burn reduction of 60%, and SUGAR Volt Core Shutdown (Ref

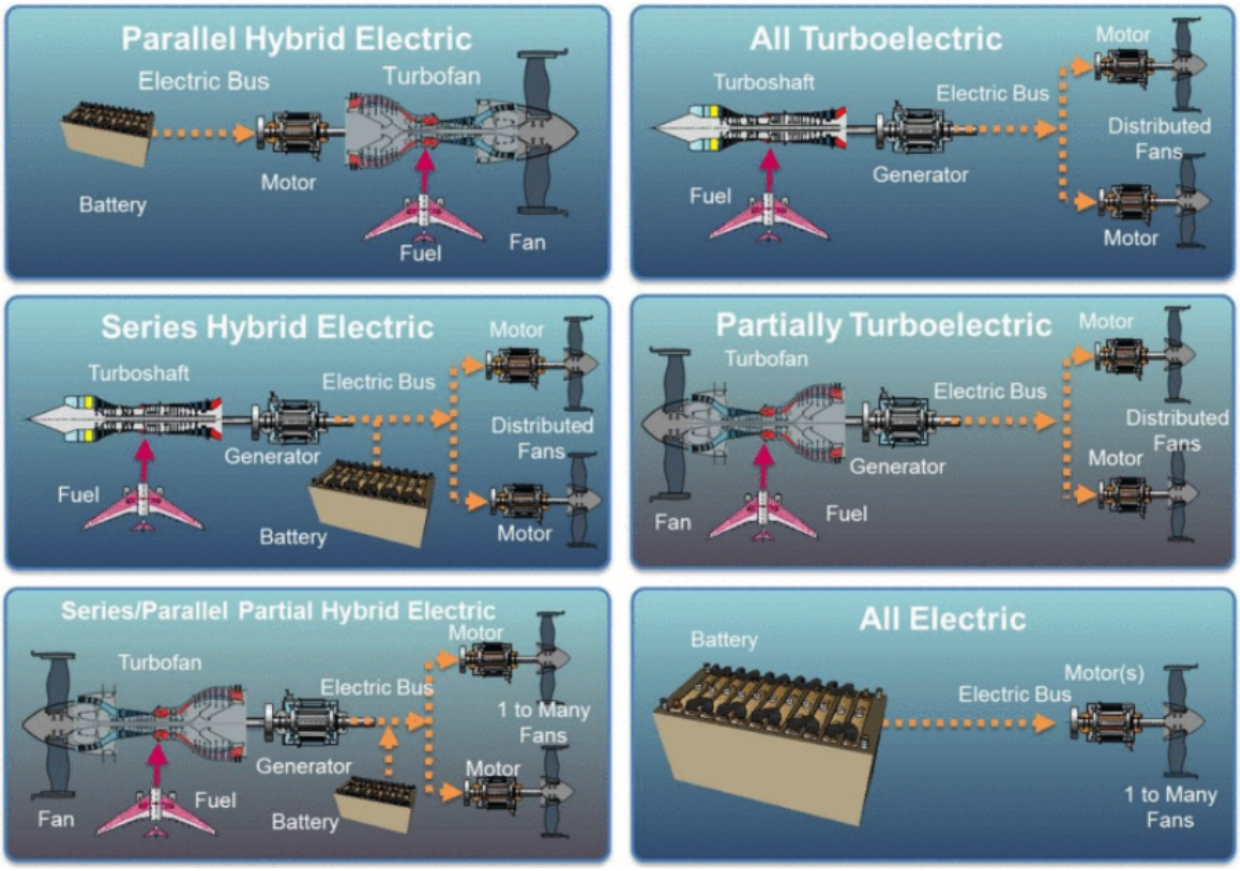

Figure 2.1. Electrified propulsion architectures [35]

Hp 7,150) shows a block fuel burn reduction of 63.7%, for a 900 nmi mission. The term 'Ref Hp' and the numbers mentioned in parenthesis for the three SUGAR Volt configurations refer to the electric motor power required by the specific configuration.

United Technologies Research Center (UTRC) studied a single-aisle aircraft utilizing a parallel hybrid-electric propulsion system (2 under-wing gas turbine engines and a 4.5MW electric drive train), with an EIS of 2035 [27]. The aircraft features a conventional high performance tube and wing configuration based on the Boeing N+4 REFINED SUGAR [36], with a seating capacity of 154 passengers. For a 900 nmi mission with a 500 Wh/kg battery energy density, the study concludes that a block fuel burn reduction of 3.4% is possible compared to N+4 REFINED SUGAR aircraft (baseline aircraft for the study).

Bauhaus Luftfahrt studied a single-aisle parallel hybrid-electric retrofit concept (EIS of 2035), with its configuration based on a 2030 conventional reference single-aisle aircraft

concept [28]. The aircraft has an economic mission range of 900 nmi with the ability to carry 180 passengers. This study uses an optimistic value of 1500 Wh/kg for the battery energy density. The study concludes that a block fuel burn reduction of up to 16% is possible with respect to the 2030 conventional reference concept aircraft.

2.3 Modeling Hybrid-Electric Aircraft

As described in Section 2.2, a hybrid-electric configuration couples two different sources of energy, mostly Jet-A fuel and batteries. The energy consumption from a combination of the two energy sources over the design mission drives the Jet-A fuel and battery weight (and volume) required to complete the mission. Traditional sizing approaches and legacy sizing tools work well for conventional all-fuel burning aircraft (some modified versions seem to work for all-electric aircraft also) but are unable to satisfactorily handle aircraft with multiple sources of energy. These approaches / tools are heavily reliant on the widely-used Bréguet range / endurance equations (for cruise / loiter flight segments) and empirical methods (for the other flight segments) to determine the amount of fuel needed to complete the mission (with the power consumed at discrete time intervals remaining unknown). This makes it hard for the traditional sizing approaches / legacy tools to appropriately capture the interplay between the two energy sources (as most of them were developed keeping a single aircraft propulsion source in mind). With the need to model and analyze aircraft that utilize multiple sources of energy, there is is a need to develop new sizing approaches to properly model such aircraft, particularly, hybrid-electric aircraft.

Finger et al. [37] developed an initial sizing methodology for series and parallel hybrid-electric general aviation aircraft using a modified constraint diagram. The authors added an additional dimension of power hybridization (i.e., split between electric and combustion engine power) to the classical constraint diagram and compared the new approach with traditional sizing approaches. The authors concluded that traditional sizing approaches do not work for hybrid-electric aircraft. Later, Finger et al. [38] used the developed initial sizing methodology to assess the benefits possible from parallel hybrid-electric powertrains for four different classes of aircraft (general aviation, regional transport, VTOL air taxi, and

UAV), and concluded that hybrid-electric propulsion systems are best suited for aircraft with high-power requirements for short duration (which could be met by the electrical system).

De Vries et al. [39] provided a preliminary sizing method for hybrid-electric aircraft with distributed propulsion. The work accounted for the propulsion–airframe integration effects considering a regional jet-size aircraft with leading-edge distributed propulsion (using several different hybrid-electric powertrain models). De Vries et al. [40] developed a range equation for aircraft with a generic hybrid-electric powertrain. The work assumes a constant power split between the two energy sources, with the conventional all fuel-burning configurations and fully-electric configurations acting as the limit cases of the hybrid-electric powertrain. Voskuijl et al. also developed a similar modified Bréguet range equation for hybrid-electric aircraft.

Pornet et al. [41] developed an extension to conventional sizing methods by including the electric power required as a part of the traditional engine look-up tables, and then integrating the required electrical energy over the complete mission. The work considered a hybrid retrofit aircraft based on a 2035 reference aircraft and concluded that batteries with very high gravimetric energy densities would be required to see significant benefits in fuel burn.

Brejle and Martins [42] developed a conceptual design toolkit – OpenConcept – built on top of the NASA-led OpenMDAO 2 framework. The tool features component-level cost modeling and thermal energy management, allowing the inclusion of economic and thermal constraints in optimization studies. The tool utilizes efficient gradients to enable gradient-based optimization methods for such studies. The authors perform a retrofit study considering a series hybrid-electric propulsion architecture for the King Air while minimizing both fuel burn and trip cost for varying design ranges and assumed battery specific energy levels. Brejle and Martins [34] also summarized the aircraft modeling and simulation approaches developed for analyzing aircraft with electrified propulsion.

Chakraborty and Mishra [43] developed an energy-based vehicle sizing and performance analysis methodology to enable the modeling of unconventional aircraft concepts, including aircraft with electrified propulsion. The methodology allows to estimate the propulsive power and energy requirements of a flight vehicle as well as its weight. The work presents a

generalized methodology for aircraft sizing combining flight performance, mission analysis, energy sizing concepts, and consideration of vehicle trim and geometry parameterization, allowing to size a diverse range of air vehicle including fixed-wing and vertical takeoff and landing aircraft. The authors demonstrate the methodology using a conventional fixed-wing general aviation aircraft, a UAM concept, and a hybrid lift airship. However, the work does not include any sizing optimization studies considering hybrid-electric propulsion systems.

Zamboni et al. [44] developed a method for conceptual design of hybrid-electric aircraft using an outside to inside power-path approach (from propulsive shaft to energy source) based on the propulsive control laws defined for each segment. The work considered a turboprop regional aircraft with parallel, series/parallel and distributed series configurations, and utilized rubber-sizing to scale all the components of the propulsion system while sizing the aircraft, allowing for a rapid exploration of the vast design space.

NASA is developing the Layered and Extensible Aircraft Performance System (LEAPS) tool [45] as a successor to the proven aircraft modeling tool Flight Optimization System (FLOPS) [46] to better model aircraft with electrified propulsion. Welstead et al. [45] and Capristan and Welstead [47] provide details about the energy based approach utilized in LEAPS to allow it to easily handle multiple energy sources for aircraft propulsion. NASA intends to release the LEAPS code in the public domain in the future, however, the release date is not clear [45]. Marien et al. [48], [49] used LEAPS (in conjunction with FLOPS as LEAPS is still under development) to conduct a series of parametric studies that explored the performance impact of battery size, motor size, range, and amount of electrification, for a regional jet-size hybrid-electric aircraft. The authors concluded that the turboprop configuration saw a significant fuel burn reduction, the turbofan configuration saw no benefit from the hybrid-electric configuration, and the operating cost for hybrid-electric aircraft is expected to be higher compared to their respective baselines.

All the above studies (and many more) present a strong argument for the need to modify existing traditional sizing approaches or develop new sizing methodologies to appropriately model aircraft with electrified propulsion, including hybrid-electric aircraft. To aptly study the fleet-level benefits possible from the introduction of hybrid-electric aircraft in future airline fleets, it is important to model the hybrid-electric aircraft characteristics appropri-

ately. Since most of the aforementioned (and other) hybrid-electric aircraft sizing codes are not publicly available, the author has developed a MDO sizing tool to identify optimal single-aisle parallel hybrid-electric aircraft designs using a "flight-mechanics-based" mission analysis approach. The MDO sizing tool addresses multiple disciplines (including aerodynamics, propulsion, performance, weights) using a single aircraft sizing code.

Most of the studies available in the literature do not consider the impact of downsizing the gas turbine engines for a parallel hybrid-electric configuration. Downsizing the gas turbine engines essentially means a reduction in the gas turbine engine core size, which in turn could lead to lower fuel burn (and lower carbon emissions). Concurrently, the aircraft should be able to climb at a gradient of at least 2.4% with the downsized gas turbine engine in case of an engine failure. The MDO sizing tool presented in this work considers this aspect while making sure that the aircraft can meet all the performance constraints (including meeting the OEI condition).

Another neglected aspect in most of the existing hybrid-electric aircraft sizing studies concerns the volumetric constraints associated with placing the batteries in the aircraft. For instance, if the batteries are placed inside the cargo hull in the aircraft fuselage, there will be a reduction in the cargo carrying capability (in terms of volume) of the aircraft. This reduction in the cargo capacity of the aircraft might make the aircraft less attractive for airlines. Hence, there is a need to account for the battery volume / placement while sizing the aircraft so that the fuselage can be sized accordingly. The MDO sizing tool presented in this work addresses this aspect by uniquely re-sizing the fuselage based on the required battery volume, concurrently as a part of the aircraft sizing process. Moreover, the sizing tool can identify the optimal climb, cruise, and descent speeds, along with the optimal cruising altitude, for both conventional and hybrid-electric aircraft configurations.

Another important aspect of appropriately modeling a hybrid-electric aircraft is considering the off-design performance characteristics of the aircraft. When the sized hybrid-electric aircraft is flown at a lower payload, or for a lower range (or both), the battery energy required to assist the gas turbine engine during takeoff and climb (to the cruising altitude) could be lower than the total battery energy onboard the sized aircraft (because the aircraft is lighter due to lower payload, or due to lower amount of fuel in the fuel tanks considering a

shorter mission, or both). Since batteries essentially count as "dead weight" that is carried by the aircraft on its mission, it makes most sense to utilize (or discharge) them completely (as per their safety limits) while minimizing the fuel burn (and carbon emissions) over the complete mission. This means that there is a need to identify a method / approach to optimize the power split between the two propulsion sources, i.e., gas turbine engine and electric motor, while they compete to meet the aircraft thrust requirements. For the parallel hybrid-electric aircraft considered in this work – with electric power augmentation considered only for takeoff and climb segment – this could mean that the optimal power split between the two propulsion sources could allow the aircraft to partially (or fully) cruise using battery energy, if that minimizes the fuel burn for the off-design mission in consideration.

Perullo and Mavris [50] reviewed the existing energy management optimization techniques in the literature and combined aircraft sizing with optimal energy management using a nested optimization approach. The authors used mathematical formulations from model predictive control to optimize energy management within the vehicle sizing process (inspired by the developments in ground vehicles). Trawick et al. [51] compared various power management optimization methods for determining the optimal power split between two energy sources, including optimal control, dynamic programming, and"rule-based" power schedules. Based on the results, the authors provided a general methodology and concluded that the choice of the optimal power schedule would be governed by the computational resources at hand and the improvement in fuel burn for the chosen power schedule compared to the baseline schedule. Lee et al. [52] developed an approach to simultaneously optimize flight path trajectory and power split strategy using a differential dynamic programming setup. The authors concluded that some fuel burn reduction benefits are possible at the aircraft level when we generate optimal flight path and power split trajectories for hybrid-electric aircraft compared to a constant electric power case, with higher benefits expected at a fleet-level. However, the study did not include the flight speed and altitude restrictions as per FAA guidelines in its analyses of the different flight phases. Wang and Mesbahi [53] proposed an optimal control problem formulation to identify the optimal power allocation strategy to minimize the fuel consumption and regularize the state of charge of the battery pack. The authors also derived inspiration from the results to propose some rule-based power alloca-

tion strategies for hybrid-electric aircraft. However, the study only considered a light aircraft with internal combustion engines, where the engine dynamics are much simpler than a gas turbine engine. The authors note that the optimal control problem could become highly complex when mid-scale or large-scale hybrid-electric aircraft (with gas turbine engines) are considered, requiring the use of alternate approaches in those cases.

These studies signify the importance of implementing an optimal power split strategy to minimize the fuel burn (and carbon emissions) for hybrid-electric aircraft operating on off-design missions. While most of the studies in the literature use some variation of an optimal control problem or dynamic programming problem formulation to solve for the optimal power split between the two propulsion sources, this work uses a more "traditional" optimization approach to solve the same problem – set up in the form of an energy management tool. The energy management tool is developed as an extension to the hybrid-electric aircraft sizing tool and consists of a single-objective constrained nonlinear optimization problem at its core. The tool can simultaneously optimize the power split between the two propulsion sources and identify the optimal climb, cruise, and descent speeds, along with the optimal cruising altitude, for different payload-range combinations. The aircraft performance metrics (primarily fuel burn) so obtained from the energy management tool are utilized to conduct fleet-level studies.

2.4 Airline Fleet Allocation

This work employs the Fleet-Level Environmental Evaluation Tool (FLEET) to study the fleet-level environmental impact of U.S. commercial aviation. FLEET models the behavior of a profit-seeking airline, assuming that it is one large "aggregate" U.S.-based airline. FLEET's core profit-maximizing optimization algorithm is an adaptation of a resource allocation problem [7]. However, several studies exist in the literature that perform aircraft allocation by solving an assignment problem, commonly known as a Fleet Assignment Model (FAM). Most of these studies employ linear programming problems to model aircraft assignment decisions while using profit maximization or cost minimization as the objective function.

Abara [54] solved the fleet assignment problem as an integer linear programming model, where the objective function could either maximize profit or minimize operating cost by maximizing the utilization of a particular fleet type. The work developed a time-space network to track individual aircraft (both in the air and on the ground) to ensure feasible aircraft assignment. Hane at al. [55] performed fleet assignment by formulating a large multi-commodity flow problem, with an objective function to minimize operating cost. The operating cost also included the cost of spilling a passenger because of lack of capacity. They tackled the optimization problem using different methods like interior point algorithm, dual steepest-edge simplex, etc. to find optimal integer solutions. Smith et al. [56] tackled a similar problem by using a station decomposition approach to solve a subnetwork fleet assignment model instead of using the entire network. Jacobs et al. [57] integrated FAM with origin and destination revenue management model (O&D FAM) using Benders decomposition, addressing both passenger flows within the network and demand uncertainty. All these studies considered flight leg-based passenger demand assumption. Barnhart et al. [58], [59] introduced the Itinerary-based Fleet Assignment Model (IFAM), capable of capturing network effects and more accurately estimating spill and recapture of passengers, an improvement over the then existing FAM models. This approach integrated an itinerary-based demand model with FAM to capture the effects of hub-and-spoke network operations on optimal fleet assignment decisions. Some other variations in tackling the fleet assignment problem are available in Berge and Hopperstad [60], Rushmeier and Kontogiorgis [61], Antoine et al. [62], Grönkvist [63], Sherali et al. [64], Li and Tan [65], for example. There exist some other studies in the literature that integrate fleet assignment with other stages in the airline planning process such as schedule design, crew scheduling, and maintenance routing. Such models are available in Barnhart et al. [66], Clarke et al. [67], Desaulniers et al. [68], Rexing at al. [69], Lohatepanont and Barnhart [70], Sherali et al. [71], Caetano and Gualda [72], Kenan et al. [73], Keji et al. [74], and others.

The computational expense associated with solving fleet assignment and scheduling problems is high. FAM consists of large-scale optimization problems, leading to considerable challenges in solving them to optimality (or near optimality) in reasonable time frames. In reality, airlines use a scheduling problem to assign individual aircraft by tracking their unique

tail numbers. This formulation of a scheduling problem requires tracking the individual aircraft, time-of-day issues, etc., and is substantially more difficult to solve than an allocation problem because of the large increase in decision variables, constraints, etc.

As mentioned before, FLEET's central optimization algorithm solves a resource allocation problem to maximize the profit of an airline while satisfying passenger demand on its route network. This essentially allows the airline to choose which (and how many) aircraft need to be allocated on a specific route, based on aircraft operation profitability and passenger demand forecast on that route. The allocation tool needs to quickly allocate flights throughout the air transportation network, satisfy demand, and calculate the fleet-level environmental metrics based on the allocation results. To comply with this requirement, the allocation tool in FLEET does not schedule aircraft. By removing the scheduling component, the tool used for the studies in this work simply allocates a number of aircraft to various roundtrips, without taking into consideration when the flights will actually occur. This helps FLEET to find feasible fleet allocation solutions to meet all the constraints in a reasonable time frame (usually in minutes). With the solve time reduced for the allocation problem formulation, changes in the fleet-mix, constraints or any other parameter of the model are evaluated quickly and allow a quick analysis of how fleet-level metrics are impacted [7], [75], [76].

2.5 Fleet-level Environmental Impact Modeling

FLEET's model-based approach of forecasting demand and allocating aircraft to meet future demand – while meeting the airline's objective of profit maximization – allows it to predict CO_2 emissions from a more-realistic airlines operation and profitability perspective [7].

There exist several studies that model fleet-level carbon emissions from commercial aviation, while assessing the ability to meet future carbon emission targets given the different economic, technological and demand growth scenarios. Nolte et al. [77] use a fleet forecast model to predict the fleet-level aviation CO_2 emissions with the introduction of technological advancements in the aviation fleet. The work assigns yearly fuel consumption and traffic

to each active aircraft (based on the yearly forecast of the number of each type of aircraft required to meet the predicted demand), utilizing the assigned fuel values to calculate the fleet-level CO_2 emissions (using the block fuel consumption data for each type of aircraft). Sgouridis et al. [78] employ the Global Aviation Industry Dynamics (GAID) model to predict the fleet-wide carbon emissions as a function of technological efficiency improvements, operational efficiency improvements, use of alternative fuels, demand shift and market-based incentives. The GAID model [79] employs a system dynamics approach to model primary aviation industry stakeholders including aircraft manufacturers, airlines, and passengers. The study recommends that an approach based on a portfolio of mitigating measures and policies spanning across technology and operational improvements, use of biofuels, demand shift and carbon pricing is required to promote sustainable growth of the aviation industry. Hileman et al. [80] predict the fleet-wide life cycle greenhouse gas intensity by using the product of aircraft energy consumed per payload–distance flown and the jet fuel life cycle greenhouse gas emissions factor. The work predicts the carbon emissions as a function of aviation growth, aircraft efficiency, operational efficiency, and life cycle greenhouse gas emissions of aviation fuels. Hassan et al. [81] perform a probabilistic assessment of aviation CO_2 emission targets by formulating an optimization problem that minimizes the available seat miles to achieve partial equilibrium that matches aviation supply with the demand. The study employs FAA aerospace forecast (and further extrapolation of that data) to evolve the fleet size up to year 2050 and calculates the system CO_2 emissions based on the system fuel burn, while considering aircraft technologies, operational improvements and sustainable biofuels.

The most recent additions to the approaches for modeling fleet-wide future carbon emissions include considering biofuels as a fuel source for aviation. Sgouridis et al. [78], Hileman et al. [80], and Hassan et al. [81] conclude that biofuel usage will be the major contributor to meet the aviation CO_2 emission targets.

References [82]–[84] describe the impact the of biofuels on aviation emissions using the Fleet-Level Environmental Evaluation Tool (FLEET), the tool utilized in this work and described in the Chapter 4. Chao at al. [85] use FLEET to study the potential impacts of biofuel options and emissions trading scheme on the carbon emissions of U.S. airlines.

The study indicates that the fleet-wide CO_2 emissions might not reduce with the usage of biofuels alone and will require the implementation of a domestic emission scheme which would stimulate biofuel demands and decrease the fleet-level carbon emissions to the emission reduction targets.

Although several research efforts studied the fleet-level impacts of technological advancements, demand growth, and operational improvements on the environment, none of the studies attempt to model and simulate the behavior of an airline seeking to maximize its profit over its whole route network.

The aforementioned studies rely on external forecasts to predict fleet-wide carbon emissions, neglecting the airline decision modeling portion of the problem. FLEET employs a year-by-year approach in its simulation which models the evaluation of passenger demand, airline fleet mix, and available aircraft technology level. This makes FLEET independent of an external forecast for airline operations, an external forecast for passenger demand, and of a prescribed fleet mix evolution. Using a series of modules that represent various aspects of the commercial aviation system connected by feedback loops, FLEET allows airline ticket fares, passenger demand, airline fleet size and airline fleet composition to evolve over time. By including routes and operations that reflect most of the airline operations with at least one airport in the U.S., the results from FLEET provide a fleet-level prediction of the environmental impacts (including CO_2 emissions trends) of U.S. commercial aviation, while also taking into account the impact of the COVID-19 pandemic.

3. MODELING HYBRID-ELECTRIC AIRCRAFT

Modeling an aircraft computationally requires information about the aircraft's fuel consumption, performance characteristics (including, but not limited to, payload-range capability), and operating costs. Aircraft sizing is the technique to determine the size (wing, fuselage, tails, and engine), weight, and performance characteristics of an aircraft that can complete a specified mission. Some of the important sizing variables include thrust-to-weight ratio, wing loading, wing aspect ratio, wing sweep, wing taper ratio, wing thickness-to-chord ratio, and fuselage fineness ratio. Based on the sizing design variables, the empty weight of the aircraft and the weight of fuel required to complete the mission are determined; the fuel weight is dependent on the aerodynamic characteristics and the propulsion system considered for the aircraft. Traditionally, the well-known Bréguet range equations (for cruise flight segment) and empirical equations (for other flight segments; based on existing aircraft data) are employed to determine the fuel fraction or fuel weight required to complete different segments of the design mission (for a given set of sizing variables), leading to iterative sizing of an aircraft. However, these historical data-based approaches to determine fuel fraction for sizing are not sufficient for sizing a hybrid-electric aircraft. A hybrid-electric configuration couples two different sources of energy; this work considers Jet-A fuel and batteries as the two energy sources. The energy consumption from a combination of the two energy sources over the design mission drives the weight and volume of fuel and battery required to complete the mission. Hence, hybrid-electric aircraft sizing needs power requirement information for each flight segment to implement the power-split between the gas turbine engine (powered by the Jet-A fuel) and the electric motor (powered by the batteries). Section 3.1 presents the "flight-mechanics-based" hybrid-electric aircraft sizing tool developed by the author to model these partially-electric aircraft of the future. Section 3.3 discusses an energy management tool developed by the author to optimally utilize the battery energy onboard the sized hybrid-electric aircraft when flying on an off-design mission.

This work considers a parallel hybrid-electric single-aisle aircraft with electric power augmentation available only for takeoff and climb segments when sizing the aircraft. The

tool can be expanded to include other types of aircraft, like business, regional, or twin-aisle size hybrid-electric and all-electric aircraft.

3.1 Hybrid-Electric Aircraft Sizing Tool

The hybrid-electric aircraft sizing tool is set up as a Multidisciplinary Design Optimization (MDO) toolbox that consists of a single aircraft sizing code addressing different disciplines. The tool simulates an aircraft's trajectory in two-dimensions considering three degrees-of-freedom (3-DOF) – two translational (surge, heave) and one rotational (pitch), while using the angle of attack, climb/descent angle, and throttle position as control parameters. This generates detailed information about the aircraft's energy requirements for discrete time steps. The aircraft's energy requirements drive the size of the gas turbine engine, the electric motors, and the batteries. The following are some of the distinguishing features of the hybrid-electric aircraft sizing tool presented in this work:

- Considers hybrid-electric propulsion only for takeoff and climb segments with electric motors operating at full throttle; no electric motor power is available during the cruise, descent, and landing segments during sizing. This is a modeling choice based on engineering intuition – this would apply the electric power in flight conditions when the most power is needed from the gas turbine engines
- Allows to "re-size" the gas turbine engine while meeting energy requirements for takeoff, climb, and cruise segments
- Considers one-engine-inoperative (OEI) condition during takeoff climb for a hybrid-electric powertrain
- Allows for fuselage re-sizing ("stretching") to accommodate the required battery packs inside the aircraft's fuselage without sacrificing the aircraft's cargo capacity
- Utilizes a Simultaneous Analysis and Design (SAND) approach to concurrently enable aircraft sizing and fuselage re-sizing while avoiding a traditional iterative sizing

loop to converge on the aircraft weight and performance metrics, which saves total computational cost and time

The following sub-sections provide details about the problem setup and the different modules that allow the tool to incorporate all the above-mentioned hybrid-electric aircraft sizing features. There are five modules in the sizing tool – geometry, propulsion, aerodynamics, mission, and weight. The sizing tool is then used to conduct design trade studies considering different battery energy densities (both gravimetric and volumetric), electric motor characteristics, and system efficiencies (Section 3.2).

3.1.1 Optimization Problem Setup

The sizing optimization problem is set up as a single-objective nonlinear programming problem with nonlinear constraints. The problem consists of continuous design variables only and can be solved using gradient-based approaches. The objective function of the problem is to minimize the weight of Jet-A fuel, while satisfying some performance constraints, including constraints on takeoff and landing field lengths, climb gradient for OEI condition, cruise and service ceilings, thrust available during cruise (implemented using the gas turbine engine throttle setting, also referred to as power code, PC), and the guessed aircraft takeoff gross weight and volume required by the battery. The last two constraints are a part of the Simultaneous Analysis and Design (SAND) approach implemented as a part of the problem setup. In the SAND approach, the guessed aircraft takeoff gross weight and the guessed volume required by the battery are design variables in the problem. The guessed values are used to complete the sizing loop, and the constraint ensures that the guessed aircraft weight and battery volume are less than or equal to the calculated aircraft weight and battery volume. Using the less-than-or-equal-to constraints rather than equality constraints helps to reduce the computational cost associated with the SAND approach. This approach allows the sizing tool to get rid of the traditional iterative aircraft sizing loop while also allowing the tool to account for the change in fuselage dimensions (and subsequently aerodynamic characteristics and empty weight) associated with installing the required battery in the aircraft (without compromising on cargo volume).

The sizing optimization problem is formulated as follows:

minimize:

$$W_{Fuel}$$

subject to:

$$takeoff\ field\ length \leq 7,500 \text{ ft [1]}$$
$$landing\ field\ length \leq 7,000 \text{ ft [2]}$$
$$OEI\ climb\ gradient \geq 2.4\% \text{ [3]}$$
$$cruise\ ceiling \geq 25,000 \text{ ft [4]}$$
$$service\ ceiling \geq 28,000 \text{ ft [5]}$$
$$PC_{GTE}^{top-of-climb} \leq 47 \text{ [6]}$$
$$TOGW^{calculated} \leq TOGW^{guess} \text{ [7]}$$
$$V_{Batt}^{calculated} \leq V_{Batt}^{guess} \text{ [8]}$$

design variables:

$$S_{wing},\ AR_{wing},\ \Lambda_{wing},\ t/c_{wing},$$
$$Pmax_{turbine}^{SLS},\ Pmax_{emotor},\ TOGW^{guess},\ V_{Batt}^{guess}$$

where, the first four design variables are related to aircraft geometry, followed by the maximum sea-level static shaft power of the gas turbine engine, maximum rated power of all electric motors combined, guessed takeoff gross weight, and the guessed battery volume. Table 3.1 shows the upper and lower bounds for all the sizing design variables.

Table 3.1. Sizing tool: Upper and lower bounds for the sizing design variables

Sizing Design Variables	**Lower Bound**	**Upper Bound**
Wing Area (S_{wing}) [ft^2]	1,100	1,500
Wing Aspect Ratio (AR_{wing})	8	12
Wing Sweep at 25 % (Λ_{wing}) [deg]	15	40
Wing Thickness-to-Chord Ratio (t/c_{wing})	0.09	0.17
Max SLS Power of GTE ($Pmax_{GTE}^{SLS}$) [MW]	10	25
Max Power of E-Motor ($Pmax_{emotor}$) [MW]	0	8
Guess Takeoff Gross Weight ($TOGW^{guess}$) [lbs]	80,000	250,000
Guess Battery Volume (V_{Batt}^{guess}) [ft^3]	0	300

Figure 3.1 depicts the hybrid-electric aircraft sizing tool. The sizing optimization problem passes the design variables to the propulsion, geometry, aerodynamics, and mission modules. The aerodynamics module uses additional information from the propulsion and geometry modules to provide lift and drag information to the mission module. The mission module uses information from the propulsion and geometry modules to calculate the fuel and battery weights. Similarly, the weights module uses information from the propulsion and geometry modules to provide the aircraft empty weight. The takeoff gross weight calculations close the sizing loop and the objective value and detailed mission data is returned to the optimizer for constraint analysis. Figure 3.1 also showcases the inputs and outputs for all five modules.

For combinations of design variables that prevent the aircraft from climbing or cruising (for instance, when the total thrust available is too low to accelerate and climb for the guessed aircraft takeoff gross weight), the problem employs a backup mission to obtain a value for the mission fuel weight for the current set of sizing design variables. The objective function in that case is set as the sum of the weight of fuel from the backup mission and a penalty based on the segment it fails. The sizing tool is set up in MATLAB and is adapted to use MATLAB's gradient-based solvers, like Sequential Quadratic Programming (`fmincon` solver [86]), and non gradient-based solvers, like Nelder-Mead Simplex (`fminsearch` solver [87]), to solve the optimization problem. The tool is agnostic to the choice of the solver and can be adapted easily to use other gradient-based and non gradient-based solvers. A multi-start approach is preferred for non-global solvers to identify the best solution to the posed sizing optimization problem in case there are multiple local minima.

3.1.2 Sizing Tool Modules

3.1.2.1 Geometry Module

The geometry module utilizes information from the aircraft's Computer-Aided Design (CAD) model to provide fuselage dimensions (length, height, and width) to the aerodynamics and weight modules. The sizing design variable V_{Batt}^{guess}, which concerns the required battery volume, drives the length of the fuselage (with the fuselage height and width staying constant).

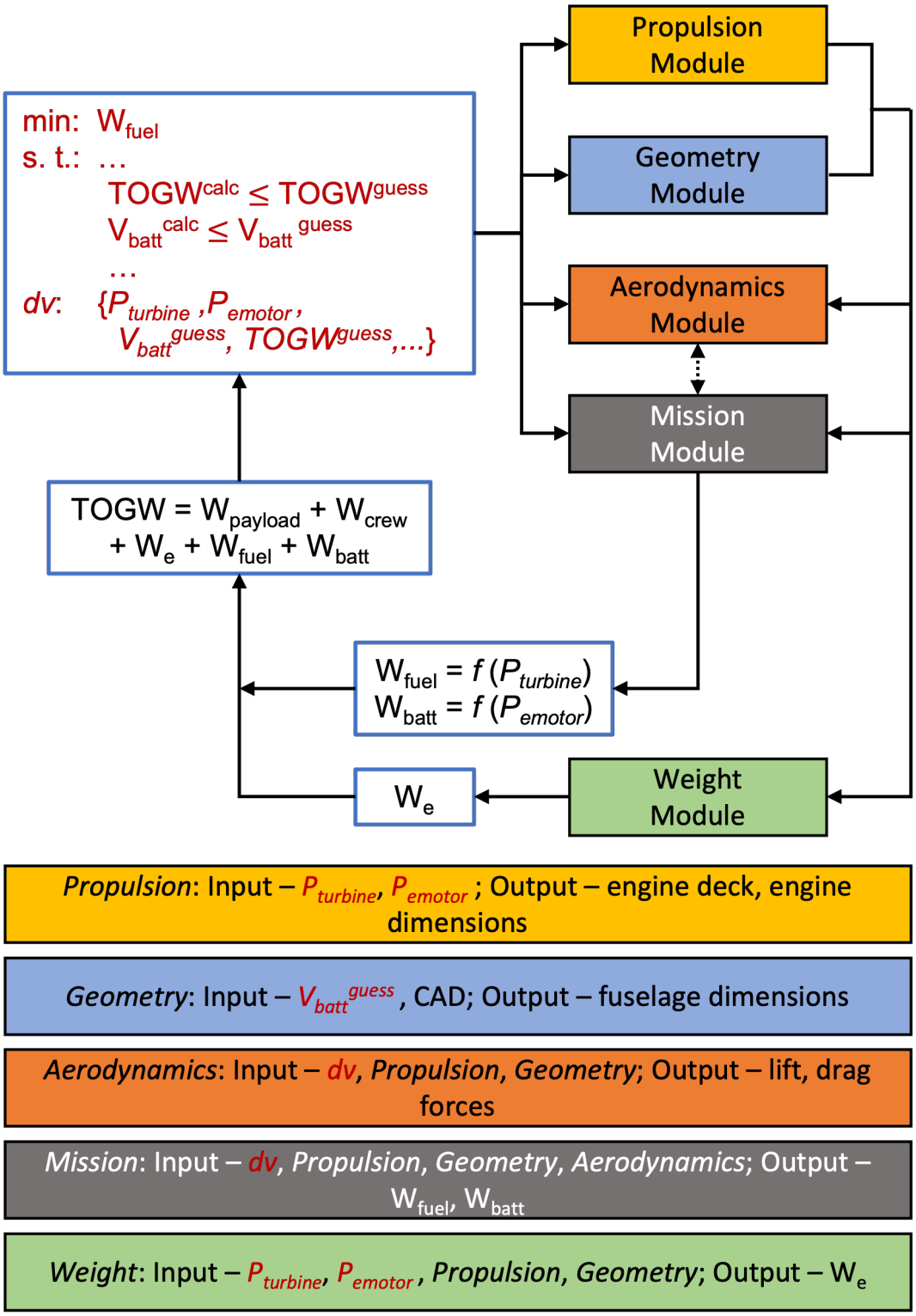

Figure 3.1. A simplified flowchart depicting the hybrid-electric aircraft sizing tool

Baseline CAD Model

The baseline CAD model uses a Boeing 737-800 aircraft as a starting point to lay out the cabin cross-section. The model uses human comfort bubbles to set the seat, aisle, and final fuselage width. The human comfort bubbles make sure that every passenger has enough space to sit comfortably on any seat in the aircraft by taking into account the passenger headroom, arm movement room, and legroom. The dimensions used for the human comfort bubbles are 6.5 inches for the head, 10.9 inches for the shoulders, 12.2 inches for the arms, and 6.5 inches for the feet. Using a seat width of 17 inches, an armrest width of 2 inches, and an aisle width of 20 inches, the maximum fuselage width comes out to be 148.21 inches for the baseline model. Figure 3.2 shows the cabin cross-section with the human comfort bubbles, seats, luggage bins, and a 95 percentile human (with 74 inches height) to illustrate the headroom in the aisle when standing. The cargo area visible in the cabin cross-section in Figure 3.2 has a maximum height of 46.35 inches and a maximum width of 120 inches. The cargo area is sized to accommodate a LD3-45 container [88]. LD3-45 is a standard container designed for a single-aisle aircraft (initially designed for the Airbus 320-family) with maximum dimensions of 96 inches (width) x 45 inches (height) x 60.4 inches (depth). The maximum fuselage height for the baseline model is 158.23 inches.

Next, the location of the passenger seats and the exits are determined using the Layout of Passenger Accommodations (LOPA). The seat pitch is set to 30 inches, which leads to an all economy single-class cabin with 185 seats; there are 29 rows of six abreast seating, two rows of four abreast seating, and one row of three abreast seating. The exit doors are located at the beginning and end of the passenger cabin, along with an emergency exit over the wing, on both sides of the fuselage. The passenger compartment length is 80 ft, and the total length of the fuselage is 124.75 ft. Figure 3.3 shows the LOPA for the baseline CAD model.

Figure 3.4 shows the lofted fuselage. The fuselage consists of two cargo compartments – forward and aft. The forward compartment stretches 302 inches and can fit up to five LD3-45 containers; the cargo capacity is approximately 766 ft^3. The aft compartment has a length of 428 inches (borrowed from Boeing 737-800 aircraft), can fit up to four LD3-45

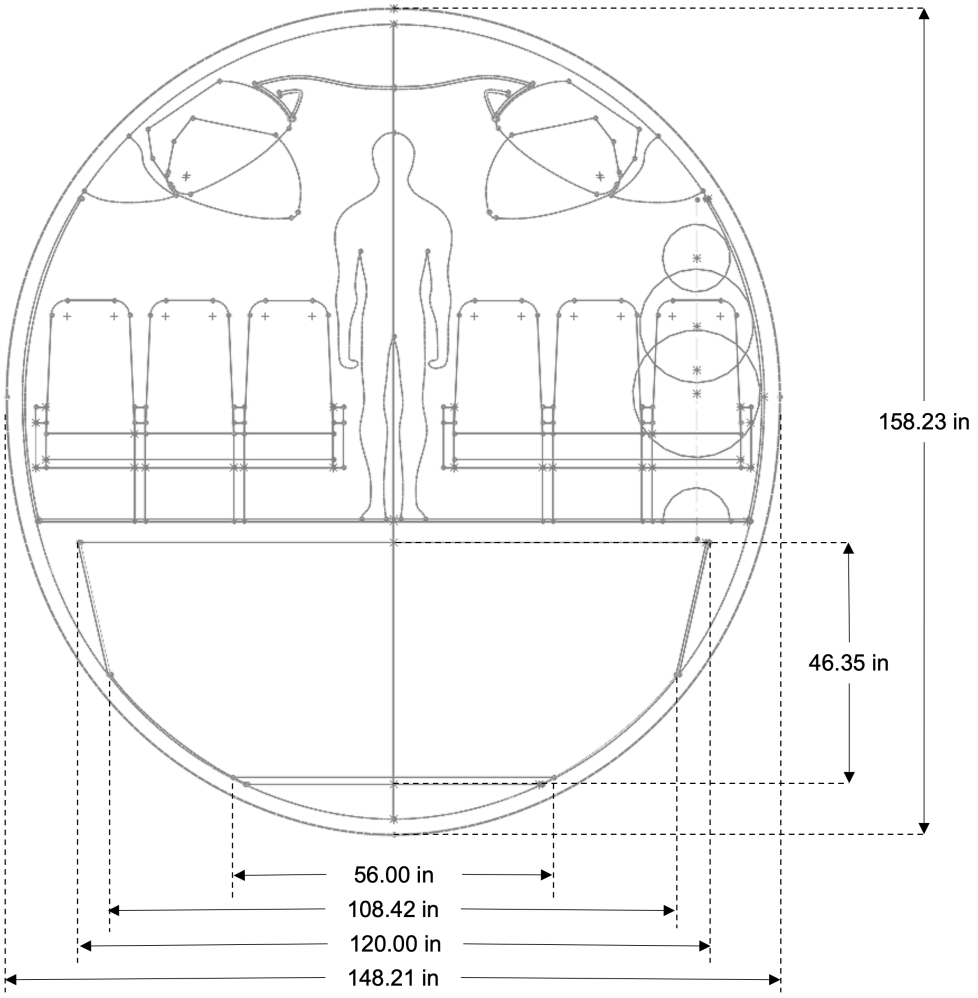

Figure 3.2. Cabin cross-section for the baseline single-aisle aircraft; shows the human comfort bubble, seat placement, luggage bins, a 95 percentile human, and cargo area

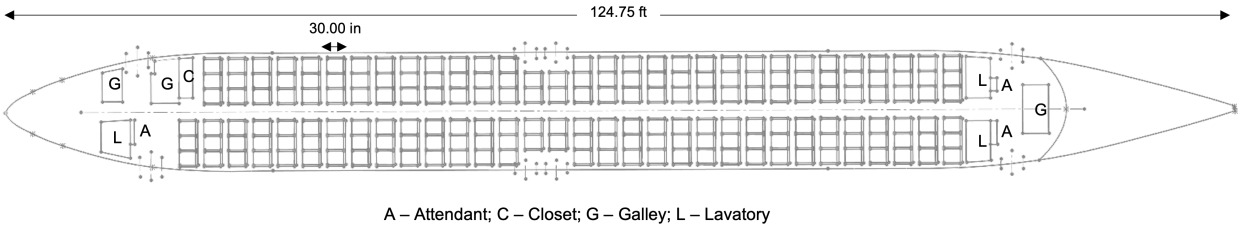

Figure 3.3. Layout of Passenger Accommodations (LOPA) for the baseline single-aisle aircraft

containers before the fuselage starts to taper, and has a cargo capacity of approximately 869 ft^3. The total cargo volume available in the baseline CAD model is approximately 1,635 ft^3. The author notes that the final fuselage dimensions of the baseline single-aisle aircraft are very similar to a Boeing 737-800 aircraft which served as a starting point to loft the fuselage.

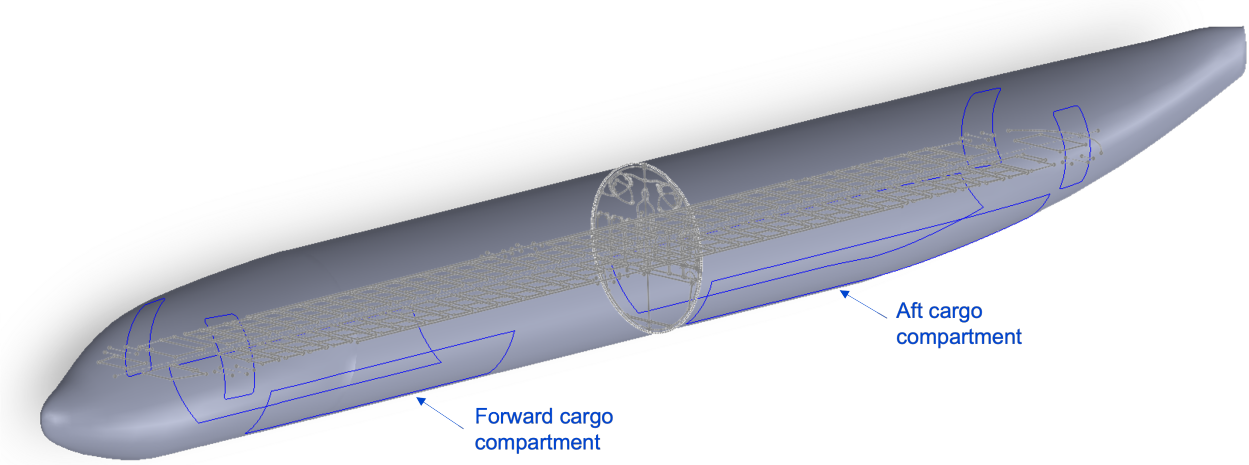

Figure 3.4. Lofted fuselage with cargo compartments for the baseline single-aisle aircraft

Fuselage Stretching for Hybrid-Electric Aircraft Sizing

This work considers changes to the fuselage length of the baseline CAD model when sizing a hybrid-electric aircraft. The fuselage is "stretched" to accommodate the required battery without sacrificing the aircraft's available total cargo volume; the fuselage length is governed by the sizing design variable V_{Batt}^{guess}. The battery is assumed to be stored in the "extra" cargo volume of the stretched fuselage.

Considering the cabin cross-section of the baseline CAD model shown in Figure 3.2, the area of the cargo hold is approximately 25 ft^2, taking into account all unusable spaces due to the shape of the hull. Now considering the cargo hold in three dimensions, ignoring battery placement specifics, storing 25 ft^3 of batteries would require an additional fuselage length of 1 ft. This means that the fuselage length needs to increase by 1 ft for every 25 ft^3 of battery volume. The fuselage is "stretched" at the constant fuselage cross-section area without impacting the tapered sections near the nose or tail. A sample location where the

fuselage stretch could be implemented is the location where the cabin cross-section sketch is shown inside the lofted fuselage in Figure 3.4.

This work uses a simple linear interpolation to convert the required battery volume (provided by V_{Batt}^{guess}) to a change in total fuselage length and the passenger cabin length. For example, a value of 145 ft^3 for V_{Batt}^{guess} would lead to a (145/25 =) 5.8 ft increase in the fuselage and passenger cabin length. The linear interpolation allows the sizing problem to stay continuous in the overall design space.

Another approach to place the required batteries in a hybrid-electric aircraft could be to store them under the main floor. This would require a redesign of the cabin cross-section (and hence the fuselage) using a CAD model for every combination of sizing design variables. Storing the batteries under the main floor would be beneficial if the volume required by the batteries is at least 742.5 ft^3. This value is comes from the passenger cabin floor dimensions of the baseline CAD model assuming a battery layer height of 1 ft — 82.5 ft (cabin length) x 9 ft (cabin width) x 1 ft (layer height). Given that the upper bound for the guessed battery volume design variable (V_{Batt}^{guess}) is set to 300 ft^3, it does not make sense to use this approach to resize the fuselage in the current work. Additionally, storing the batteries under the main floor might lead to some challenges with battery maintenance / pack replacement in the longer run.

3.1.2.2 Propulsion Module

The propulsion module takes into consideration the gas turbine engine and the electric motor. This work considers a turbofan engine as the gas turbine engine of choice for modeling a single-aisle parallel hybrid-electric aircraft. Given the fidelity of the sizing tool presented in this work, the author assumes a straightforward integration of the electric motors with the Low Pressure Turbine (LPT) shaft of the gas turbine engine. In simple terms, the electric motor provides power to the LPT shaft to drive the fan using a gearbox (only modeled via an efficiency, $\eta_{transmission}$), in addition to the power provided by the turbofan engine core through combustion. Figure 3.5 shows a sketch to illustrate the simplistic integration of the electric motor with the gas turbine engine. The total power input to the fan is described by

Equation 3.1. Equation 3.2 calculates the total thrust produced by the power input to the fan. Using Equation 3.1, Equation 3.2 can be re-written as Equation 3.3, given the simplistic propulsion system modeling considered in this work.

$$P_{input} = P_{turbine} + P_{emotor} \tag{3.1}$$

$$T_{total} = \frac{P_{input}}{V} * \eta_{fan} \tag{3.2}$$

$$T_{total} = \frac{\eta_{fan}}{V} * (P_{turbine} + P_{emotor}) \tag{3.3}$$

Hence, we can determine the total thrust generated by the propulsion system using the shaft power of the gas turbine engine, $P_{turbine}$, and the power of the electric motor, P_{emotor}.

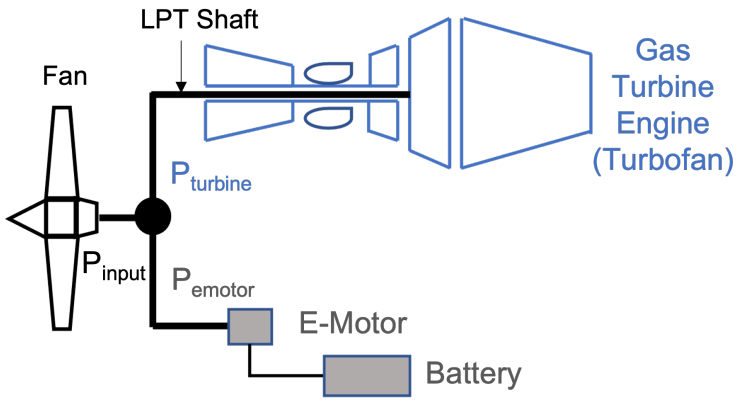

Figure 3.5. Simple illustration depicting the integration of the electric motor with the gas turbine engine

The power augmentation by the electric motors during takeoff, initial climb, and climb segments allows the sizing optimization problem to downsize the turbofan engine core (while keeping the fan size constant). The design variables — $Pmax^{SLS}_{turbine}$ and $Pmax_{emotor}$ — from the sizing optimizer govern the "size" of the gas turbine engine and the electric motor, respectively.

Gas Turbine Engine Modeling

The gas turbine engine modeling for this work started with developing a simplistic high bypass ratio turbofan engine model using the equations provided in the appendix of Mattingly's book [89]. However, with issues related to finding appropriate detailed engine data to validate the performance of the turbofan engine model, and the need to use detailed engine data like LPT shaft power at various Mach number, altitude, and throttle setting combinations, the author decided to use the Numerical Propulsion System Simulation (NPSS) software [90] to model the engine. NPSS is a proven gas turbine modeling software that is widely used in both the industry and academia. NPSS provides a six-column engine deck with Mach number, altitude, throttle setting / power code, net thrust, fuel flow, and shaft power as outputs (with a capability to add more user-based data / columns, if needed). The baseline engine modeled in NPSS mimics a CFM56-7B27 engine; Figure 3.6 shows an excerpt from the six-column engine deck. The engine deck from NPSS provides all the required data to model the fuel burn and LPT shaft power characteristics of a gas turbine engine. The gas turbine engine is "re-sized" based on the value of the sizing design variable $Pmax^{SLS}_{turbine}$, which signifies the maximum sea-level static shaft power of the gas turbine engine. Current work does not call NPSS as a part of the sizing loop to re-size the gas turbine engine for every combination of design variables, rather it uses a simplistic rubber engine sizing approach to maintain fidelity with the other modules of the sizing tool. As a part of the rubber engine sizing approach, the baseline engine deck is scaled to generate the updated engine deck based on the ratio of $Pmax^{SLS}_{turbine}$ and $Pmax^{SLS}_{turbine_{baseline}}$. The thrust, shaft power, and fuel flow characteristics at different altitudes and Mach number are then calculated using linear interpolation or using a surrogate model of the engine deck.

Electric Propulsion Modeling

The electric propulsion system includes the electric motors, batteries, and their wiring connections. The sizing design variable $Pmax_{emotor}$ drives the size of the electric motor. The power drawn from electric motor determines the battery power required for a discrete time step in the mission profile. Equation 3.4 provides the relation between electric motor power

Mach	Altitude(ft)	PowerCode	NetThrust(lbf)	FuelFlow(lb/min)	ShaftPower(hp)
0.00	0.0	50	26889.73	10190.33	29555.30
0.00	0.0	46	23304.59	8608.42	24867.68
0.00	0.0	38	16133.75	5818.45	15847.97
0.00	0.0	30	8963.23	3232.45	7243.74
0.00	0.0	24	3764.55	1629.99	2230.48
0.00	0.0	21	1344.48	1007.17	616.86
0.10	0.0	50	25037.47	10493.60	30459.39
0.10	0.0	46	21699.42	8890.13	25792.09
0.10	0.0	38	15022.40	6091.71	16813.11
0.10	0.0	30	8345.78	3477.83	8089.66
0.10	0.0	24	3505.24	1795.94	2711.71
0.10	0.0	21	1251.89	1081.22	810.23

Figure 3.6. Sample six-column engine deck from NPSS

(P_{emotor}) and battery power (P_{batt}) , where η_{emotor} is the electric motor efficiency, $\eta_{transmission}$ is the transmission efficiency, η_{PMAD} is the Power Management and Distribution (PMAD) system efficiency, and $\eta_{battery}$ is the battery discharge efficiency.

$$P_{emotor} = \eta_{emotor} * \eta_{transmission} * \eta_{PMAD} * \eta_{batt} * P_{batt} \tag{3.4}$$

The integration of battery power required over the takeoff, initial climb, and climb segments provides the battery energy and the battery weight required for the complete sizing mission. Equation 3.5 provides the relation between battery energy (E_{batt}) and battery weight (W_{batt}), where *Esb* is the gravimetric energy density of the battery, and *MaxDischarge* is the maximum percentage of energy that can be discharged from the battery without permanently damaging it.

$$E_{batt} = Esb * MaxDischarge * W_{batt} \tag{3.5}$$

3.1.2.3 Aerodynamics Module

The aerodynamics module provides aircraft lift and drag data to the mission module for solving the equations of motion for discrete time steps. This module takes into consideration the fuselage dimensions from the geometry module to generate the lift and drag data. Given the fidelity of the sizing tool, current work uses simplistic semi-empirical equations for calculating the lift and drag forces on the aircraft.

The module calculates the lift at any discrete time step using airfoil information and wing design variables from the sizing problem. Equations 3.6 to 3.8 provide details about the lift

force calculations. First, the wing lift-curve slope (C_{L_α}) is determined using the wing design variables, as shown in Equation 3.6 [91], where, the value of β is calculated as $\sqrt{1-M^2}$ (where M is the Mach number), the value of η is set to 1.0, and the value of $(\frac{S_{exposed}}{S_{ref}}) * F$ is set to 0.98 as recommended by Raymer [91].

$$C_{L_\alpha} = \frac{2 * \pi * AR}{2 + \sqrt{4 + \frac{AR^2 * \beta^2}{\eta^2} * (1 + \frac{tan^2 \Lambda}{\beta^2})}} * (\frac{S_{exposed}}{S_{ref}}) * F \tag{3.6}$$

The product of the wing lift-curve slope and the angle of attack (α) gives the coefficient of lift (Equation 3.7), which further provides the lift force on the aircraft using Equation 3.8.

$$C_L = C_{L_\alpha} * (\alpha - (\alpha_0 + \delta\alpha_0)) \tag{3.7}$$

$$L = q * S_w * C_{L_\alpha} * (\alpha - (\alpha_0 + \delta\alpha_0)) \tag{3.8}$$

In Equation 3.8, q is the dynamic pressure of the freestream air, S_w is the wing area, α_0 is the zero-lift angle of attack, and $\delta\alpha_0$ is the change in the zero-lift angle of attack due to flaps, slats, and spoilers. The zero-lift angle of attack (α_0) is determined using airfoil characteristics like design lift coefficient, design angle of attack, and lift curve slope, as shown in Equation 3.9 [92],

$$\alpha_0 = \alpha_i - \frac{c_{l_i}}{c_{l_\alpha}} \tag{3.9}$$

where, α_i is the airfoil's design angle of attack, c_{l_i} is the airfoil's design lift coefficient, and c_{l_α} is the airfoil's lift curve slope. This work estimated the zero-lift angle for the Boeing 737 wing airfoil as the same zero-lift angle as the NACA 23012 airfoil. This is because the airfoil section of the 737 is not readily available in public literature. The change in the zero-lift angle of attack ($\delta\alpha_0$) due to flaps, slats, and spoilers is calculated using Equation 3.10 from Raymer [91].

$$\delta\alpha_0 = \delta\alpha_{0\,airfoil} * \frac{S_{flap}}{S_{ref}} * cos(\Lambda) \tag{3.10}$$

The value of $\delta\alpha_{0\,airfoil}$ is determined using linear interpolation based on the known values for change in airfoil's zero-lift angle due to a certain degree of flap deflection. Raymer [91]

estimates that the change in airfoil's zero-lift angle due to flaps is -15 deg at landing (70 deg flap deflection) and -10 deg at takeoff (40 deg flap deflection). Using this information, linear interpolation provides the value of $\delta\alpha_{0\,airfoil}$ for a certain flap deflection; the value of $\delta\alpha_{0\,airfoil}$ for a clean configuration (no flap deflection) is zero. All these calculations assume that the lift-curve slope remains constant.

This work uses simplistic textbook-based approaches to calculate aircraft drag. The parasite drag coefficient (C_{D_0}) is determined using the parasite drag buildup empirical equations based on chapter 12 from Raymer [91]. The laminar flow percentage for the wings, tails, and fuselage is set to 50%, 50%, and 25%, respectively, considering the hybrid-electric aircraft will have an EIS date of 2035. The increment in parasite drag coefficient due to flap deflection is calculated using Equation 3.11 from Raymer [91],

$$\Delta C_{D_{0\,flap}} = F_{flap} * \frac{C_f}{C} * \frac{S_{flapped}}{S_{ref}} * (\delta_{flap} - 10) \tag{3.11}$$

where δ_{flap} is the flap deflection, and the value of F_{flap} is set to 0.0074 considering slotted flaps. The induced drag coefficient is simply calculated using Equation 3.12,

$$C_{D_i} = (\frac{1}{\pi * AR * e}) * C_L^2 \tag{3.12}$$

where e is the Oswald efficiency factor – set to 0.8 for this work. The increment in induced drag coefficient due to flap deflection is calculated using Equation 3.13 from Raymer [91],

$$\Delta C_{D_{i\,flap}} = k_f^2 * (C_{L_{alpha}} * \delta\alpha_0)^2 * cos\Lambda \tag{3.13}$$

where, k_f is set to 0.28 considering half-span flaps. The additional drag due to the extension of the landing gear is modeled using Sun et al. [93] and the drag due to the spoilers is modeled using Raymer [91]. The final drag is the sum of parasite drag, parasite drag increment due to flap deflection (if any), induced drag, induced drag increment due to flap deflection (if

any), and additional drag due to landing gear and spoilers (if any). Equation 3.14 depicts the total drag force on the aircraft.

$$D = q * S_w * (C_{D_0} + \Delta C_{D_{0\,flap}} + C_{D_i} + \Delta C_{D_{iflap}} + \Delta C_{D_{LG,spoiler}}) \tag{3.14}$$

3.1.2.4 Mission Module

The mission module calculates the fuel weight, battery weight, and battery volume required for the complete mission. The mission profile is split into several flight segments that adhere to Part 25 rules; Figure 3.7 shows the mission profile for the sizing mission; each straight line in the figure represents a mission sub-segment (note that the cruise segment is not shown to scale, and can vary with the design requirements of the aircraft). The flight segments are modeled using "flight-mechanics-based" simulation techniques which includes solving equations of motion for discrete time steps for each segment. This is necessary to know the aircraft thrust or power requirements for finer time steps in the mission profile; this information forms the basis for sizing the electric motor, re-sizing the gas turbine engine, and estimating the battery weight and volume. Figure 3.8 provides the free body diagram used to calculate the aircraft's state at a given time. Equations 3.15 and 3.16 show the equations of motion for the free body diagram in Figure 3.8.

$$T * cos\alpha - D - W * sin\gamma = \frac{W}{g} * a \tag{3.15}$$

$$L + T * sin\alpha - W * cos\gamma = 0 \tag{3.16}$$

Equations 3.15 and 3.16 can be simplified using Equations 3.7, 3.11-3.14 to contain only four control parameters: α (angle of attack), γ (climb/descent angle), T (thrust), and a (aircraft acceleration). Equations 3.17 and 3.18 show the simplified equations of motion.

$$\begin{aligned} T * cos\alpha - q * S_w * (C_{D_0} + \Delta C_{D_{0\,flap}} + \Delta C_{D_{iflap}} + \Delta C_{D_{LG,spoiler}}) \\ -q * S_w * (\frac{1}{\pi * AR * e}) * (C_{L_\alpha} * (\alpha - \alpha_0))^2 - W * sin\gamma = \frac{W}{g} * a \end{aligned} \tag{3.17}$$

$$q * S_w * C_{L_\alpha} * (\alpha - (\alpha_0 + \delta\alpha_0)) + T * sin\alpha - W * cos\gamma = 0 \tag{3.18}$$

For every flight segment, two of the four control parameters are known using the characteristics of the flight segment, leading to two equations (Equations 3.17 and 3.18) with two unknowns. The solution of the equations of motion determines the fuel burn and battery energy (and hence battery weight and volume) required to complete the concerned time step.

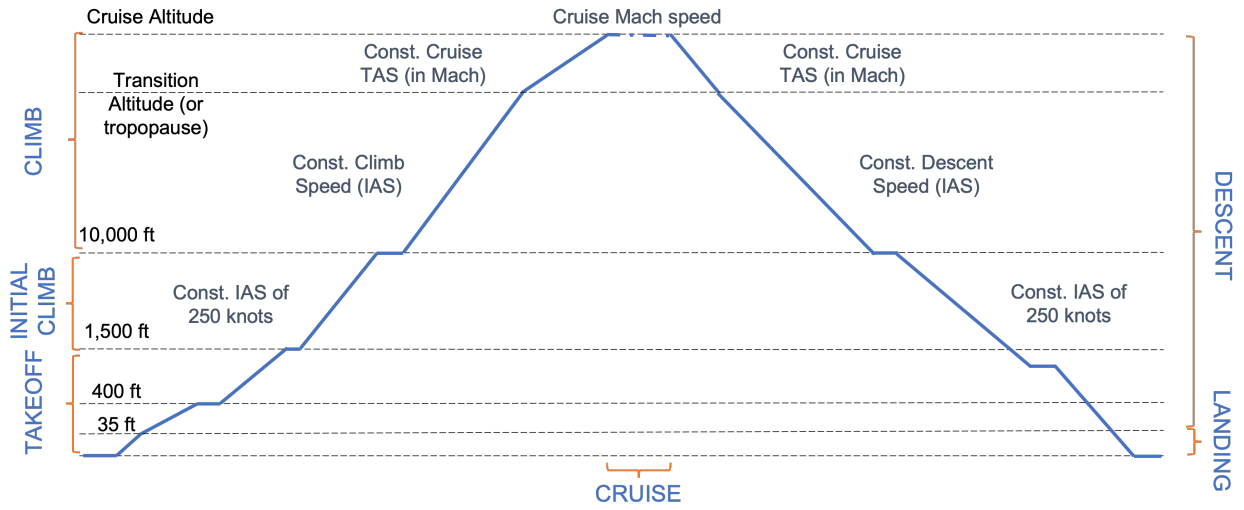

Figure 3.7. Mission profile for the sizing mission

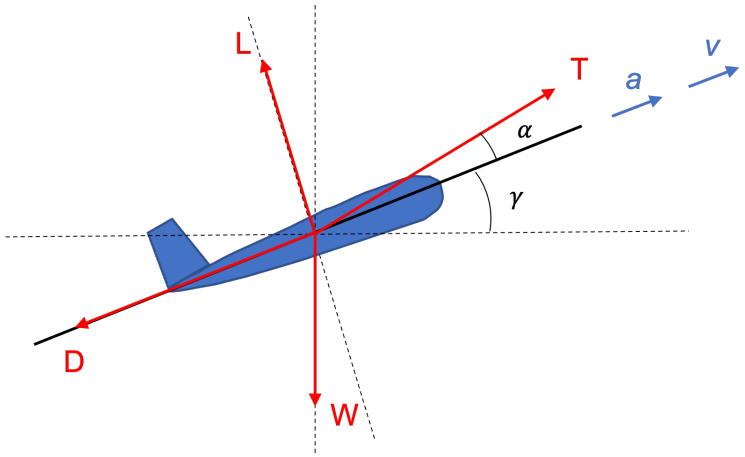

Figure 3.8. Aircraft free body diagram

The takeoff, initial climb, and climb segments use maximum throttle setting for the electric motor (along with sub-segment specific throttle setting for the gas turbine engines) when sizing the hybrid-electric aircraft; for sizing, no electric motor power is available during the cruise, descent, and landing segments.

Takeoff Segment

The takeoff segment is divided into five sub-segments – ground roll and takeoff segments 1-4. Ground roll models the acceleration of the aircraft from rest to rotation velocity (1.1 times stall velocity) at maximum throttle setting for the gas turbine engines. Takeoff segment 1 models the lift-off and climb to the obstacle height of 35 ft (with acceleration) using maximum throttle setting for the gas turbine engines. The climb angle is a product of the rotation rate and the time elapsed. Takeoff segment 2 models the climb from 35 ft to 400 ft at steady speed using maximum throttle setting for the gas turbine engines. Similar to takeoff segment 2, takeoff segment 3 models the acceleration of the aircraft at a constant altitude of 400 ft to 1.25 times stall velocity. Takeoff segment 4 models the climb from 400 ft to 1,500 ft at steady speed using maximum continuous thrust throttle setting for the gas turbine engines. Figure 3.9 provides detailed modeling information about the takeoff segment.

Takeoff Balanced Field Length: The takeoff balanced field length is the total takeoff distance when the accelerate-stop distance required is equal to the takeoff distance required. Both the accelerate-stop distance and the takeoff distance are dependent on the decision speed, *V1*, which is the speed at which if there is an engine failure, the aircraft can either brake to a halt or continue with the takeoff using the same distance. The accelerate-stop distance is modeled in three steps – 1) ground roll until *V1* speed, 2) engine failure at *V1* speed followed by pilot reaction time, and 3) ground roll with braking using the remaining engine(s) until the aircraft stops. The takeoff distance or accelerate-go distance is modeled in four steps – 1) ground roll until *V1* speed, 2) engine failure at *V1* speed followed by pilot reaction time, 3) ground roll using the remaining engine(s) until the aircraft reaches takeoff safety speed (1.15 times stall velocity), and 4) rotate, transition and climb to obstacle height of 35 ft using the remaining engine(s). The accelerate-stop and accelerate-go distances are

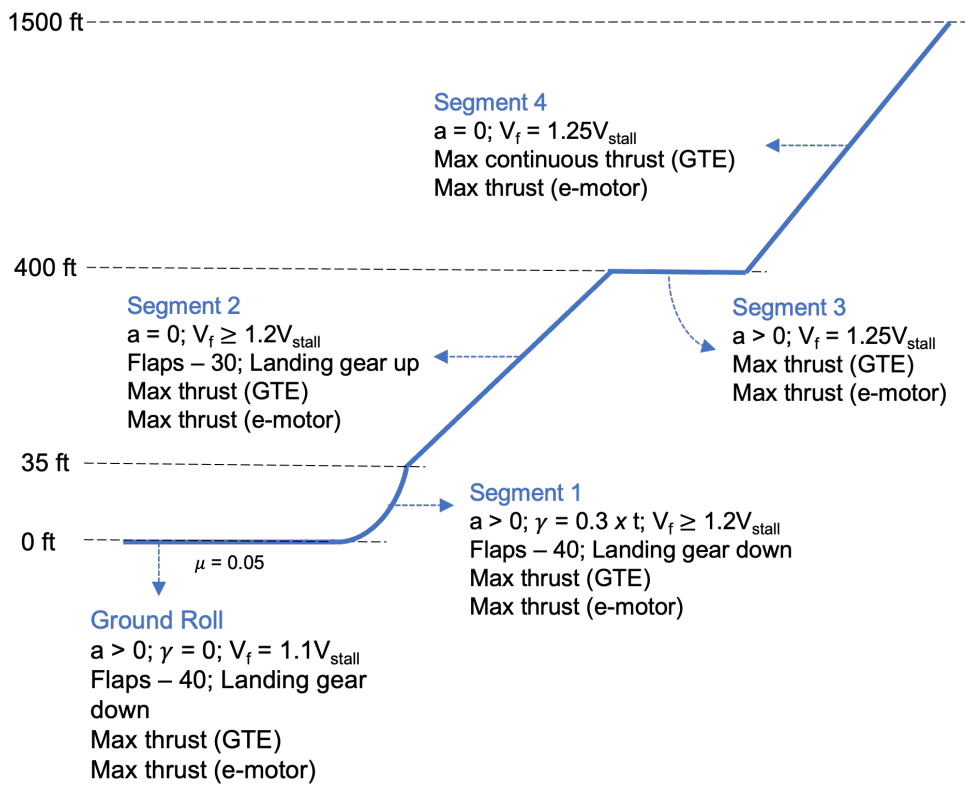

Figure 3.9. Detailed standard mission profile and modeling information for the takeoff segment

calculated for a range of *V1* values and the value that leads to the same accelerate-stop and accelerate-go distance is chosen as the decision speed, *V1*. The takeoff balanced field length is the field length at the determined decision speed, *V1*.

One-Engine-Inoperative (OEI) Condition: The OEI condition is modeled as a part of the takeoff segment. In this work, losing an engine signifies that the engine's fan is no longer working, which means that neither the gas turbine engine core, nor the electric motors attached to the failed engine can contribute to any thrust. The aircraft accelerates from rest to the decision speed, *V1*, on the ground with all engines operating, with an engine failure occurring just after reaching the *V1* speed; the *V1* velocity is calculated as a part of the balanced takeoff field length calculations. The reaction time for the pilot is assumed to be 3 seconds, following which the aircraft accelerates to the takeoff safety speed using the remaining engine(s) only. FAR Part 25 rules mandate that an aircraft reaches *V2* velocity

(1.2 times stall velocity) at or before 35 ft. This condition is implemented using a uni-variate bounded optimization problem – the problem solves for the optimum aircraft rotation rate that minimizes the difference between the aircraft velocity at 35 ft and *V2* velocity. Using the optimum rotation rate, the aircraft climbs from ground level to 35 ft, and then further to 400 ft using the remaining engine(s). In case no rotation rate exists that can allow the aircraft to accelerate to *V2* velocity and climb to 35 ft, or the climb gradient from 35 ft to 400 ft using the remaining engine(s) is less than the required climb gradient of 2.4%, the design fails the third constraint in the sizing optimization problem (Section 3.1.1).

Initial Climb Segment

The FAA requirements limit the Indicated Air Speed (IAS) of all aircraft below 10,000 ft to 250 knots. This segment models the acceleration and climb of the aircraft to 250 knots IAS and 10,000 ft, respectively, taking into consideration the FAA requirements. The segment is divided into two sub-segments. Initial climb segment 1 models the acceleration of the aircraft to 250 knots IAS at a constant altitude of 1,500 ft, using maximum continuous thrust throttle setting for the gas turbine engines. Initial climb segment 2 models the climb from 1,500 ft to 10,0000 ft at a steady speed (250 knots IAS) using maximum continuous thrust throttle setting for the gas turbine engines.

Climb Segment

The climb segment models the climb of the aircraft from 10,000 ft to cruising altitude. The climb segments constitutes of three sub-segments – climb segments 1-3. Climb segment 1 models the acceleration of the aircraft to the chosen climb speed (V_{climb}) at a constant altitude of 10,000 ft, using maximum continuous thrust throttle setting for the gas turbine engines. The climb speed is set to 280 knots IAS for the standard mission. Climb segment 2 models the climb from 10,000 ft to the Mach transition altitude or the tropopause (whichever is lower) at steady V_{climb} speed (280 knots IAS for standard mission) using maximum continuous thrust throttle setting for the gas turbine engines. Above 10,000 ft, the difference between the aircraft's IAS and True Air Speed (TAS) becomes significant. This means that even

though the aircraft climbs from 10,000 ft at a constant IAS, the aircraft's TAS is increasing (acceleration is greater than zero). The acceleration for such a flight phase is calculated based on the difference in the TAS at the current altitude and the TAS at the previous known altitude. The Mach transition altitude is the altitude at which the climb speed in TAS is equivalent to the cruise Mach number. Once the aircraft reaches the Mach transition altitude or the tropopause (36,089 ft) – whichever comes earlier – the aircraft climbs to cruising altitude at a constant TAS equivalent to the cruise Mach speed (while the IAS starts to decrease). This final climb to the cruising altitude is modeled under climb segment 3. In case the aircraft hits the cruising altitude before reaching the Mach transition altitude, the aircraft accelerates to the cruise Mach speed at the constant cruising altitude using maximum continuous thrust throttle setting for the gas turbine engines. Figure 3.10 provides detailed modeling information about the initial climb and climb segments.

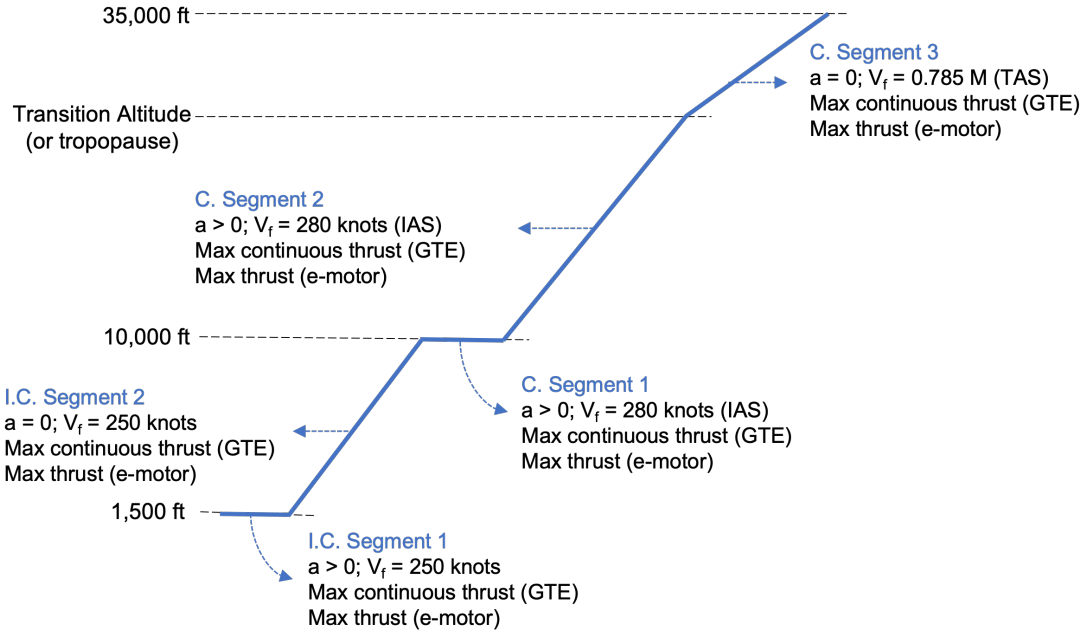

Figure 3.10. Detailed standard mission profile and modeling information for the initial climb (denoted by I.C.) and climb (denoted by C.) segments

Cruise and Service Ceilings: The cruise and service ceiling calculations work as constraints for the sizing optimization problem (refer to Section 3.1.1). The cruise ceiling is the altitude at which the rate of climb of the aircraft is 300 ft/min, while the service ceiling is

the altitude at which the rate of climb of the aircraft is 100 ft/min. Both the calculations use climb segments 1 to 3 with maximum thrust throttle setting for the gas turbine engines and the electric motors. In case the aircraft cannot meet the cruise and service ceiling thresholds, the design fails the fourth and the fifth constraint in the sizing optimization problem.

Cruise Segment

The cruise segment models a steady level flight, i.e., cruising at a constant Mach number (no acceleration) at a constant altitude. For a standard mission, the cruise Mach number is set to 0.785 M and the cruise altitude is set to 35,000 ft. This work does not consider a cruise-climb condition where the aircraft keeps climbing as it gets lighter during cruise. Using the condition that the thrust required is equivalent to the drag during cruise, the throttle setting for the gas turbine engines is back-calculated. There exists a constraint in the sizing optimization problem (refer to Section 3.1.1) to ensure that the gas turbine engines can provide the required thrust during cruise even after downsizing; the constraint checks that the throttle position for the gas turbine engines does not exceed maximum continuous thrust throttle position (considered as power code of 47) at top-of-climb (beginning of cruise).

Descent Segment

The descent segment is split into six sub-segments – descent segments 1-6. Descent segment 1 models the descent at constant TAS (equivalent to the cruise Mach number) from cruising altitude to the altitude at which the IAS becomes equivalent to the descent speed, $V_{descent}$ (IAS increases as the aircraft descends at constant TAS). $V_{descent}$ is set to 280 knots IAS for the standard mission. Descent segment 2 models the descent of the aircraft to 10,000 ft at constant $V_{descent}$ IAS. The aircraft's TAS decreases to maintain a constant IAS, and the deceleration is calculated based on the difference in the TAS at the current altitude and the TAS at the previous known altitude. Descent segment 3 models the deceleration of the aircraft from $V_{descent}$ IAS to 250 knots IAS at a constant altitude of 10,000 ft to meet the FAA speed limit requirements under 10,000 ft. Descent segment 4 models the descend from 10,000 ft to 1,000 ft at a constant IAS of 250 knots. Descent segment 5 models the

deceleration of the aircraft from 250 knots to approach velocity (1.3 times stall velocity) at a constant altitude of 1,000 ft. Finally, descent segment 6 models the descent from 1,000 ft to the obstacle height of 50 ft at a steady speed (approach velocity). All the six sub-segments in the descent segment use idle thrust throttle setting for the gas turbine engines. Figure 3.11 provides detailed modeling information about the descent segment.

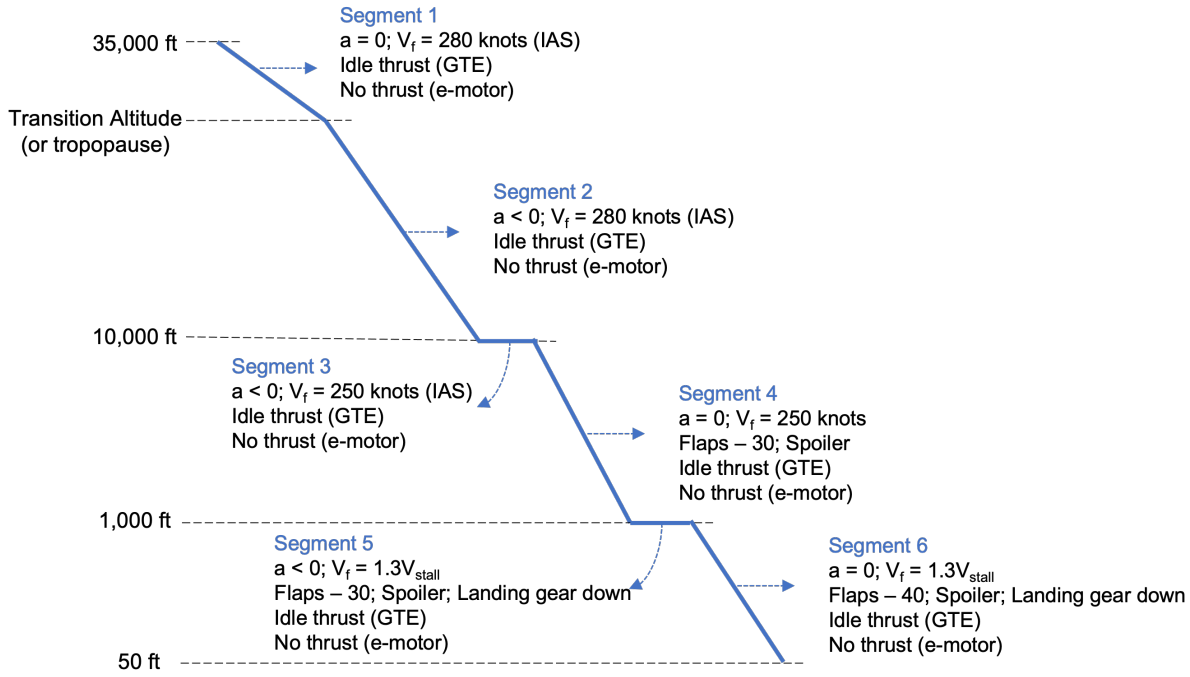

Figure 3.11. Detailed standard mission profile and modeling information for the descent segment

Landing Segment

The landing segment consists of three sub-segments – approach, flare, and ground roll. Approach models the descent of the aircraft from the obstacle height of 50 ft to flare height at constant approach velocity. The flare height is calculated using the approach presented in chapter 17 of Raymer's book [91]. Using a preset descent angle of 3 degrees, the throttle setting for the gas turbine engines is back-calculated. Flare models the deceleration of the aircraft from approach velocity to touchdown velocity (1.15 times stall velocity). Ground roll models the deceleration of the aircraft from touchdown velocity to rest at idle throttle setting

for the gas turbine engines (includes a free roll phase of two seconds after touchdown). The coefficient of friction for the runway is set to 0.5 to include the braking effect; the impact of thrust reversers is not directly modeled. The landing balanced field length is calculated based on the approach presented in Raymer [91] (1.666 times the sum of approach, flare, free roll, and ground roll distances).

Reserve Segment

This work does not model the reserve segment directly, rather it uses an estimate provided by Lammen et al. [94]. The reserve fuel estimate is based on IACO's Annex 6 Operation of Aircraft [95] and is set to a constant value of 3968.28 lbs (1.8 metric tonnes) accounting for alternate, contingency and reserve missions. This work did not include batteries for the reserve segment because the operating mission would need to carry the batteries needed for the missed approach climb out, but not use them in nearly all cases. Since the reserve segment would only be used at the end of a normal operation, carrying fuel for this is the lightest way to meet a reserve requirement. Again, a "typical" mission would not burn this, so it would not contribute to CO_2 emissions for a normal operation.

Taxi Segment

The taxi segment is modeled using a taxi-out time of 10 minutes and a taxi-in time of 10 minutes. This work does not consider an onboard electric taxi system (ETS) because of the weight penalty (electric motors on the landing gear) and thermal management issues at the landing gear associated with them. Additionally, ETS is only beneficial if the taxi-in and taxi-out time is greater than 5 minutes each as the gas turbine engines need 5 minutes to warm-up and cooldown [96]. Also, this work does not consider electric taxiing using gas turbine engines running on batteries during aircraft sizing. The tool can be easily adapted to include onboard ETS or electric taxiing using batteries as a part of the sizing problem. Another way to study the impact of electric taxiing using batteries on mission fuel burn could be to consider electric taxiing as a part of the energy management tool presented in

Section 3.3, where the sized aircraft with the onboard battery pack uses batteries for taxi-out first.

Climb Optimizer – Best Climb Speed

The climb optimizer is a feature modeled as a part of the hybrid-electric aircraft sizing tool. This feature determines the optimum climb speed (V^*_{climb}) and climb gas turbine engine throttle settings (th^*_1, th^*_2, th^*_3) for minimum fuel-to-climb or minimum time-to-climb conditions. The climb optimization problem is set up as an unconstrained bounded minimization problem with climb fuel or climb time as the objective function. The aircraft climbs from 10,000 ft to cruise ceiling while calculating the fuel burnt and time consumed using the climb speed and gas turbine engine throttle settings (for climb segments 1-3) as design variables. The climb speed has upper and lower bounds of 260 knots IAS and 300 knots IAS, respectively, while the throttle settings are bounded by the maximum continuous thrust setting and the idle thrust setting.

minimize:

$$W_{Fuel} \text{ or } t_{climb}$$

design variables:

$$V_{climb},\ th_1,\ th_2,\ th_3$$

The fuel burn and time elapsed calculations are based on the three climb sub-segments discussed earlier.

Best Cruise Mach/Best Cruise Altitude (BCM/BCA)

Best Cruise Mach/Best Cruise Altitude (BCM/BCA) is another feature modeled as a part of the hybrid-electric aircraft sizing tool; this feature could act as a continuation to the previously discussed climb optimizer. The goal here is to find the optimum cruise Mach number and cruise altitude that leads to maximum specific air range. The BCM/BCA optimization problem is set up as an unconstrained bounded minimization problem with

specific air range as the objective function, and cruise Mach number and cruise altitude as the design variables.

minimize:

$$-\ SpecificAirRange$$

design variables:

$$M_{cruise},\ Alt_{cruise}$$

The maximum specific air range is dependent on the aircraft weight at the beginning of cruise. This work solves the BCM/BCA optimization problem for different weights as the aircraft climbs from 10,000 ft. To reduce the computational expense, the BCM/BCA calculations are ignored below 25,000 ft.

The aircraft accelerates from 250 knots IAS to V^*_{climb} IAS using th^*_1 gas turbine engine throttle setting, and then climbs to 25,000 ft at constant V^*_{climb} IAS using th^*_2 gas turbine engine throttle setting. As the aircraft climbs above 25,000 ft, for the current weight and altitude, the BCM/BCA solver finds the optimum Mach number and cruise altitude that maximizes the specific air range of the aircraft. If the difference between the calculated optimum cruise altitude (Alt^*_{cruise}) and the current altitude at which BCM/BCA calculations were performed is less than a threshold value (100 ft in this case), then the calculated M^*_{cruise} and Alt^*_{cruise} values are chosen as the best cruise Mach number and the best cruise altitude. If the difference between Alt^*_{cruise} and the current altitude is higher than the threshold value, then the aircraft climbs to a higher altitude and the BCM/BCA calculations are re-performed. The threshold value governs the computational intensity of the BCM/BCA feature; another intensity control parameter could be the altitudes at which the BCM/BCA calculations are conducted (for example, every 100 ft or 60 seconds after an altitude of 25,000 ft or lower).

Descent Optimizer

The descent optimizer is the third feature modeled as a part of the hybrid-electric aircraft sizing tool. This feature determines the optimum descent angle to allow the aircraft to glide from cruising altitude to 10,000 ft, while reaching 250 knots IAS at 10,000 ft; the throttle

setting for the gas turbine engines is set to idle. The descent optimization problem is set up as an unconstrained bounded minimization problem with an objective function of minimizing the square of the difference between the calculated IAS in knots at 10,000 ft after gliding and 250 knots IAS. The descent angle is the only design variable in the problem, with its value ranging between -4 and -1 degrees.

minimize:

$$(V_{calculated} - 250)^2$$

design variable:

$$\gamma_{descent}$$

After descending to 10,000 ft (while meeting FAA's speed limit of 250 knots IAS at 10,000 ft), the aircraft descends further using descent segments 3-6, followed by landing using the landing sub-segments discussed earlier.

Implementation of Mission Optimizers

The climb, BCM/BCA, and descent optimizers work as inner optimizers with the aircraft sizing optimizer acting as the main or outer optimizer. Figure 3.12 provides a flowchart depicting all three misson optimizers. In case the inner optimizers are unable to find an optimal solution, the mission switches back to the standard mission, hence, making sure that a good, nearly optimal design is not discarded by the main optimizer due to the failure of mission-specific inner optimizers. All three inner optimizers are "switched off" during aircraft sizing (the standard mission is used); they are "switched on" for some cases as a part of the off-design mission calculations, as discussed in Section 3.3.

3.1.2.5 Weight Module

The weight module provides the operating empty weight of the aircraft based on the fuselage dimensions from the geometry module and the size of the propulsion system (considering both the gas turbine engine and the electric motors). This work uses the FLOPS weight

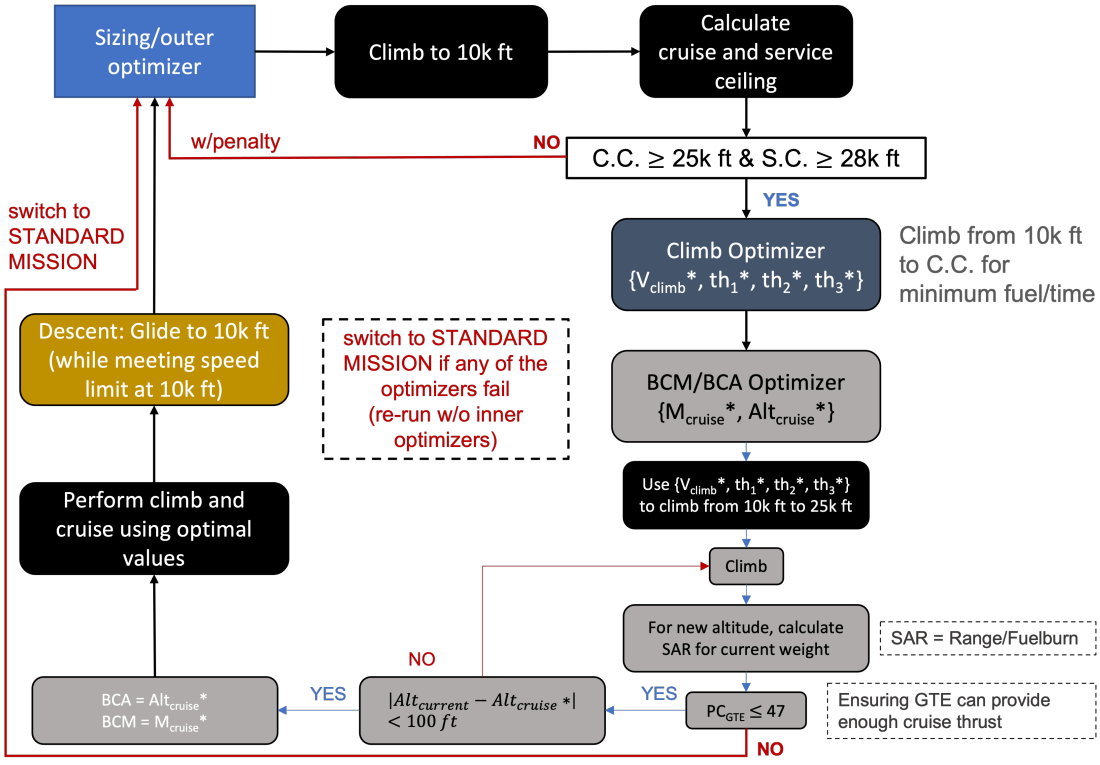

Figure 3.12. Flowchart depicting the three mission optimizers

estimation method [97] to estimate the weight of structural components (including horizontal tail, vertical tail, fuselage, landing gear, nacelles and air induction systems, and paint), propulsion system (including gas turbine engines, thrust reversers, fuel system, tanks, and plumbing), systems and equipment items (including surface controls, auxiliary power unit, instruments, hydraulics, electrical, avionics, furnishings and equipment, air conditioning, and anti-icing), and operating items (including crew and baggage, unusable fuel, engine oil, and passenger service). The weight of the wing (part of the structural components) is estimated using the empirical equation presented in Raymer [91]. These historically-based estimators rely upon a traditional tube-and-wing configuration common for current passenger transport aircraft and assumes predominantly aluminum material.

The propulsion system for a hybrid-electric aircraft has additional components – electric motors, gearbox, wiring, converters, etc. The weight of the electric motors is governed by the power density of the electric motors; the power density is the quantity of power that a motor can output per unit volume – essentially a power-to-mass ratio with units kW/lb. The

weight of the gearbox for connecting the electric motor to the gas turbine engine is based on the WATE tool [98]. The WATE tool uses a PW 1000G engine to estimate the gearbox weight, because it is the only geared turbofan engine whose data is publicly available. With the unavailability of other simple approaches for gearbox weight estimation, this work uses the power-to-weight ratio of the PW1000G gearbox (30,000 hp/250 lbs [99]) to estimate the weight of the gearbox. Additionally, 500 lbs of miscellaneous weight is added to the propulsion system to account for the thermal management system, wiring, converters, etc.

For the single-aisle aircraft considered in this work, the passenger weight and crew weight is considered to be 200 lbs per person (including luggage). This work uses an additional weight margin of 5% on the non-operating components (structural components, the propulsion system, and the systems and equipment items) to take into account the uncertainty associated with estimating the operating empty weight using semi-empirical equations.

3.1.3 Tool Validation

The described sizing tool is validated using an existing conventional all fuel-burning aircraft – Boeing 737-800; this approach of validating with an existing aircraft is common in other studies of hybrid-electric aircraft. Figure 3.13 compares the payload-range chart for the aircraft sized using the presented sizing tool with the publicly available payload-range chart of the Boeing 737-800 aircraft [100]. The error percentage ranges between $\pm 5\%$ across the payload-range chart, which seems pretty reasonable given the fidelity of the presented sizing tool. The author believes that the error margin could reduce further if the presented sizing tool considered cruise-climb during the cruise segment as the Boeing 737-800 aircraft usually uses cruise-climb to reduce fuel burn on longer missions than the sizing code predicts.

3.2 Hybrid-Electric Aircraft Sizing

This work considers a single-aisle parallel hybrid-electric aircraft with a design range of 900 nmi. For sizing the aircraft, the aerodynamic parameters of the wing are governed by the chosen airfoil, which in the current work is a NACA 23012 airfoil. The airfoil design lift

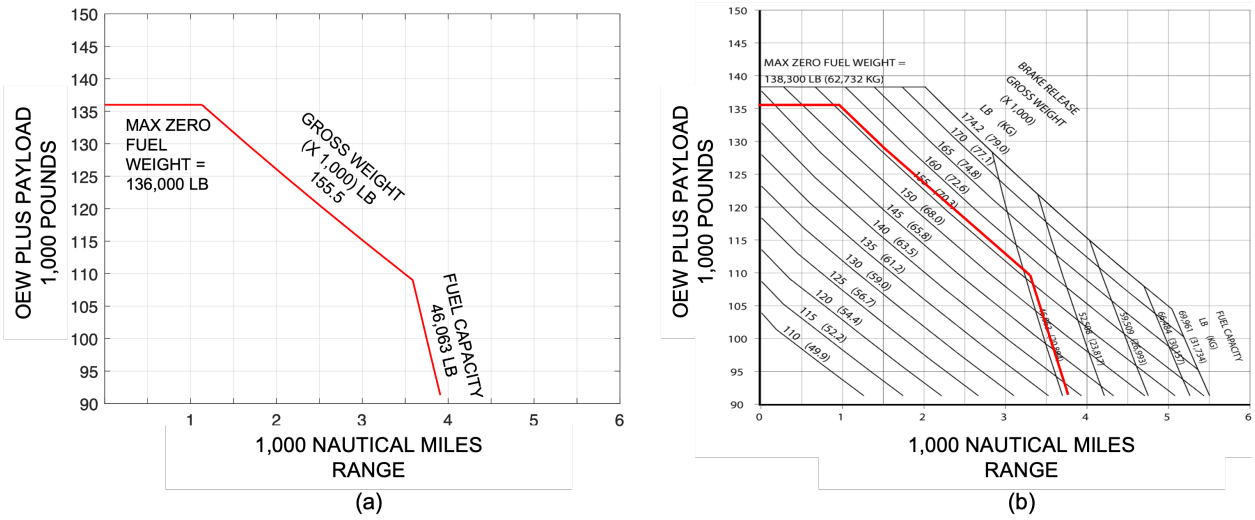

Figure 3.13. Comparison of payload-range charts – (a) Boeing 737-800 sized using the presented sizing tool, (b) actual Boeing 737-800 aircraft data [100]

coefficient, design angle of attack, and the lift curve slope are based on the NACA 23012 airfoil, and the wing zero-lift angle of attack and wing lift curve slope are calculated using the airfoil values as per the discussion in Section 3.1.2.3. The wing taper ratio is not included as a part of the problem design variables because the aerodynamic and weight prediction fidelity do not capture the effect of taper adequately, and is set to Boeing 737-800's known value, i.e., 0.2012. Similarly, the values for the horizontal and vertical tail sweep are set to 33.4 deg and 39.4 deg, respectively, and the values for the horizontal and vertical tail thickness-to-chord ratio are set to 0.109 and 0.06, respectively, based on the Boeing 737-800 aircraft. The propulsion system consists of two gas turbine engines (turbofans) with electric motors connected to their LPT shaft. Given the uncertainty associated with predictions for future battery and electric motor characteristics, this work considers four different battery and electric motor technology cases with low, medium, high, and very high uncertainties (or risk) for year 2035. The battery and electric motor technology cases are discussed in Section 3.2.1.

The aircraft can carry 185 passengers in a single-class all-economy configuration, with two pilots and three crew members onboard the aircraft. For the aircraft sizing, the design mission is based on the standard mission discussed in Section 3.1.2.4; i.e., a climb speed of

280 knots, a cruise speed of 0.785 M, a cruise altitude of 35,000 ft, and descent speed of 280 knots. The taxi time is set to 20 minutes and the current results do not consider electric taxiing. As mentioned before, for cases where the sizing tool optimizer cannot complete the mission for a given combination of design variables, the optimizer uses a backup mission (to ensure that the search for an optimal set of aircraft design variables can continue, even if the mission analysis would not close for the hybrid-electric aircraft). The backup mission for the current sizing runs is a 1,900 nmi design mission using a conventional (all fuel-burning) single-aisle aircraft that is sized similar to a Boeing 737-800 aircraft.

The following points summarize the design and operation assumptions made while sizing the hybrid-electric aircraft:

- Hybrid-electric propulsion is only used during takeoff, initial climb, and climb segments, with the electric motors set to full throttle
- Batteries can only be charged at the gate; no in-flight charging is considered
- Batteries can only be discharged to the maximum discharge limit to maintain safety
- Battery packs are embedded in the fuselage and cannot be altered for daily operations, i.e., it is not possible to add or remove a battery pack from the fuselage before a flight
- Aircraft is required to meet the one-engine-inoperative condition using a single propulsor, i.e., one gas turbine engine with the associated electric motors
- Reserve segment is conducted using fuel only; no extra batteries are added for the reserve segment
- Changes in the layout of passenger accommodation due to fuselage stretching, i.e., conversion to dual-class cabin, are not considered

3.2.1 Hybrid-Electric Aircraft Cases

This work considers four hybrid-electric propulsion technology cases, categorized by the uncertainty / risk associated with the future battery and electric motor performance predictions. The uncertainty increases from case 1 to case 4, with case 1 having the lowest

uncertainty and case 4 having the highest uncertainty. The current work is agnostic to a specific battery chemistry and uses information from other battery studies to assume the battery gravimetric and volumetric energy densities (how much energy is available in 1 kg and 1L of battery), battery maximum discharge capacity (how much can we safely discharge the battery without affecting its life), and battery efficiency (how much charge can a battery actually hold). Table 3.2 summarizes the four hybrid-electric propulsion technology cases considered in this work.

The battery characteristics for the four cases are adapted from different studies to ensure that this work can explore the impact of the most conservative and the most optimistic battery technology predictions (and all those in between) on aircraft design, analysis, and fleet-level utilization. Case 1 is the low uncertainty case because it uses battery technology that seems to achievable by 2035. The battery gravimetric energy density is set to 500 W-h/kg, based on the Battery500 Consortium goals [101]. The volumetric energy density is assumed to be 700 W-h/L, which seems achievable by 2035 given the current battery technology forecasts. Case 2 is the medium uncertainty case and uses battery gravimetric and volumetric energy densities of 750 W-h/kg and 1200 W-h/L, respectively, adapted from the Boeing SUGAR Volt studies [26]. Case 3 is the high uncertainty case and uses optimistic values of 1000 W-h/kg and 1300 W-h/L for the battery gravimetric and volumetric energy density, respectively. These values are based on the long-term 20 year horizon (starting 2016) provided by Lents et al. [102]. The battery maximum discharge rate and battery efficiency for the first three cases (cases 1, 2, and 3) are assumed to be 90% and 96%, respectively, and are adapted from values used in the single-aisle parallel hybrid-electric study by Lents and Hardin [27]. Case 4 is the very high uncertainty case and uses highly optimistic values of 1500 W-h/kg and 1700 W-h/L for battery gravimetric and volumetric energy density, respectively. These battery energy density values are adapted from the 2035 battery technology expectations provided by Zamboni [103], and could only be achieved by highly advanced Metal-Air (or similar) batteries. The battery maximum discharge rate and battery efficiency for case 4 are assumed to be 95% and 97%, respectively.

With limited information available about future high power density electric motors, this work assumes that cases 1, 2, and 3 have the same electric motor characteristics. These

characteristics are based on the NASA Motor NRA results summarized in a recent study by Lents and Hardin [27]; the electric motor power density is 6.8 kW/lb and the motor efficiency is 97%. Case 4 assumes highly optimistic values for the electric motor characteristics with a power density of 9 kW/lb and an efficiency of 99%. The performance characteristics of future superconducting electric motors with cryogenic cooling could match these values as they are expected to showcase power densities close to 11 kW/lb (25 kW/kg) in the next 15-20 years.

The efficiency of the power management and distribution (PMAD) system in the form of inverters, converters and cables, is assumed to be 98% for cases 1, 2, and 3, and 99% for case 4. Current modeling assumes that a gearbox is required to connect the electric motor to the gas turbine engine's LPT shaft. The transmission efficiency for the gearbox is assumed to be 95% for cases 1, 2, and 3, and 97% for case 4.

Table 3.2. Hybrid-electric aircraft propulsion technology cases considered in this work

Parameters		Case 1	Case 2	Case 3	Case 4
Battery	Gravimetric Energy Density [W-h/kg]	500	750	1000	1500
	Volumetric Energy Density [W-h/L]	700	1200	1300	1700
	Max Battery Discharge	90%	90%	90%	95%
	Efficiency (η_{batt})	96%	96%	96%	97%
Electric Motor	Power Density [kW/lb]	6.80	6.80	6.80	9.00
	Efficiency (η_{emotor})	97%	97%	97%	99%
PMAD Efficiency (η_{PMAD})		98%	98%	98%	99%
Gearbox Transmission Efficiency (η_{trans})		95%	95%	95%	97%
Risk		Low	Medium	High	Very High

3.2.2 Hybrid-Electric Aircraft Sizing Results

This section presents the hybrid-electric aircraft sizing results considering the four hybrid-electric propulsion technology cases discussed in the previous section. As mentioned in the Section 3.1, resizing / stretching the fuselage to accommodate the required batteries while sizing a hybrid-electric aircraft is important to ensure that there is no reduction in a hybrid-electric aircraft's cargo volume due to the placement of the battery packs. However, a

stretched fuselage would lead to a higher empty weight and a higher parasite drag, both of which contribute to an increase in the propulsive power required to complete the mission, ultimately leading to a higher fuel burn. In such a case, airlines operating a hybrid-electric aircraft might be willing to trade the reduced cargo capacity with lower mission fuel burn. To demonstrate the impact of fuselage resizing / stretching on the conceptual design of a hybrid-electric aircraft, the sizing results presented here consider two options for each hybrid-electric propulsion technology case – 1) without fuselage resizing (denoted by $woFuse$), and 2) with fuselage resizing (denoted by $wFuse$); this leads to a total of eight hybrid-electric aircraft.

Table 3.3 shows the aircraft sizing results for the eight hybrid-electric aircraft, along with a conventional (all fuel-burning) aircraft sized for 900 nmi. These hybrid-electric aircraft results consider that the maximum combined electric motor power available during sizing is limited to 8 MW (the upper bound for the sizing problem design variable, $Pmax_{emotor}$, is set to 8 MW, as shown in Table 3.1). This means that the sizing optimizer can choose any value between 0 MW and 8 MW for the maximum combined electric motor power while sizing the aircraft.

3.2.2.1 Conventional Aircraft vs Hybrid-Electric Aircraft

With the current modeling, single-aisle parallel hybrid-electric aircraft lead to fuel savings ranging between 2.7% and 9.3%, compared to a conventional aircraft sized for the same mission. As expected, the more optimistic hybrid-electric propulsion technology cases lead to higher fuel savings, and the $woFuse$ option leads to higher fuel savings compared to the $wFuse$ option. The second last row in Table 3.3 (Δ Fuel) provides the exact fuel savings for each hybrid-electric aircraft case compared to the conventional aircraft (sized for 900 nmi). When compared to a Boeing 737-800 aircraft operating on a 900 nmi off-design mission, the fuel savings from the hybrid-electric aircraft are much higher. The sized Boeing 737-800 aircraft (sized for a 1,990 nmi mission) consumes approximately 11,563.7 lbs of fuel to fly a 900 nmi mission with the same payload (37,000 lbs) and same reserve fuel (3,968.28 lbs) as all other aircraft considered here. The last row in Table 3.3 (Δ Fuel(B737-800@900nmi))

Table 3.3. Summary of the hybrid-electric aircraft sizing results considering both without fuselage resizing ($woFuse$) and with fuselage resizing ($wFuse$) approaches; electric motors' combined maximum rated power limited to 8 MW

Parameters	No Hybrid-Electric	Case 1		Case 2		Case 3		Case 4	
		woFuse	wFuse	woFuse	wFuse	woFuse	wFuse	woFuse	wFuse
Design Range [nmi]	900	900	900	900	900	900	900	900	900
S_{wing} [ft²]	1241.35	1248.51	1323.74	1200.02	1299.86	1178.71	1215.79	1133.69	1175.18
AR_{wing}	12.00	12.00	12.00	12.00	12.00	12.00	12.00	12.00	12.00
Λ_{wing} [deg]	36.68	36.94	25.31	24.90	25.20	24.27	24.73	19.79	19.99
t/c_{wing}	0.11	0.14	0.14	0.14	0.12	0.12	0.10	0.10	0.10
$Pmax^{SLS}_{GTE}$ [MW]	15.99	13.96	14.60	13.40	13.99	13.21	13.49	13.01	13.22
$Pmax_{emotor}$ [MW]	0.00	8.00	8.00	8.00	8.00	8.00	8.00	7.99	8.00
Fuel Weight [lbs]	10362.32	10117.30	10189.15	9723.84	9834.72	9584.73	9682.37	9402.73	9471.69
Battery Weight [lbs]	0.00	10824.88	10423.05	7023.90	6923.56	5255.48	5249.19	3130.01	3125.25
Battery Volume [ft³]	0.00	123.86	119.26	70.32	69.32	64.76	64.68	44.24	44.17
Reserve Fuel Weight [lbs]	3968.28	3968.28	3968.28	3968.28	3968.28	3968.28	3968.28	3968.28	3968.28
Payload Weight [lbs]	37000	37000	37000	37000	37000	37000	37000	37000	37000
Operating Empty Weight [lbs]	88678.50	89309.68	90493.38	85673.24	89392.33	85947.17	88340.91	84947.23	86491.45
Takeoff Gross Weight [lbs]	140009.10	151220.13	152073.85	143389.26	147118.90	141755.66	144240.74	138448.24	140056.66
Δ Fuel	-	-2.36%	-1.67%	-6.16%	-5.09%	-7.50%	-6.56%	-9.26%	-8.59%
Δ Fuel (B737-800 @ 900nmi)	-13.58%	-15.62%	-15.02%	-18.90%	-17.98%	-20.06%	-19.25%	-21.58%	-21.01%

provides the fuel savings for each hybrid-electric aircraft with respect to the Boeing 737-800 aircraft; the fuel savings range between 15.0% to 21.6%, depending on the hybrid-electric propulsion technology.

All the sized hybrid-electric aircraft choose the upper bound for the combined maximum rated power of all electric motors ($Pmax_{emotor}$) to maximize the fuel burn benefit, i.e., 8MW. The propulsor setup could be visualized as two 2 MW electric motors attached to the LPT shaft of each of the two gas turbine engines, making a total of four electric motors present on the hybrid-electric aircraft. The gas turbine engine core size also reduces as the hybrid-electric propulsion technology improves, saving more fuel. Interestingly, the gas turbine engines for all the hybrid-electric aircraft are sized by the top-of-climb constraint rather

than the one-engine-inoperative constraint. The top-of-climb constraint ensures that the gas turbine engines alone can provide enough thrust for the aircraft to cruise, while making sure that the power code for the engines does not exceed the maximum continuous thrust setting, i.e., 47 (a power code of 50 corresponds to maximum thrust). The sixth constraint presented as a part of the sizing optimization problem represents this feature (refer to Section 3.1.1). The next "almost active" performance constraint for all the hybrid-electric aircraft is the balanced takeoff field length.

As visible in Table 3.3, all the hybrid-electric aircraft choose the upper bound for the wing aspect ratio, i.e., 12. This is an attribute of the low-fidelity nature of the aerodynamics and weights module, wherein the structural impacts of having very high aspect ratio wings cannot be assessed meticulously. The wing area (S_{wing}), wing sweep (Λ_{wing}), and wing thickness-to-chord ratio (t/c_{wing}) reduce as we move from case 1 to case 4, for both $woFuse$ and $wFuse$ options. This is a direct outcome of the hybrid-electric aircraft becoming lighter overall as we utilize higher technology – lighter and more efficient – batteries and electric motors, along with smaller core gas turbine engines.

Comparison with Relevant Aircraft Sizing Study: Comparing the Case 2 hybrid-electric aircraft without fuselage resizing ($woFuse$) with the Boeing SUGAR Volt parallel hybrid-electric aircraft [25], [26] (as it seems to be the most relevant aircraft study available in the literature), we see that the block fuel burn per seat is higher for the Case 2-$woFuse$ aircraft. The SUGAR Volt 'No Shutdown' (Ref Hp 7,150) aircraft has a block fuel per seat value of 32.69 lb while the Case 2-$woFuse$ aircraft presented in Table 3.3 has a block fuel per seat value of 52.56 lb; the author chose to compare the presented aircraft with the 'No Shutdown' version of the SUGAR Volt aircraft because of their similar electric motor rating. This difference in block fuel per seat values is an artifact of the different sizing approaches followed by the two studies under comparison. The sizing approach presented in this work considers gas turbine engine downsizing and OEI condition/constraint for determining the size of the hybrid propulsion system, while using lower-fidelity approaches to model the electric motor-gas turbine engine integration and the aerodynamic characteristics. On the other hand, the SUGAR Volt study uses a higher-fidelity NPSS environment to model an advanced gas turbine engine ($hFan + 2$) and its integration with the electric motors, along

with higher-fidelity aerodynamic analysis to include a much more efficient truss-braced wing configuration [26].

3.2.2.2 Impact of Fuselage Resizing

Comparing hybrid-electric aircraft without fuselage resizing ($woFuse$) and hybrid-electric aircraft with fuselage resizing ($wFuse$) in Table 3.3, it can be seen that the gross takeoff weight for $wFuse$ aircraft is higher, for all four hybrid-electric propulsion technology cases. This is because the stretching of the fuselage to accommodate the battery packs leads to an increase in the weight of the fuselage, which in turn increases the operating empty weight, propulsion system size and weight, and ultimately the fuel required to complete the mission – all contributing to a higher gross takeoff weight. Additionally, due to the drag and weight penalty associated with increasing the length of the fuselage, the optimal battery size (weight and volume) for the $wFuse$ hybrid-electric aircraft is lower than the $woFuse$ hybrid-electric aircraft. This is true for all four cases. Hence, the $wFuse$ hybrid-electric aircraft are less efficient compared to the $woFuse$ hybrid-electric aircraft. Being heavier than the $woFuse$ aircraft, the $wFuse$ aircraft showcase a bigger wing, a higher wing sweep (except for case 1), and gas turbine engines with higher thrust rating.

For case 1, the $wFuse$ hybrid-electric aircraft consumes 71.9 lbs of extra fuel compared to the $woFuse$ aircraft, while saving 123.9 ft^3 of cargo volume by stretching the fuselage to accommodate the batteries (although the cargo volume required by the batteries for $wFuse$ aircraft is 119.3 ft^3, if the fuselage was not resized, the cargo volume required by the batteries would be 123.9 ft^3). For reference, the total cargo volume available in the aircraft without fuselage stretching (based on the baseline CAD model presented in Section 3.1.2.1) is approximately 1,635 ft^3. Hence, the cargo volume required to accommodate the batteries for case 1 is less than 8% of the total cargo volume available in the aircraft. Based on this information, it is possible that airlines might not prefer the $wFuse$ version because that aircraft burns 71.9 lbs of extra fuel per flight while saving only a small percentage of cargo volume (although the extra fuel required by the $wFuse$ aircraft seems small at an aircraft-level, the fleet-level implications could be notable). Similarly, for cases 2, 3, and

4, the $wFuse$ hybrid-electric aircraft consume 110.9 lbs, 97.6 lbs, and 69.0 lbs of extra fuel compared to the $woFuse$ aircraft, while only saving 70.3 ft^3 (4.3%), 64.8 ft^3 (4.0%), and 44.2 ft^3 (2.7%) of cargo volume, respectively. For the fleet-level studies conducted in this work in Chapter 5, the author considers only the $woFuse$ hybrid-electric aircraft; the energy management tool results presented in Section 3.4 also consider the same.

3.2.2.3 Impact of Higher Electric Motor Power

Given that all the eight hybrid-electric aircraft presented in Table 3.3 chose the upper bound (8 MW) for the electric motors' maximum rated combined power ($Pmax_{emotor}$), this section explores what happens if the upper bound for the maximum rated power is raised to 20 MW. Increasing the maximum possible electric motor rated power should allow us to see how much more fuel savings are possible if we have the technology to connect (and fit) more than than two electric motors to the LPT shaft of each gas turbine engine. Table 3.4 summarizes the aircraft sizing results for the eight hybrid-electric aircraft with the electric motors' combined maximum power limited to 20 MW.

The fuel savings increase with an increase in the maximum rated combined power of the electric motors, ranging between 2.0% and 10.3% compared to the conventional aircraft sized for the same mission. Compared to the 8MW hybrid-electric aircraft, we see a fuel savings of at least 35.5 lbs (and a maximum fuel saving of 123.7 lbs) across all cases. The $woFuse$ and $wFuse$ hybrid-electric aircraft show trends similar to those discussed in Section 3.2.2.2. The $woFuse$ hybrid-electric aircraft showcase 20 MW of combined electric motor power for cases 2, 3, and 4, indicating that more fuel savings could be possible if very high power density electric motors become available in the future. As expected, the combined electric motor power for the $wFuse$ aircraft cases is lower than (or equal to) $woFuse$ aircraft cases due to the drag and weight penalty associated with increasing the length of the fuselage. For the $wFuse$ option, only case 4 showcases a combined electric motor power of 20 MW, all other cases showcase lower combined electric motor power. Given the current electric motor technology forecasts, compact electric motors with a power rating greater than 2 MW might not be feasible in the near future. Hence, the possibility of attaching electric motors with a

Table 3.4. Summary of the hybrid-electric aircraft sizing results considering both without fuselage resizing ($woFuse$) and with fuselage resizing ($wFuse$) approaches; electric motors' combined maximum rated power limited to 20 MW

Parameters	No Hybrid-Electric	Case 1		Case 2		Case 3		Case 4	
		woFuse	wFuse	woFuse	wFuse	woFuse	wFuse	woFuse	wFuse
Design Range [nmi]	900	900	900	900	900	900	900	900	900
S_{wing} [ft^2]	1241.35	1250.02	1292.16	1195.85	1208.81	1152.57	1190.00	1121.55	1169.93
AR_{wing}	12.00	12.00	12.00	12.00	12.00	12.00	12.00	12.00	12.00
Λ_{wing} [deg]	36.68	25.52	24.16	24.95	24.87	30.17	24.64	24.81	24.50
t/c_{wing}	0.11	0.15	0.14	0.12	0.14	0.12	0.12	0.11	0.13
$Pmax^{SLS}_{GTE}$ [MW]	15.99	14.05	14.04	13.91	14.06	13.69	13.76	13.30	13.40
$Pmax_{emotor}$ [MW]	0.00	12.00	9.15	20.00	18.88	20.00	18.92	20.00	20.00
Fuel Weight [lbs]	10362.32	10040.77	10153.67	9628.34	9773.99	9465.94	9558.67	9292.16	9350.04
Battery Weight [lbs]	0.00	13264.96	11775.01	10674.20	10472.01	7880.07	7781.06	4653.55	4644.09
Battery Volume [ft^3]	0.00	151.77	134.73	106.87	104.84	97.10	95.88	65.77	65.64
Reserve Fuel Weight [lbs]	3968.28	3968.28	3968.28	3968.28	3968.28	3968.28	3968.28	3968.28	3968.28
Payload Weight [lbs]	37000	37000	37000	37000	37000	37000	37000	37000	37000
Operating Empty Weight [lbs]	88678.50	88537.19	90338.55	89733.05	90345.88	89316.82	90327.77	87163.62	87275.03
Takeoff Gross Weight [lbs]	140009.10	152811.20	153235.51	151003.88	151560.16	147631.12	148635.77	142077.61	142237.44
Δ Fuel	-	-3.10%	-2.01%	-7.08%	-5.68%	-8.65%	-7.76%	-10.33%	-9.77%
Δ Fuel (B737-800 @ 900nmi)	-13.58%	-16.26%	-15.32%	-19.70%	-18.48%	-21.05%	-20.28%	-22.50%	-22.02%

combined power rating greater than 4 MW to the LPT shaft of a gas turbine engine is very low, making the installation of 20 MW rated electric motors on an aircraft (10 MW combined power electric motors on each gas turbine engine LPT shaft) infeasible. The author uses this reasoning to consider only 8 MW hybrid-electric aircraft for all the energy management / aircraft performance and fleet-level studies presented in this work.

3.2.2.4 Maximum Hybrid-Electric Aircraft Range

As the design range of the hybrid-electric aircraft increases, the size of the electric motors (and hence the size of the hybrid portion of the propulsion system) will start to reduce. As

the aircraft flies a longer mission, it needs to carry more fuel for the cruise segment. To compensate for the added fuel weight, the longer-range aircraft would like to reduce the "dead" weight, i.e., battery weight, to reduce fuel consumption over the mission, compared to a hybrid-electric aircraft sized for a shorter design range. The battery weight is directly reduced by reducing the combined maximum rated power of all electric motors ($Pmax_{emotor}$). There should exist a sweet-spot for the amount of electric power augmentation (for takeoff, initial climb, and climb segments) required by the aircraft so that it can minimize the mission fuel burn, even while carrying some "dead" weight for the longer mission; the sizing optimization problem should be able to capture this tradeoff. However, there will be a design range where the aircraft will not be able to carry any batteries to minimize the fuel burn, leading to a conventional (all fuel-burning) aircraft ($Pmax_{emotor}$=0). This design range will be the maximum range for the hybrid-electric aircraft in consideration. The maximum design range will vary with hybrid-electric propulsion technology, with case 1 showcasing the lowest maximum design range and case 4 showcasing the highest maximum design range.

Table 3.5 summarizes the case 1 $woFuse$ hybrid-electric aircraft characteristics as we increase the design range (in unequal intervals) from 900 nmi to 1,800 nmi. The maximum hybrid-electric aircraft range for a case 1 $woFuse$ aircraft is approximately 1,800 nmi because the combined maximum rated power of all electric motors is almost zero (the value of $Pmax_{emotor}$ is actually 0.001 MW, which is why the battery weight and volume are slightly greater than zero). These results show that the electric system's contribution to the total power required by the aircraft (during takeoff, initial climb, and climb) will reduce if we increase the design range of the hybrid-electric aircraft, reducing the overall fuel burn benefit possible from a hybrid-electric propulsion system.

3.2.3 Optimization Algorithm Selection

The aircraft sizing optimization problem is a single-objective constrained nonlinear programming problem with continuous design variables (refer to Section 3.1.1 for more details). The sizing tool is set up in MATLAB and is adapted to use both gradient-based solvers, like Sequential Quadratic Programming (SQP), and non gradient-based solvers, like Nelder-Mead

Table 3.5. Summary of the hybrid-electric aircraft characteristics considering higher design ranges – for case 1 without fuselage resizing ($woFuse$); electric motors' combined maximum rated power limited to 8 MW

Case 1 – *woFuse* Parameters	Design Range [nmi]					
	900	1200	1500	1650	1750	1800
$Pmax_{emotor}$ [MW]	8.00	6.63	4.58	2.08	0.51	0.00
$Pmax^{SLS}_{GTE}$ [MW]	13.96	14.77	15.33	16.55	16.69	16.10
Fuel Weight [lbs]	10117.30	13278.09	16506.32	18207.74	19240.88	19657.843
Battery Weight [lbs]	10824.88	9519.65	7372.77	3532.12	1004.84	2.43
Battery Volume [ft³]	123.86	108.92	84.36	40.41	11.50	0.03

Simplex. The sizing results presented in Section 3.2.2 use the non gradient-based Nelder-Mead Simplex solver – implemented using a MATLAB package, `fminsearchcon` [104] – to find the optimal solution to the sizing problem at hand. Given the way the sizing optimization problem is set up as an SAND formulation, the Nelder-Mead Simplex solver seems to perform better than the gradient-based SQP solver.

Initially, the author used the gradient-based SQP solver, `fmincon`, to solve the sizing optimization problem. However, the SQP solver took too many function evaluations to find a sub-optimal solution with a MATLAB exitflag of 2 (the change in design variables was less than the step size tolerance and maximum constraint violation was less than the constraint tolerance); an exitflag of 1 is desirable in MATLAB because it indicates meeting first-order optimality conditions. On closer inspection, the problem had some scaling issues with respect to the objective function and the constraints. To remedy this issue, the author scaled the objective function by dividing it by a large number ($obj_{updated} = obj/20000$), wherein the large number was arbitrarily chosen based on some trial-and-error runs. Resolving the scaling issue reduced the number of function evaluations required by SQP to reach a solution, however, the solution was still sub-optimal as the exitflag did not change from 2. On further inspecting the solution obtained from SQP after fixing the scaling issue, the author noted that the Hessian matrix of the objective function had at least one eigenvalue that very close to zero (on the order of 10^{-10}). This indicated that the Hessian matrix was not positive-definite, causing

the SQP solver to have problems with the final search steps. This issue was noted with all the hybrid-electric aircraft sizing runs (with many different starting points) and might be due to the battery and fuel weight constraints that obviate the sizing code iterations.

While searching for an approach to fix the issues faced by the SQP solver for the sizing problem at hand, the author found multiple studies in the literature that indirectly point to a similar issue. In most of these studies, the authors either developed their own methods to efficiently calculate gradients or modify SQP, or used non gradient-based solvers like Nelder-Mead Simplex or Genetic Algorithms. Brejle and Martins [42] developed an aircraft design tool with efficient gradients; the authors use analytic gradients to enable the use of OpenMDAO 2's Newton solvers and combine it with gradient-based optimization to solve conceptual design problems for aircraft with unconventional propulsion architectures. The SUAVE [105] aircraft conceptual design and optimization tool uses a gradient-based solver SNOPT [106]; SNOPT is a software for large-scale linear and quadratic programming and essentially uses a modified SQP algorithm to solve aircraft design optimization problems. The Program for Aircraft Synthesis Studies (PASS) [107] – an aircraft preliminary design tool created by Desktop Aeronautics, Inc. – used non gradient-based approaches like Genetic Algorithms and Nelder-Mead Simplex methods to conduct aircraft conceptual design studies, with the argument that the design space at the conceptual design stage is often noisy and ill behaved, making it hard to use traditional gradient-based solvers [108], [109]. Since solver development was out of scope for this work, the author chose to use the non gradient-based Nelder-Mead Simplex solver to solve the sizing optimization problem at hand.

Nelder-Mead Simplex solver usually works well for problems that cannot be easily solved by gradient-based solvers. However, the Nelder-Mead Simplex solver is not a global solver and requires a feasible starting point to begin the search for the optimal solution. Being independent of the objective and constraint function gradients and Hessians, the Nelder-Mead Simplex solver is able to tackle the problems faced by the SQP solver with the final search steps using direct random searches. This comes at the expense of more computational time as the Nelder-Mead Simplex solver requires more function evaluations to find the optimal solution. Since the author had the sub-optimal solutions from SQP available for all the hybrid-electric aircraft considered in this work, the author used them as the starting

point for the Nelder-Mead Simplex solver. The final sizing results (presented in Section 3.2.2) showed a MATLAB exitflag of 1 (using `fminsearchcon` [104]), which signifies that the function converged to an optimal solution while satisfying all constraints (`fminsearchcon` employs a post-processing assessment of the Kuhn-Tucker conditions to ensure optimality).

3.3 Hybrid-Electric Aircraft Energy Management Tool

The hybrid-electric aircraft sized using the "flight-mechanics-based" sizing tool is based on the sizing rule that the electric motors operate at full throttle during the takeoff, initial climb, and climb segments. This means that the installed battery in the sized aircraft is just enough to ensure that all the battery energy is consumed (to safety limits) at top-of-climb, provided the electric motors are operated at full throttle (until the beginning of the cruise segment) and the aircraft is flying for 900 nmi at 100% load factor. However, when these aircraft will be introduced as part of airline fleets for daily operations, they will rarely be operated at their design mission. Most of the airline operations will include off-design missions, i.e., operating at different route lengths and at various load factors (depending on demand and frequency of service for a given city-pair).

For off-design missions, changing the usage of the installed battery energy, i.e., choosing when and how much battery power should be used during the mission, has the potential to lead to lower overall mission fuel burn. There are two main reasons for this preferable outcome — 1) aircraft weight reduces when fuel is burned but stays constant when battery energy is utilized to provide propulsive power – a reduction in aircraft weight leads to lower propulsive power requirement for the remaining flight segments, which means that an optimal combination of fuel burn and battery energy consumption could lead to lower overall mission fuel burn, and 2) when the aircraft is flown at a lower payload, or for a lower range (or both), the battery energy required to assist the gas turbine engine during takeoff and climb (to the cruising altitude) could be lower than the total battery energy onboard the sized aircraft (because the aircraft is lighter due to lower payload, or due to lower amount of fuel in the fuel tanks considering a shorter mission, or both), which means that an optimal battery energy management scheme could lead to better utilization of the battery across all flight segments

to minimize overall fuel burn. Additionally, combining the energy management scheme with an optimal flight path for the off-design mission could lead to even further reductions in the overall mission fuel burn. Determining an optimal flight path for the sized aircraft includes identifying the optimal climb, cruise, and descent speeds, along with the optimal cruising altitude, for different payload-range combinations.

An optimal energy management for the fuel and battery energy onboard a hybrid-electric aircraft – operating at an off-design mission – can be achieved by optimizing the power split between the two propulsion sources, i.e., the gas turbine engine and the electric motor, while they compete to meet the aircraft thrust requirements. Since batteries essentially count as "dead weight" that is carried by an aircraft on its mission because they do not decrease in weight as they discharge, it makes most sense to utilize (or discharge) them completely (as per their maximum safe discharge limit) while minimizing the fuel burn over the complete mission. For the parallel hybrid-electric aircraft considered in this work – with electric power augmentation considered only for takeoff, initial climb, and climb segments during sizing – this could mean that the optimal power split between the two propulsion sources could allow the aircraft to partially (or fully) cruise using battery energy, if that minimizes the fuel burn over the flight envelope for the off-design mission in consideration.

This section presents an energy management tool – derived from the "flight-mechanics-based" sizing tool (Section 3.1) – to minimize the fuel burn of a hybrid-electric aircraft on an off-design mission by identifying the optimal combination of throttle settings (to control the power split) for the gas turbine engines and the electric motors during takeoff, initial climb, climb, and cruise. The tool is set up with an optimization problem at its core that minimizes the overall mission fuel burn and forces the aircraft to completely discharge the batteries (to their safety limit) during the mission to gain maximum fuel burn benefit. The optimal gas turbine engine and electric motor throttle settings showcase an optimal energy management scheme that resonates with how the airlines might end up flying these aircraft as a part of their daily operations (focusing on profitability in operation / minimum fuel cost for every mission).

The energy management tool can also be integrated with the "flight-mechanics-based" sizing tool presented in this work. The integration, though straightforward in implementa-

tion, will lead to sizing a hybrid-electric aircraft that is highly specialized to "fly" the design mission at 100% load factor. Such an aircraft is expected to perform worse when operating at off-design missions, making it unfavorable for use by airlines. Additionally, the integration will lead to much higher computational costs for sizing the aircraft as the number of design variables for the optimization problem will at least double, which is not ideal for an aircraft conceptual sizing / exploration study.

3.3.1 Optimization Problem Setup

The energy management optimization problem is set up as a single-objective nonlinear programming problem with nonlinear constraints; the problem consists of continuous design variables only. The objective function of the problem is to minimize the mission fuel weight, while satisfying the SAND mission fuel weight constraint (refer to Section 3.1.1 for SAND constraint). The design variables for this problem include the gas turbine engine and electric motor throttle positions for takeoff and climb segments, along with the guessed mission fuel weight. The guessed mission fuel weight acts as both a design variable and a constraint in the problem. The guessed fuel weight value (or takeoff weight) is used to complete the mission performance calculations (using the Mission Module), and the constraint ensures that the difference between the guessed mission fuel weight and the calculated mission fuel weight is less than a specified tolerance. This is different from the sizing problem setup where the difference between the guessed value and the calculated value was set to less than, or equal to, zero. The current setup allows the problem to solve quicker while using a buffer fuel weight set by the tolerance. The SAND approach further leads to a lower number of total function evaluations because it allows the user to get rid of the traditional iterative procedure of guessing the mission fuel weight (or takeoff weight), solving for optimal mission fuel weight, and then using the calculated value as the new guess for the next iteration (if the difference between the calculated and guessed values is greater than the required tolerance).

The current setup assumes that the gas turbine engine and electric motor throttle positions for takeoff ground roll and takeoff segments 1 & 2 (refer to Mission Module in Section 3.1.2.4) are set to maximum to allow the aircraft to takeoff and climb to obstacle height

(and accelerate to safety speed) as quickly as possible. Additionally, the current setup does not consider any battery power utilization during the descent, landing, or reserve segments, which means that the batteries are completely discharged (to their safe discharge limits) by the end of the cruise segment. For combinations of design variables (throttle positions) that prevent the aircraft from climbing (for instance, when the total combined thrust is too low to accelerate and climb for the guessed aircraft fuel weight / takeoff weight), the problem employs a backup mission to obtain a value for the mission fuel weight for the current set of design variables. The objective function in that case is set as the sum of the weight of fuel from the backup mission and a penalty based on the takeoff, initial climb, or climb sub-segment it fails. The backup mission fuel weight is set to be equal to the block fuel of the sized hybrid-electric aircraft, flying 900 nmi at 100% payload.

This work considers two approaches for the energy management tool to minimize the overall mission fuel burn for off-design missions. These approaches differ in terms of implementation of the power split between the two propulsion sources for the cruise segment, with the power split implementation staying the same for the takeoff, initial climb, and climb segments. The optimal flight path identification scheme can be integrated with both the energy management approaches without much modifications.

3.3.1.1 Approach 1: "Rule-based" Cruise

The "rule-based" cruise approach assumes that the electric motor throttle position is set to maximum for the cruise segment. This means that the battery energy remaining after the climb segment is consumed by operating the electric motor at full throttle during cruise until all the onboard batteries are safely discharged. In this optimization problem setup, the design variables consider the throttle positions for the gas turbine engine and the electric motor for takeoff (segment 3 onward), initial climb, and climb segments only. The energy management problem for approach 1 ("rule-based" cruise) is formulated as follows:

minimize:

$$W_{Fuel}$$

subject to:

$$W_{Fuel}^{calculated} - W_{Fuel}^{guess} \leq tol$$
$$W_{Fuel}^{guess} - W_{Fuel}^{calculated} \leq tol$$

design variables:

$$th_{TO_3},\ th_{TO_4},\ th_{iCl_1},\ th_{iCl_2},\ th_{Cl_1},\ th_{Cl_2},\ th_{Cl_3},$$
$$eth_{TO_3},\ eth_{TO_4},\ eth_{iCl_1},\ eth_{iCl_2},\ eth_{Cl_1},\ eth_{Cl_2},\ eth_{Cl_3},\ W_{Fuel}^{guess}$$

where, the first seven design variables represent the throttle position for the gas turbine engine, followed by seven design variables that represent the throttle position for the electric motor, and the last variable that represents the guessed mission fuel weight. Table 3.6 shows the upper and lower bounds for all the design variables. The constraints signify the SAND approach; the value of the fuel weight tolerance, *tol*, is set to 25 lbs to reduce computational runtime. The optimization algorithm employed for solving this problem is the Nelder-Mead Simplex, implemented using a MATLAB package – `fminsearchcon` [104]. The solution of the posed optimization problem will provide the optimal "rule-based" energy management solution – for the route and load factor in consideration – that will lead to minimum overall mission fuel burn (and hence CO_2 emissions).

Table 3.6. Energy management tool: Upper and lower bounds for the "free cruise" energy management design variables

Design Variables	**Lower Bound**	**Upper Bound**
GTE throttle position ($th_{TO}, th_{iCl}, th_{Cl}$)	22	49
E-motor throttle position ($eth_{TO}, eth_{iCl}, eth_{Cl}$)	0.2	0.999
Guess Fuel Weight (W_{Fuel}^{guess}) [lbs]	2,000	W_{Fuel}^{sizing}

3.3.1.2 Approach 2: "Variable Throttle" Cruise

The "variable thottle" cruise approach assumes that the cruise segment has multiple electric motor throttle positions. This allows the optimizer to choose when and how much battery energy to use during the cruise segment to minimize overall fuel burn. This enables the possible tradeoff where the energy management scheme "waits" for aircraft to get lighter during cruise to better use the available battery energy towards the end of the cruise segment.

This scheme could lead to lower overall fuel burn when compared to the "rule-based" cruise approach where the aircraft has to use all the available battery energy when it is the heaviest (segment-wise), i.e., at the beginning of cruise.

The number of electric motor throttle positions available (n) for a given mission depends on the mission length. In the current setup, the mission length is divided by 100 and round-down to the nearest integer to calculate the number of electric motor throttle positions available as design variables in the optimization problem. For instance, a mission length of 300 nmi has three electric motor throttle positions, and a mission length of 900 nmi has nine electric motor throttle positions available as design variables. The gas turbine engine throttle for the cruise segment is back-calculated based on the total thrust required to cruise and the equivalent thrust provided by the electric motor (based on the throttle setting).

Hence, in this optimization problem setup, the design variables consider the throttle positions for the gas turbine engine and the electric motor for the takeoff (segment 3 onward), initial climb, and climb segments, along with electric motor throttle positions for the cruise segment. The energy management problem for approach 2 ("variable throttle" cruise) is formulated as follows:

minimize:

$$W_{Fuel}$$

subject to:

$$W_{Fuel}^{calculated} - W_{Fuel}^{guess} \leq tol$$
$$W_{Fuel}^{guess} - W_{Fuel}^{calculated} \leq tol$$
$$\Delta E_{Batt}^{avail} \leq 0$$

design variables:

$$th_{TO_3},\ th_{TO_4},\ th_{iCl_1},\ th_{iCl_2},\ th_{Cl_1},\ th_{Cl_2},\ th_{Cl_3},$$
$$eth_{TO_3},\ eth_{TO_4},\ eth_{iCl_1},\ eth_{iCl_2},\ eth_{Cl_1},\ eth_{Cl_2},\ eth_{Cl_3},$$
$$eth_{Cr_1}, ..., eth_{Cr_n},\ W_{Fuel}^{guess}$$

where, the first seven design variables represent the throttle position for the gas turbine engine during takeoff, initial climb, and climb, followed by seven design variables that represent the throttle position for the electric motor during takeoff, initial climb, and climb. The next n design variables represent the the throttle position for the electric motor during cruise, and the last variable represents the guessed mission fuel weight. Table 3.7 shows the upper and lower bounds for all the design variables. The first two constraints signify the SAND approach; the value of the fuel weight tolerance, tol, is set to 25 lbs to reduce computational runtime. There is an additional constraint in this problem setup that ensures that the battery energy is completely depleted to safety limits by the end of the cruise segment. The optimization algorithm employed for solving this problem is Genetic Algorithm, implemented using MATLAB's *ga* package [110]. This problem did not use the Nelder-Mead Simplex algorithm because it usually tends to be ineffective for problems with 15 or more design variables [111].

Table 3.7. Energy management tool: Upper and lower bounds for the "variable throttle" energy management design variables

Design Variables	**Lower Bound**	**Upper Bound**
GTE throttle position (th_{TO}, th_{iCl}, th_{Cl})	22	49
E-motor throttle position (eth_{TO}, eth_{iCl}, eth_{Cl})	0.2	0.999
E-motor throttle position (eth_{Cr})	0.0	0.999
Guess Fuel Weight (W_{Fuel}^{guess}) [lbs]	2,000	W_{Fuel}^{sizing}

An important thing to note here is that it is not possible for the aircraft to save all its battery energy for the cruise segment. This is because the hybrid-electric aircraft has downsized gas turbine engines that always need some electric power augmentation to enable the aircraft to takeoff and climb safely, which means that the aircraft cannot climb without expending battery energy. However, there could arise a case where the hybrid-electric aircraft has to fly on a very short route with a low payload. In that case, the aircraft could climb by using the gas turbine engines only and save the battery energy for cruise. However, the author believes that the overall mission fuel burn might still be higher than the option where some battery energy was expended to takeoff and climb because the gas turbine engines will have to operate at near full throttle.

3.4 Hybrid-Electric Aircraft Performance

The performance characteristics of a hybrid-electric aircraft depend on the energy management scheme implemented for the off-design mission. This section presents the hybrid-electric aircraft performance for a sample route considering the different energy management approaches, including "rule-based" cruise energy management, and "variable throttle" cruise energy management. The aircraft performance results showcase the energy management tool's capabilities and the possible benefits of identifying the optimal power split between the gas turbine engine and the electric motor for a given off-design mission.

The sample route chosen for demonstration is LGA-ORD (great circle distance of 637 nmi). The author chose this route because it was the second busiest domestic route in the US in June 2022 (according to OAG database). Additionally, it is assumed that the load factor for this route is 80%, which is equivalent to 148 passengers (this is synonymous with most FLEET studies which assumes a load factor of 80% for all routes in its network). Since the hybrid-electric aircraft operating on this route would be lighter than the sized aircraft because of lower payload weight and lower fuel weight (due to reduced mission length and payload weight), this route will allow us to see the benefits of the different energy management schemes to reduce overall mission fuel consumption.

The results presented in this section for the sample route consider only the 'case 1 - 8MW' hybrid-electric aircraft. For the fleet-level studies, the energy management tool is run for all the routes in FLEET's route network (Section 4.1.3) and for all four hybrid-electric aircraft cases.

3.4.1 No Energy Management

Considering hybrid-electric aircraft performance without any energy management schemes helps illustrate the benefits provided by the energy management tool. Without any energy management scheme, the hybrid-electric aircraft is operated using the sizing rules, i.e., the electric motors operate at full throttle during takeoff, initial climb, and climb segments, and the gas turbine engines operate as per the description in the sizing tool's Mission Module 3.1.2.4. Any battery energy remaining after the climb segment (if any) is not utilized in this

case. Without any energy management scheme, a ‘case 1 - 8MW’ hybrid-electric aircraft flown on the LGA-ORD route at 80% load factor requires a total mission fuel of 7,104.98 lbs, with an equivalent battery weight of 666.82 lbs remaining unutilized. This considers that the aircraft follows the standard mission defined in Section 3.1.2.4, with a climb speed of 280 knots, a cruise speed of 0.785 M, a cruise altitude of 35,000 ft, and a descent speed of 280 knots. Figure 3.14 shows the mission profile, mission fuel burn, gas turbine engine throttle positions, and electric motor throttle positions, along with other information for the LGA-ORD route, with ‘case 1 - 8MW’ hybrid-electric aircraft operating at 80% load factor.

GTE throttle position	th_{TO3}	49.000
	th_{TO4}	49.000
	th_{iCl1}	49.000
	th_{iCl2}	49.000
	th_{Cl1}	49.000
	th_{Cl2}	49.000
	th_{Cl3}	49.000
E-motor throttle position	eth_{TO3}	1.000
	eth_{TO4}	1.000
	eth_{iCl1}	1.000
	eth_{iCl2}	1.000
	eth_{Cl1}	1.000
	eth_{Cl2}	1.000
	eth_{Cl3}	1.000
	eth_{Cr}	-
	eth_{Cr1}	-
	eth_{Cr2}	-
	eth_{Cr3}	-
	eth_{Cr4}	-
	eth_{Cr5}	-
	eth_{Cr6}	-
TOW [lbs]		140807.81
Fuel Weight [lbs]		7104.98

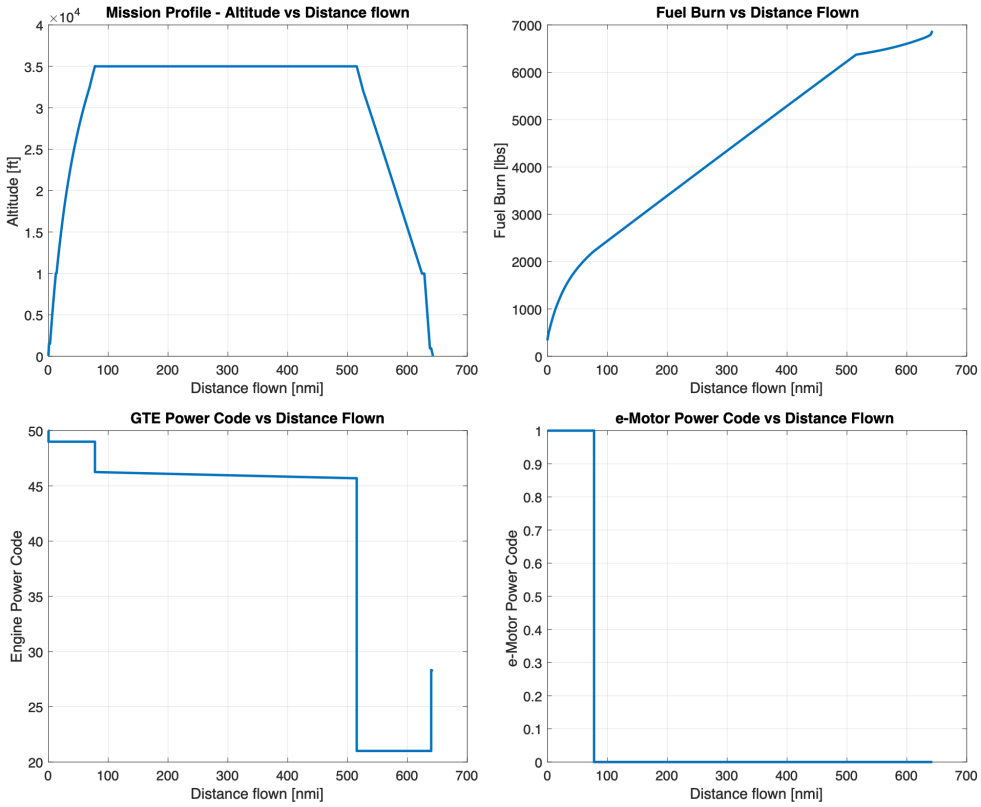

Figure 3.14. No energy management: Mission profile, mission fuel burn, gas turbine engine throttle positions, and electric motor throttle positions – LGA-ORD route with ‘case 1 - 8MW’ hybrid-electric aircraft operating at 80% load factor

3.4.2 Approach 1: "Rule-based" Cruise Energy Management

The "rule-based" cruise energy management scheme assumes that the electric motor throttle is set to maximum for the cruise segment until all the onboard batteries are completely (safely) discharged. The total mission fuel burn for a 'case 1 - 8MW' hybrid-electric aircraft using the "rule-based" cruise scheme on LGA-ORD route is 6,962.87 lbs (using the standard mission). Figure 3.15 shows the mission profile, mission fuel burn, gas turbine engine throttle positions, and electric motor throttle positions, along with other information for the LGA-ORD route, with 'case 1 - 8MW' hybrid-electric aircraft operating at 80% load factor. As expected, the energy management scheme chooses to use a higher throttle position for the electric motors in the later stages of the climb. As the gas turbine engines provide a higher percentage of the total required power in the early stages of climb, the aircraft becomes lighter compared to the case where electric motors would have provided a higher percentage of the required initial power. The lighter aircraft now needs lesser thrust / energy in the later stages of climb, allowing the aircraft to reap a higher benefit from using the electric motors in the later stages. The optimal combination of the gas turbine engine and electric motor throttle positions ensures that the aircraft has enough thrust to complete the mission, while minimizing overall mission fuel burn.

3.4.3 Approach 2: "Variable Throttle" Cruise Energy Management

The "variable throttle" cruise energy management scheme assumes that the cruise segment has multiple electric motor throttle positions, along with the throttle positions for the takeoff, initial climb, and climb segments. Given that the route length for the LGA-ORD route is 637 nmi, there are six electric motor throttle positions available for the cruise segment. The total mission fuel burn for a 'case 1 - 8MW' hybrid-electric aircraft using the "variable throttle" cruise scheme on LGA-ORD route is 6,958.88 lbs (using the standard mission). Figure 3.16 shows the mission profile, mission fuel burn, gas turbine engine throttle positions, and electric motor throttle positions, along with other information for the LGA-ORD route, with 'case 1 - 8MW' hybrid-electric aircraft operating at 80% load factor. As with the previous energy management scheme, the "variable throttle" energy

GTE throttle position	th_{TO3}	44.784
	th_{TO4}	44.939
	th_{iCl1}	44.997
	th_{iCl2}	44.597
	th_{Cl1}	44.914
	th_{Cl2}	45.120
	th_{Cl3}	44.849
E-motor throttle position	eth_{TO3}	0.753
	eth_{TO4}	0.746
	eth_{iCl1}	0.772
	eth_{iCl2}	0.858
	eth_{Cl1}	0.793
	eth_{Cl2}	0.832
	eth_{Cl3}	0.785
	eth_{Cr}	1.000
	eth_{Cr1}	-
	eth_{Cr2}	-
	eth_{Cr3}	-
	eth_{Cr4}	-
	eth_{Cr5}	-
	eth_{Cr6}	-
TOW [lbs]		140665.70
Fuel Weight [lbs]		6962.87

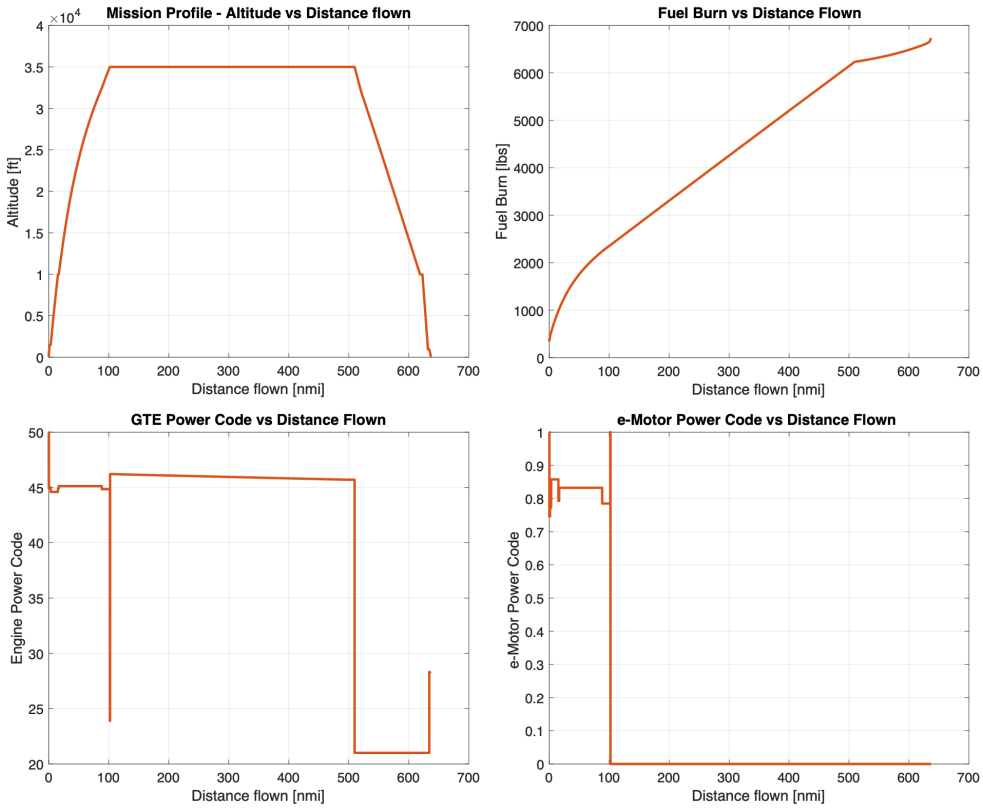

Figure 3.15. "Rule-based" cruise energy management: Mission profile, mission fuel burn, gas turbine engine throttle positions, and electric motor throttle positions – LGA-ORD route with 'case 1 - 8MW' hybrid-electric aircraft operating at 80% load factor

management scheme "waits" for the aircraft to get lighter during climb and cruise to better use the available battery energy towards the end of the climb and cruise segments. This "waiting" scheme for the cruise segment leads to lower overall fuel burn when compared to the "rule-based" approach where the aircraft has to use all the available battery energy when it is the heaviest (segment-wise), i.e., at the beginning of cruise.

3.4.4 Comparison of Different Energy Management Schemes

Table 3.8 compares the different energy management schemes to determine the hybrid-electric aircraft performance characteristics; the different gas turbine and electric motor throttle positions show the optimal power split between the two energy sources onboard the

GTE throttle position	th_{TO3}	45.111
	th_{TO4}	45.124
	th_{iCl1}	45.422
	th_{iCl2}	45.000
	th_{Cl1}	44.960
	th_{Cl2}	45.844
	th_{Cl3}	44.947
E-motor throttle position	eth_{TO3}	0.750
	eth_{TO4}	0.757
	eth_{iCl1}	0.750
	eth_{iCl2}	0.752
	eth_{Cl1}	0.826
	eth_{Cl2}	0.800
	eth_{Cl3}	0.863
	eth_{Cr}	-
	eth_{Cr1}	0.016
	eth_{Cr2}	0.026
	eth_{Cr3}	0.000
	eth_{Cr4}	0.000
	eth_{Cr5}	0.000
	eth_{Cr6}	0.047
TOW [lbs]		140661.71
Fuel Weight [lbs]		6958.88

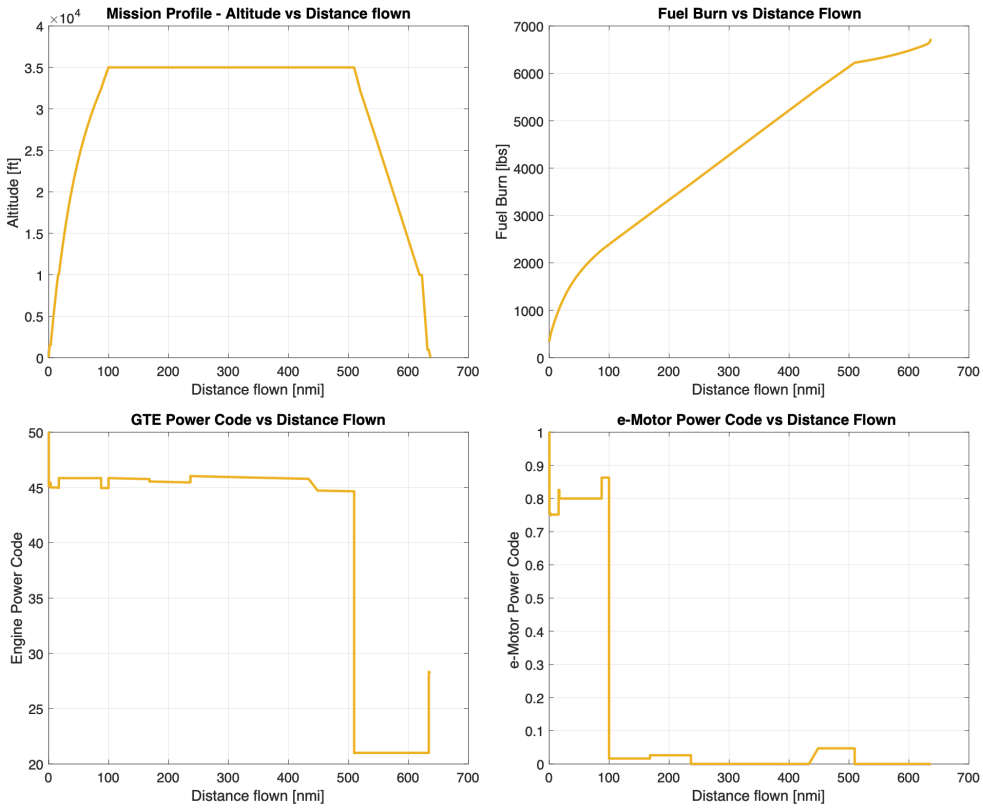

Figure 3.16. "Variable throttle" cruise energy management: Mission profile, mission fuel burn, gas turbine engine throttle positions, and electric motor throttle positions – LGA-ORD route with 'case 1 - 8MW' hybrid-electric aircraft operating at 80% load factor

aircraft. Figure 3.17 compares the mission profile, fuel burn, gas turbine engine throttle positions, and electric motor throttle positions for the different energy management approaches.

The "rule-based" cruise energy management scheme leads to a 2.00% reduction in fuel burn compared to the fuel burn using no energy management scheme, equivalent to 142.11 lbs of fuel saved per flight. The "variable throttle" energy management cruise scheme leads to a further reduction of about 4 lbs in mission fuel burn, leading to fuel savings of 2.06% (equivalent to 146.10 lbs of fuel per flight) compared to the case with no energy management scheme. All these fuel savings are corresponding to a case 1 (8MW) hybrid-electric aircraft operating on LGA-ORD route (637 nmi) at 80% load factor.

Comparing the "variable throttle" scheme with the "rule-based" scheme, the extra fuel savings from the "variable throttle" scheme seem marginal given the extra computational

Table 3.8. Energy management scheme comparison: Performance characteristics for 'case 1 - 8MW' hybrid-electric aircraft operating on LGA-ORD route at 80% load factor

Parameters		No EM	"Rule-Based" Cruise EM	"Variable Throttle" Cruise EM
GTE throttle position	th_{TO3}	49.000	44.784	45.111
	th_{TO4}	49.000	44.939	45.124
	th_{iCl1}	49.000	44.997	45.422
	th_{iCl2}	49.000	44.597	45.000
	th_{Cl1}	49.000	44.914	44.960
	th_{Cl2}	49.000	45.120	45.844
	th_{Cl3}	49.000	44.849	44.947
E-motor throttle position	eth_{TO3}	1.000	0.753	0.750
	eth_{TO4}	1.000	0.746	0.757
	eth_{iCl1}	1.000	0.772	0.750
	eth_{iCl2}	1.000	0.858	0.752
	eth_{Cl1}	1.000	0.793	0.826
	eth_{Cl2}	1.000	0.832	0.800
	eth_{Cl3}	1.000	0.785	0.863
	eth_{Cr}	-	1.000	-
	eth_{Cr1}	-	-	0.016
	eth_{Cr2}	-	-	0.026
	eth_{Cr3}	-	-	0.000
	eth_{Cr4}	-	-	0.000
	eth_{Cr5}	-	-	0.000
	eth_{Cr6}	-	-	0.047
TOW [lbs]		140807.81	140665.70	140661.71
Fuel Weight [lbs]		7104.98	6962.87	6958.88
Fuel Savings		-	-2.00%	-2.06%

time required by the scheme to find the optimal power split between the gas turbine engines and the electric motors (because of the need to use Genetic Algorithm [110] to handle the increased number of problem design variables). Additionally, the extra fuel savings from the "variable throttle" scheme are based on an ideal standard mission with no consideration of uncertainties like winds aloft and other factors. The "variable throttle" scheme distributes the battery energy for the cruise segment based on the ideal mission, "saving" the battery energy for use towards the end of the cruise segment. In case there is a change in the mission profile (due to winds or to accommodate other air traffic), we might not be able to utilize the "saved" battery energy optimally, which could lead to higher overall mission fuel burn. In reality, this will always be the case due to the high number of uncertainties faced by the operators on a daily basis, making the "variable throttle" scheme less useful. Hence, for

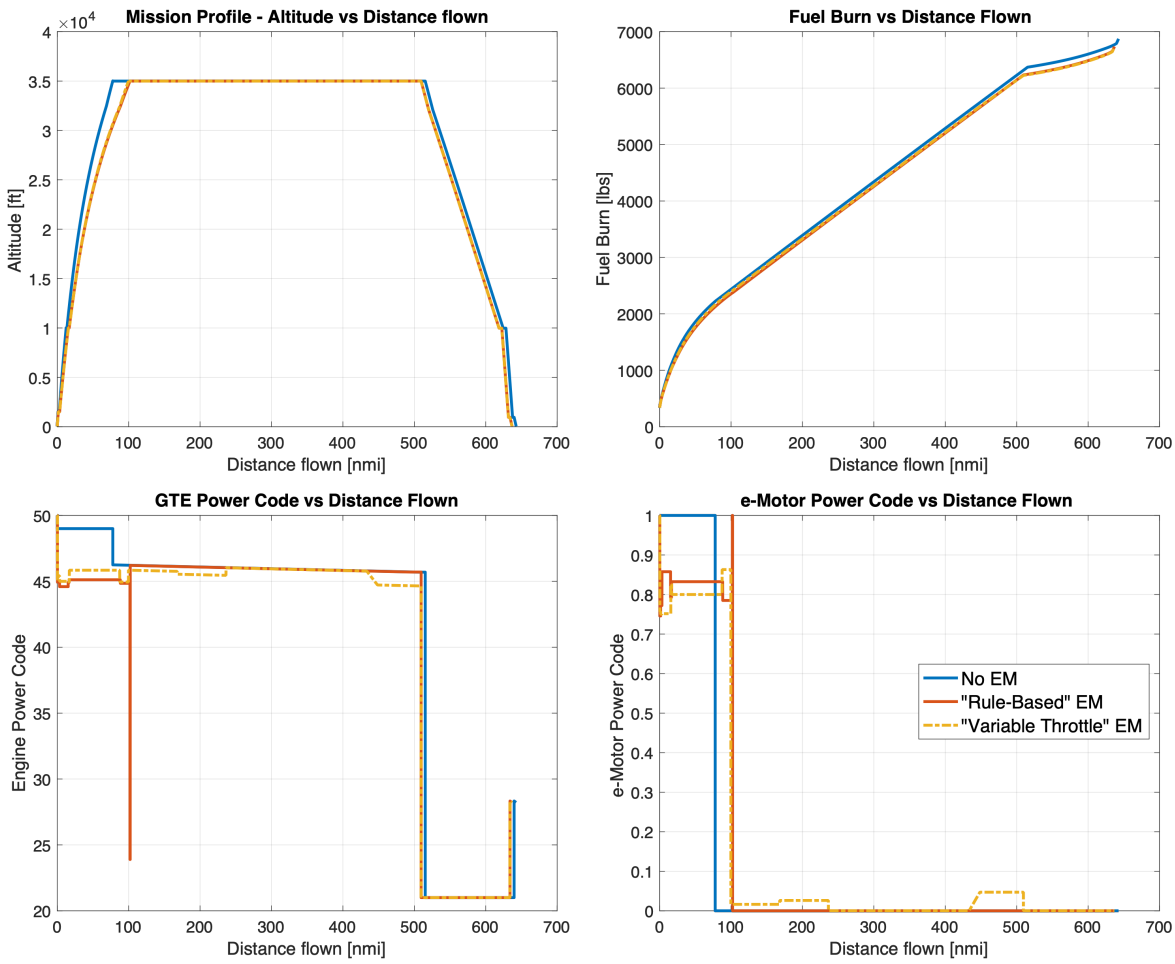

Figure 3.17. Energy management scheme comparison: Mission profile, mission fuel burn, gas turbine engine throttle positions, and electric motor throttle positions for 'case 1 - 8MW' hybrid-electric aircraft operating on LGA-ORD route at 80% load factor

the fleet-level studies conducted in this work, the author uses the "rule-based" scheme to generate the hybrid-electric aircraft performance data, as it seems more suited to represent how an airline might end up using the hybrid-electric aircraft.

3.4.5 Energy Management with Optimal Flight Path

All the energy management tool results presented until now assumed a standard mission with a climb speed of 280 knots, a cruise speed of 0.785 M, a cruise altitude of 35,000 ft, and a descent speed of 280 knots. However, concurrently optimizing the mission profile (or

flight path) and the power split between the gas turbine engines and the electric motors has the potential to lower the overall off-design mission fuel consumption for hybrid-electric aircraft even further. The optimal flight path scheme is implemented along with the energy management scheme by enabling all the mission optimizers – climb, BCM/BCA, and descent (discussed in Section 3.1.2.4) – as inner optimizers, with the energy management scheme acting as the outer (or main) optimizer. With the current tool setup, the integration of the two schemes is straight-forward (as the mission optimizers are embedded in the Mission Module), with the inclusion of climb speed (V_{climb}) as an additional design variable in the energy management optimizer (or the outer optimizer). This work considers only the "rule-based" cruise energy management scheme with the optimal flight path since it seems to be most suited to how airlines might end up using the hybrid-electric aircraft as part of their daily operations.

Table 3.9 summarizes the energy management tool results (and the hybrid-electric aircraft performance characteristics) for the "rule-based" scheme with the standard flight path and the "rule-based" scheme with an optimal flight path. The simultaneous optimization of the aircraft's energy management and flight path leads to lower mission fuel burn, with a 1.9% reduction compared to the "rule-based" scheme, and a 3.9% reduction compared to the case where no energy management scheme is implemented. This is equivalent to 134.00 lbs and 276.11 lbs of fuel saved per flight compared to the "rule-based" scheme and the no energy management scheme, respectively.

Figure 3.18 compares the mission profile, fuel burn, gas turbine engine throttle positions, and electric motor throttle positions for the "rule-based" and "rule-based" with optimal flight path schemes. The optimal flight path for the latter scheme involves cruising at a higher speed and altitude (0.789M at 37,034 ft), climbing at a slightly lower indicated airspeed, and an optimal descent to 10,000 ft with a continuous reduction in descent indicated airspeed (to meet the 250 knots speed limit at 10,000 ft). This is clearly visible in the mission profile (depicted by purple dotted line in the top-left chart) in Figure 3.18 as the aircraft climbs optimally to a higher altitude and starts to descend optimally earlier, compared to the standard mission profile (depicted by red line in the top-left chart). The less cruise distance covered by the aircraft in the "rule-based" scheme with optimal flight path seems to be a

Table 3.9. Energy management with Optimal Flight Path: Performance characteristics for 'case 1 - 8MW' hybrid-electric aircraft operating on LGA-ORD route at 80% load factor

Parameters		"Rule-Based" Cruise EM	Optimal Flight Path + "Rule-Based" Cruise EM
GTE throttle position	th_{TO3}	44.784	45.002
	th_{TO4}	44.939	46.849
	th_{iCl1}	44.997	44.989
	th_{iCl2}	44.597	45.074
	th_{Cl1}	44.914	44.984
	th_{Cl2}	45.120	45.410
	th_{Cl3}	44.849	45.012
E-motor throttle position	eth_{TO3}	0.753	0.503
	eth_{TO4}	0.746	0.826
	eth_{iCl1}	0.772	0.752
	eth_{iCl2}	0.858	0.754
	eth_{Cl1}	0.793	0.830
	eth_{Cl2}	0.832	0.615
	eth_{Cl3}	0.785	0.607
	eth_{Cr}	1.000	1.000
	eth_{Cr1}	-	-
	eth_{Cr2}	-	-
	eth_{Cr3}	-	-
	eth_{Cr4}	-	-
	eth_{Cr5}	-	-
	eth_{Cr6}	-	-
V_{climb} [knots]		280.00	279.99
M_{cruise} [Mach]		0.785	0.789
Alt_{cruise} [ft]		35000	37034
TOW [lbs]		140665.70	140531.70
Fuel Weight [lbs]		6962.87	6828.87
Fuel Savings		-	-1.92%

major factor in reducing fuel burn over the mission, as evident in the top-right chart in Figure 3.18). The gas turbine engine and electric motor throttle positions for the climb segment seem to differ noticeably for the two schemes in consideration. The "rule-based" scheme with optimal flight path uses higher gas turbine engine throttle setting and lower electric motor throttle setting during a major portion of the climb segment (visible by the gap between the red solid and purple dotted line in bottom two charts in Figure 3.18). Both the schemes still show the downward and upward "kink" in the gas turbine engine and electric motor throttles, respectively, at the beginning of cruise, signifying the use of electric motors at full throttle for a short period (accompanied by a drop in gas turbine engine throttle). However, the "kink" for the "rule-based" scheme with optimal flight path occurs later in the mission

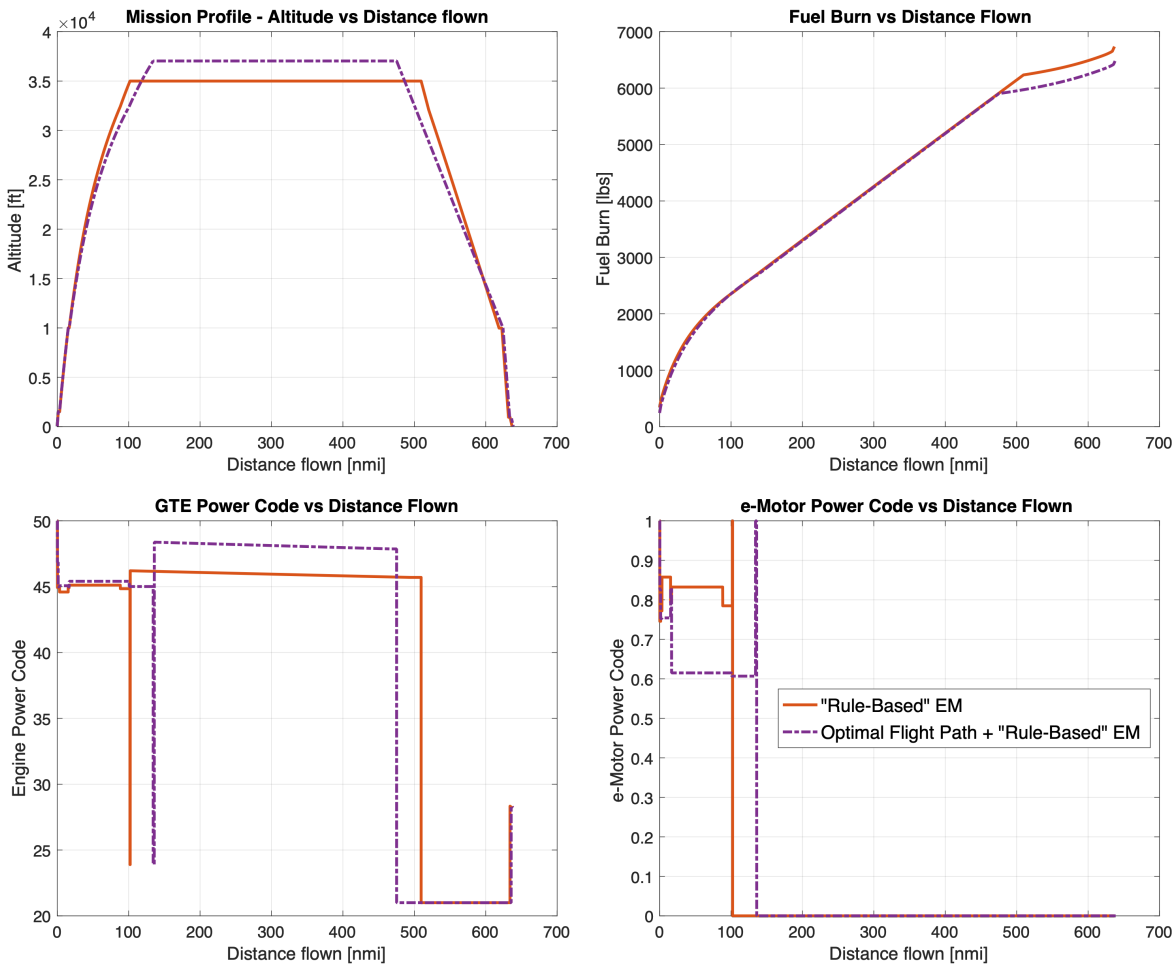

Figure 3.18. Energy management with Optimal Flight Path: Mission profile, mission fuel burn, gas turbine engine throttle positions, and electric motor throttle positions for 'case 1 - 8MW' hybrid-electric aircraft operating on LGA-ORD route at 80% load factor

as the aircraft climbs to a higher (and more optimal) cruising altitude. As expected, during cruise, the "rule-based" scheme with optimal flight path showcases a higher power code for the gas turbine engines, compared to the scheme with the standard flight path. Given the thrust lapse rate of a gas turbine engine, an engine needs to use a higher throttle position / power code to match the thrust produced by the engine at a lower altitude. Because the optimal flight path chosen by the optimizer features a higher altitude, the gas turbine engines' power code is also higher to provide sufficient thrust for constant speed cruising.

The fuel burn benefits from flying a hybrid-electric aircraft on an optimal path (with optimal energy management) are noticeable. However, in reality, the aircraft might not be able to fly as per the calculated optimal flight path due to several factors, including, restrictions by the air traffic control, winds aloft, and other weather conditions. Factoring in the real world possibility of flying an aircraft on its optimal flight path for each route during daily operations, this work uses the "rule-based" scheme with a standard mission to generate the hybrid-electric aircraft performance data for the fleet-level studies presented in Chapter 5.

4. FLEET-LEVEL MODELING

Hybrid-electric aircraft show a potential to reduce CO_2 emissions at an aircraft-level due to reduced fuel consumption compared to a conventional (all fuel-burning) aircraft. However, once these aircraft are introduced for use as a part of profit-seeking airline fleets, the overall fleet-level CO_2 emissions are not expected to reduce proportionally to individual CO_2 emissions benefits possible from these hybrid-electric aircraft. There are a number of obvious reasons for this most-likely-possible scenario – 1) there will be a limit to aircraft production and delivery based on materials, logistics, and supply chain limits, 2) airlines will not be able to suddenly retire their existing single-aisle aircraft (forced early aircraft retirement) to operate an all hybrid-electric single-aisle aircraft fleet, and, 3) hybrid-electric aircraft will have a shorter range compared to conventional aircraft, limiting the direct replacement of the conventional single-aisle aircraft with lesser carbon emitting hybrid-electric aircraft in an airline fleet.

There is a tradeoff to introducing single-aisle hybrid-electric aircraft in airline fleets. Although the fleet-level emissions from the single-aisle aircraft fleet are expected to go down once the hybrid-electric aircraft in consideration are introduced, the usage of these short-range airplanes (compared to conventional single-aisle airplanes) can cause the airlines to change how they use their whole fleet. These changes in fleet allocation and utilization could mean that the direct CO_2 emission reduction benefits possible from hybrid-electric aircraft could be offset by the changes in CO_2 emissions from the remaining fleet.

Hence, it is important to study the fleet-level impacts of introducing these short-range fuel-efficient single-aisle aircraft in airline fleets. This work attempts to simulate a profit-seeking "U.S.-flag carrier" airline's behavior when hybrid-electric aircraft are made available to its fleet in 2035, and predicts the subsequent total fleet carbon emissions, using the Fleet-Level Environmental Evaluation Tool (FLEET) [7]. Sections 4.1 and 4.2 talk about the FLEET tool and the future demand predictions, respectively. Section 4.3 talks about introducing hybrid-electric aircraft in FLEET, including aircraft performance coefficients, economic factors (aircraft and energy costs), and life-cycle CO_2 emission intensities.

4.1 Modeling Tool — FLEET

FLEET is a computational simulation tool that predicts how fleet-level environmental impacts of aviation — in the form of CO_2 emissions and airport noise — evolve over time. FLEET follows a system dynamics-inspired approach to connect computational modules that mimic the economics of airline operations, models airlines decisions regarding retirement of old aircraft and acquisition of new aircraft, and represents passenger demand growth in response to economic conditions. This set of interconnected computational modules enables the tool to assess the impact of future aircraft concepts and technologies on fleet-wide environmental metrics, while reflecting resulting relationships between carbon emissions, passenger demand/market demand, ticket prices, and airline fleet composition from 2005 to 2055. FLEET is capable of providing an estimation of how variation in external factors such as economic conditions, policy implementation, and technology availability would affect future commercial aviation environmental impacts. FLEET employs a year-by-year approach in its simulation which models the evaluation of passenger demand, airline fleet mix, and available aircraft technology level. This makes FLEET independent of an external forecast for airline operations, an external forecast for passenger demand, and of a prescribed fleet mix evolution. References [7], [83], [84], [112]–[118] talk about the various studies conducted with FLEET, considering subsonic aircraft operation only. FLEET studies considering a mixture of supersonic and subsonic commercial aircraft in airline fleet are available in references [119]–[121].

Reference [7] provides additional details about the aircraft factors (aircraft acquisition and retirement, aircraft production and delivery), economic factors (nonfuel direct operating costs (DOC), indirect operating costs (IOC), fuel cost, ticket price), market factors (projected demand, inherent demand - Gross Domestic Product (GDP) growth, price-demand elasticity), and environmental factors (environmental impact metrics, environmental policy - fuel tax) embedded in FLEET's system-dynamics-type framework. Figure 4.1 provides a representation of FLEET.

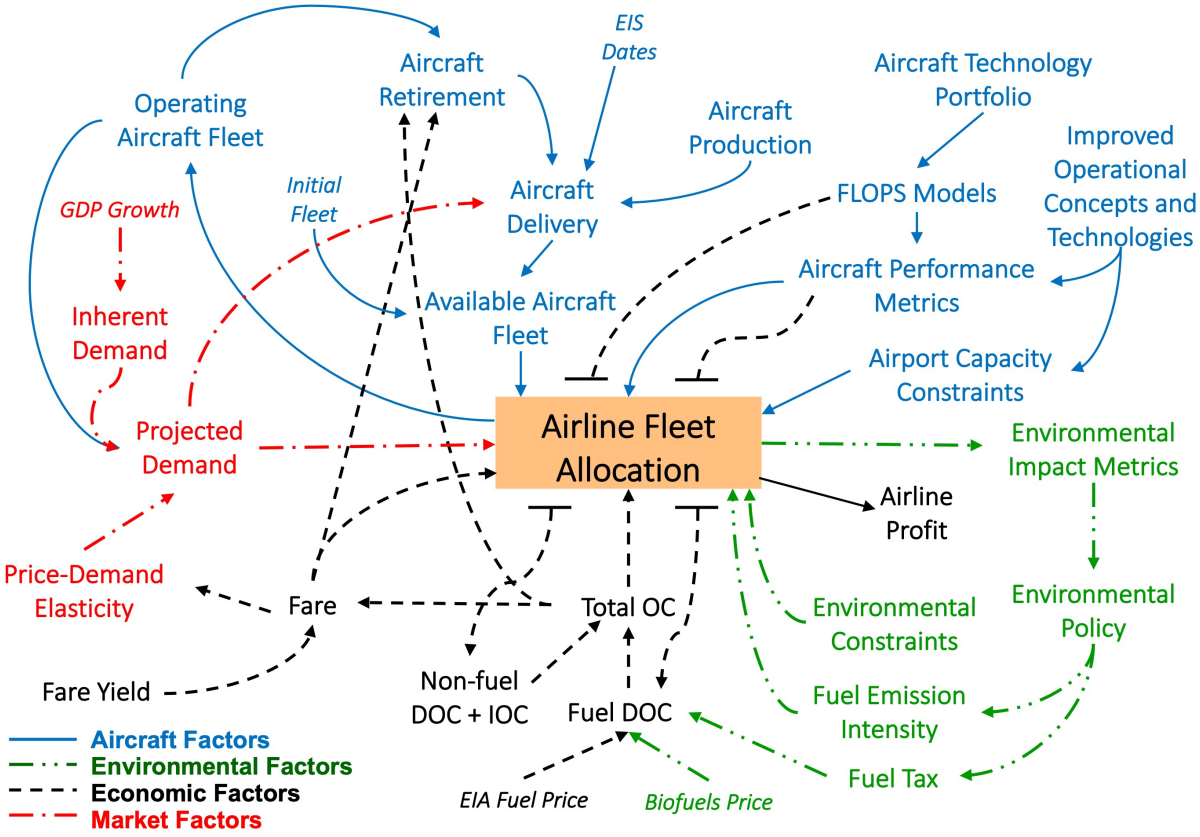

Figure 4.1. System-dynamics-inspired representation of FLEET (adapted with permission from Moolchandani et al. [7])

4.1.1 FLEET's Allocation Problem

Central to FLEET is an optimization algorithm that solves an allocation problem to maximize the profit of an airline while satisfying passenger demand on its route network. Equation 4.1 depicts the objective function for the allocation problem.

$$\sum_{k=1}^{K}\sum_{j=1}^{J} pax_{k,j} price_{k,j} - \sum_{k=1}^{K}\sum_{j=1}^{J} X_{k,j} C_{k,j} \tag{4.1}$$

In equation 4.1, $X_{k,j}$ is the number of round trips aircraft k provides on route j. The assumption of round-trip helps to remove balance constraints and reduces the number of routes, thereby reducing the size of the optimization problem. A round trip is one flight from A to B and back from B to A; it can only be an integer. $pax_{k,j}$ is the number of

passengers moved one way using aircraft k on route j today. This assumes symmetricity in the number of passengers moved between A – B and B – A. For example, if $pax_{subsonic,JFK-LHR}$ = 50, this means that 50 passengers are moved from JFK-LHR and 50 passengers are moved from LHR-JFK, leading to 100 passengers moved on the route in total. $price_{k,j}$ is the round trip ticket price for passenger on aircraft type k flying route j. This work chose to stick with round trip price because it matches the most common fare paid by passengers (matches DB1B itinerary fare). This step means that one passenger ($pax_{k,j}$) pays half of their round-trip price today. $C_{k,j}$ is the round-trip direct operating cost of aircraft k on route j. The FLOPS / sizing code output gives one-way direct operating cost. For subsonic aircraft, the output is multiplied by a factor of 2.

The allocation problem has several constraints to ensure realistic modeling of an airline's daily operations. Equations 4.2 – 4.5 depict the constraints for the allocation problem.

$$\sum_{k=1}^{K} 2X_{k,j}(BH_{k,j} + MH_{k,j} + t) \leq 24 * fleet_k \tag{4.2}$$

$$pax_{k,j} \leq cap_k X_{k,j} \tag{4.3}$$

$$\sum_{k=1}^{K} pax_{k,j} \leq dem_j \tag{4.4}$$

$$\sum_{k=1}^{K} pax_{k,j} \geq 0.9 * dem_j \tag{4.5}$$

Equation 4.2 is the count constraint; it sets the count on the number of aircraft available in fleet and the number of aircraft actually available to fly. The multiplier of 2 on the left side of the equation signifies a round-trip (as $X_{k,j}$ is number of round-trips), and the multiplier of 24 on the right side of the equation signifies the duration of one day, i.e., 24 hours. $BH_{k,j}$ is the one-way block hours from FLOPS / sizing code for aircraft k on route j, $MH_{k,j}$ is the one-way maintenance hours from FLOPS / sizing code for aircraft k on route j, t is the turnaround time. The term $fleet_k$ is the number of aircraft type k in the fleet.

Equation 4.3 is the capacity constraint; it ensures that there are enough seats to satisfy the larger one-way demand, if minimum demand constraint is imposed. In Equation 4.3, cap_k signifies the capacity of type k aircraft. In other words, the number of passengers moved by aircraft type k one way on route j today should be less than or equal to the number of seats flying each way on route j today.

Equations 4.4 and 4.5 depict the demand constraints in FLEET. Equation 4.4 ensures that FLEET does not create demand on its own, i.e., the demand to be served does not surpass the dem_{j} value. dem_{j} is the maximum value of the number of travelers between A – B and B – A. This parameter utilizes the airline market data for passenger demand each way for route A – B and route B – A. This is essentially the one-way demand in FLEET. Equation 4.5 sets a lower limit on the demand satisfied on each route.

4.1.2 Aircraft Classification

FLEET represents aircraft by class (based on number of seats) and by technology age. There are six different classes of subsonic aircraft in FLEET – 1) Small Regional Jet (up to 50 seats), 2) Regional Jet, 3) Small Single Aisle, 4) Large Single Aisle, 5) Small Twin Aisle, and 6) Large Twin Aisle. There are four different technology ages in FLEET – 1) Representative-in-class (most flown aircraft in 2005), 2) Best-in-class (aircraft with most recent entry into service dates in 2005), 3) New-in-class (aircraft currently under development that will enter service in near future), and 4) Future-in-class (aircraft that will enter into service after new-in-class aircraft). Table 4.1 lists the subsonic aircraft available in FLEET. All these aircraft (except the future-in-class) are modeled in FLOPS using the technical data available in public domain. There are no new- and future-in-class 1 aircraft available in the FLEET simulation, recognizing the dwindling number of orders for the small regional jets in the aviation market currently. The new-in-class 2 aircraft, named as CS100, is an approximate representation of the recently introduced Airbus A220, while the new-in-class 3 aircraft, named as Boeing 737-700 reengined, potentially represents the Boeing 737 MAX7 aircraft. The new-in-class 6 aircraft, named as LTA, represents a refreshed version of the Boeing 777 aircraft (the model could be considered as a representation of the upcoming Boeing 777X). Reference [122]

provides additional details about these aircraft. For the future-in-class aircraft, this work considers a "business-as-usual" scenario, wherein the author assumes a 10% reduction in fuel burn for future-in-class aircraft compared to new-in-class aircraft of the same size class. The future-in-class aircraft are modeled using what the author calls the "magic wand" approach. These future-in-class aircraft are same as the corresponding new-in-class aircraft, with their fuel burn scaled down to represent the "business-as-usual" scenario, without worrying about the technologies that need to be implemented to achieve the assumed (better) performance. Reference [117] provides details about these aircraft. These different classes and technology of aircraft represent the mix of aircraft sizes and technologies in the airline fleet.

Table 4.1. Aircraft types in FLEET with [Label] and (EIS)

	Representative-in-class	Best-in-class	New-in-class	Future-in-class
Class 1	Canadair RJ200/RJ440 [SRJ]	Embraer ERJ145 [SRJ]		
Class 2	Canadair RJ700 [RJ]	Embraer ERJ170 [RJ]	CS100 (2020)	Future RJ (2030)
Class 3	Boeing 737-300 [SSA]	Boeing 737-700 [SSA]	Boeing 737-700 reengined (2017)	Future SSA (2035)
Class 4	Boeing 757-200 [LSA]	Boeing 737-800 [LSA]	Boeing 737-800 reengined (2025)	Future LSA (2040)
Class 5	Boeing 767-300ER [STA]	Airbus A330-200 [STA]	Boeing 787 (2020)	Future STA (2030)
Class 6	Boeing 747-400 [LTA]	Boeing 777-200LR [LTA]	LTA (2025)	Future LTA (2040)

EIS, entry into service; LSA, large single aisle; LTA, large twin aisle; RJ, regional jet; SRJ, small regional jet; SSA, small single aisle; STA, small twin aisle.

4.1.3 Passenger Demand and Route Network in FLEET

FLEET predictions for routes and passenger demand build upon reported data from the Bureau of Transportation Statistics (BTS) [123]. FLEET uses historical BTS data for years from 2005 through 2018, then uses model based predictions for years 2019 and beyond. This causes FLEET to have a dynamic route network that follows how US-flag carrier airlines updated their route networks as reported in the BTS data until 2018, followed by a static route network from 2018 and beyond (i.e., FLEET does not predict the addition or deletion of routes in the future). In 2018 (and all subsequent years), there are 1,975 routes in the FLEET network that connect a subset of WWLMINET 257 airports [1]. All these routes are

[1]↑"World-Wide LMI Network (WWLMINET) 257" airports as reported by Logistics Management Institute to be those "worldwide" airports that have the most operations

either US-domestic routes or international routes with direct flights originating or ending at a US airport, because these are the only routes that appear in the BTS database.

Extracting and Processing Data from BTS Datasets

The BTS demand data employed in this work is the T-100 Segment Data (all carriers). The T-100 segment demand data comes in either monthly or yearly entries, with all data from both domestic and international carriers, passengers and cargo services (scheduled and unscheduled), all types of carriers (regional, major, small certified, etc.), and all types of aircraft configuration. This raw data contains information irrelevant to FLEET, and therefore, needs to be filtered before using it to generate the route network in FLEET. Current implementation uses yearly data for years 2005 to 2018, but the filtering approach is also applicable to monthly data.

Filtering the Data

The raw from BTS is trimmed to relevant data that can be used as an input for further processing in FLEET using the filters numbered 0 to 11 in Table 4.2. After these filters are applied to the raw data in the order listed in Table 4.2, the final demand data contains information about the number of passengers per year on directional routes by all domestic carriers combined. For instance, after filtering, the demand data for JFK – LHR route has a single entry that represents the yearly number of passengers carried by all US-flag carrier airlines combined.

Processing the Data

The filtered data is input into FLEET and additional filters for aircraft performance and airport characteristics are applied to the data. The yearly data is then transformed to daily demand (dividing the yearly demand by 365 and then ceiling the result for integer number of passengers) applicable to both directions of a route (bi-directional routes) by choosing the larger demand of the two directions to represent the demand for each direction. For instance, if JFK to LHR has a daily demand of 10,000 passengers and LHR to JFK has a

daily demand of 10,500 passengers, then the daily demand in FLEET for JFK – LHR route will be 10,500 passengers. Routes with daily demand greater than or equal to 10 passengers constitute the route network in FLEET for that year. This step is included in Table 4.2 as filter number 12.

Updated Route Network

FLEET's route network updates every year from 2005 to 2018 using the corresponding year's BTS T-100 Segment data (yearly). This causes FLEET's route network to have 1,965 routes in the year 2005 and 1,975 routes in the year 2018. FLEET's route network stays static beyond 2018, hence, there are 1,975 routes in FLEET from years 2018 to 2055. Earlier, FLEET had a static route network with 1,940 routes starting from year 2005 [7], [117], [119]. The updated route network allows FLEET to include some current "popular" trans-Pacific and trans-Atlantic routes, like SJC – HND, that were missing from FLEET's previous route network, and to remove some outdated routes, like ATL – LGW, from its route network.

4.1.4 Passenger Demand Forecast Model

The passenger demand forecast in FLEET is modeled is a function of two factors: the demand changes due to broad economic factors, referred to here as the "inherent demand growth", and the demand change due to passenger response to changes in ticket prices charged by the airlines, called the "elastic growth". In the inherent demand growth model, the demand growth is a function of GDP growth, while the elastic growth model incorporates the effects of range and availability of alternative modes of transport into its calculation [7].

Inherent Demand Growth

FLEET uses a nonlinear relationship to evaluate the demand growth rate in different continents (see reference [125]), which is based on the historical data of trips/capita vs. GDP/capita. In other words, if all the continents had the same GDP growth rate, the continents with higher GDP/capita would have a lower trips/capita growth rate. High population growth rates also dilute impacts of high GDP growth rates on GDP/capita growth.

Table 4.2. FLEET: List of filters for extracting and processing BTS T-100 Segment data (all carriers) using year 2005 as an example (adapted with permission from Jain et al. [124])

ID	Step	Purpose	Data
0	Initial BTS data for 2005 T-100 Segment (All Carriers)		Monthly records on directional routes by both different international and domestic carriers More than one record/month possible *Example: American Airlines (AA) has two entries for JFK-LAX route in Jan, one entry in Feb, four entries in Mar, etc.*
1	All origin- and destination-airports are in the WWLMINET 257 airport network	Keep entries for routes with origin or destination in the US only	Same as above
2	Filter out cargo carrier group	Keep entries for scheduled passengers service (this can include flights by regional, commuter, small certified carriers)	Same as above
3	Filter out freight configuration and seaplane configuration aircraft		Same as above
4	Filter out all cargo scheduled service, unscheduled passenger service		Same as above
5	Filter out all routes by international carriers	Keep entries for flights by US-flag carrier airlines only	Monthly records on directional routes by different domestic carriers More than one record/month possible
6	Filter for non-zero passengers & seats	Keep entries with non-zero demand only	Same as above
7	Filter for non-zero distance	Keep entries for "real" flights	Same as above
8	Aggregate to get monthly performance		Monthly records on directional routes by different domestic carriers Only one record/month *Example: AA has one entry for JFK-LAX route in Jan, Feb, Mar, etc.*
9	Group by directional routes to combine demand of all airlines on each route together	Assume one large "aggregate" U.S.-based airline, no competition considered	Monthly records on directional routes by one large "aggregate" airline representing all domestic carriers *Example: JFK-LAX route has 12 entries, one for each month, and the demand shown is sum of all airlines' demand*
10	Aggregate to get yearly performance	Aggregate monthly data into yearly data	Yearly records on directional routes by one large "aggregate" airline representing all domestic carriers *Example: One entry for JFK-LAX route for year 2005*
11	Filter for routes with regular departures performed	Keep only entries for routes with regular operations (at least 1 flight/week or 52 flights/year performed on directional routes) *Example: JFK-LAX has 105 flights performed in 2005 → kept* *JFK-IND has 50 flights performed in 2005 → out*	Same as above
12	Process in FLEET	Filter for minimum passengers per day, minimum runway length, etc. Turn yearly demand to daily demand	Daily demand on bi-directional routes by one large "aggregate" airline representing all domestic carriers

The model employs the GDP and population data of each continent in 2005 from World Bank [126] as initial settings. By using the GDP growth rate and population growth rate

historical data and predictions, the model tracks the passenger demand for each continent from 2005 to 2050.

Elastic Demand Growth

The demand for air travel also changes as passengers respond to changes in air fare; this change is represented using price-demand elasticity. In modeling price-demand elasticity, two factors affect passenger choice to fly. The first is the distance of travel – over short distances, the passengers may choose not to fly and opt for alternative modes of travel. The second factor is whether the route is domestic or international, since over many international routes, alternative modes of travel are not feasible. The elasticity values used for price-demand elasticity are based on reference [127], and appear in reference [7].

The FLEET simulations presented in this work use 2005 as the starting year for all simulations, because most stated aviation emissions goals use 2005 as the reference year. The FLEET simulation output provides information about the type(s) of and number of aircraft allocated to routes to meet passenger demand based on a number of scenarios. The scenarios are essentially a combination of low, nominal, and high values for aircraft technology, economic growth rate, and energy price. References [117], [118] provide more details about the subsonic-only FLEET scenarios. This work considers only the "Current Trends Best Guess (CTBG)" scenario from the previous work and uses it as a baseline to compare other scenarios. The CTBG scenario comprises nominal aircraft technology development, nominal economic growth, and nominal energy price evolution.

4.2 Future Demand Scenarios

The novel coronavirus (COVID-19) pandemic caused a sudden drop in air travel passenger demand and airline operations due to travel restrictions imposed worldwide. It is necessary to include this demand slump (and subsequent future demand projections) in FLEET to make better future fleet-level emission predictions. With several paths to passenger demand recovery possible (depending on the duration of the outbreak, containment

measures, consumer confidence for air travel, and economic conditions), this work utilizes the future demand scenarios presented by the author in Jain et al. [124].

The work considers six demand projection scenarios using two possibilities for airline demand recovery to pre-COVID-19 (2019) levels and three different GDP growth rates from the year of passenger demand recovery to the year 2030. The GDP growth rate directly impacts the inherent passenger demand in FLEET. These scenarios are based on two broad assumptions – 1) there is a 66% reduction in total passenger demand in 2020 [128], and 2) there will either be a V-shape recovery to 2019 air travel demand levels by 2023, or a U-shape recovery to 2019 air travel demand levels by 2024. Table 4.3 summarizes the future demand scenarios considered in this work; passenger demand for different years is listed as a percentage of pre-COVID-19 levels (2019) and the GDP growth rate is listed as a percentage of the 'Nominal' GDP growth rate in FLEET [124].

Table 4.3. Future COVID-19-related demand scenarios in FLEET

Scenario #	Description	Passenger Demand (% of pre-COVID-19 levels)					GDP Growth Rate (as % of 'Nominal')
		2020	2021	2022	2023	2024	
1	2023 recovery	34%	52%	88%	100%	--	No change
2	2023 recovery + GDP slowdown to 75% until 2030	34%	52%	88%	100%	--	75% (- 25%)
3	2023 recovery + GDP inflation to 125% until 2030	34%	52%	88%	100%	--	125% (+25%)
4	2024 recovery	34%	38%	50%	75%	100%	No change
5	2024 recovery + GDP slowdown to 75% until 2030	34%	38%	50%	75%	100%	75% (- 25%)
6	2024 recovery + GDP inflation to 125% until 2030	34%	38%	50%	75%	100%	125% (+25%)

The first three scenarios consider that the passenger demand returns to pre-COVID-19 levels (2019) by the year 2023. The total passenger demand is set to recover to 52% of pre-COVID-19 levels by 2021, 88% of pre-COVID-19 levels by 2022, and 100% of pre-COVID-19 levels by 2023 [128]. These three scenarios are distinguished by the inherent passenger demand growth rate, which is based on the GDP growth rate assumed in the

FLEET simulation. The first scenario – "2023 recovery" – assumes that the passenger demand continues to grow based on the GDP growth rate in FLEET beyond 2023. This scenario does not consider the long-term economic impacts of the COVID-19 pandemic and assumes that the GDP will continue to grow unaffected by the pandemic after 2023. The second scenario – "2023 recovery + GDP slowdown to 75% until 2030" – considers that the passenger demand grows corresponding to 75% of the GDP growth assumptions in FLEET from years 2023 to 2030. This scenario takes into consideration the long-term economic impacts of the COVID-19 pandemic and assumes that the GDP will grow at a slower rate until year 2030. The third scenario – "2023 recovery + GDP inflation to 125% until 2030" – assumes that the passenger demand grows at 125% of the inherent demand and GDP growth assumptions in FLEET from years 2023 to 2030. This scenario assumes that the GDP will bounce back stronger in the longer term and grow at a faster rate until year 2030.

The remaining three scenarios consider that the passenger demand returns to pre-COVID-19 levels (2019) by the year 2024 (one year later than the previous three scenarios). The total passenger demand is set to recover to 38% of pre-COVID-19 levels by 2021, considering the possibility that the severe travel restrictions in response to new COVID-19 variants persist [129]. The passenger demand is then assumed to recover to 50% of pre-COVID-19 levels by 2022, 75% of pre-COVID-19 levels by 2023, and to pre-COVID-19 levels by 2024. Similar to the previous three scenarios, the fourth scenario – "2024 recovery" – assumes that the GDP will continue to grow unaffected by the pandemic after 2024, the fifth scenario – "2024 recovery + GDP slowdown to 75% until 2030" – assumes that the passenger demand will grow corresponding to 75% of the GDP growth assumptions in FLEET until year 2030, and the sixth scenario – "2024 recovery + GDP inflation to 125% until 2030" – assumes that the passenger demand will grow at 125% of the GDP growth assumptions in FLEET until year 2030.

Figure 4.2 shows the V-shaped and "almost" U-shaped passenger demand recovery in FLEET to pre-COVID-19 (2019) levels by 2023 and 2024, respectively. This work only considers scenario 1 ("2023 recovery") and scenario 4 ("2024 recovery") as the representative scenarios for fleet-level studies with the introduction of single-aisle hybrid-electric aircraft.

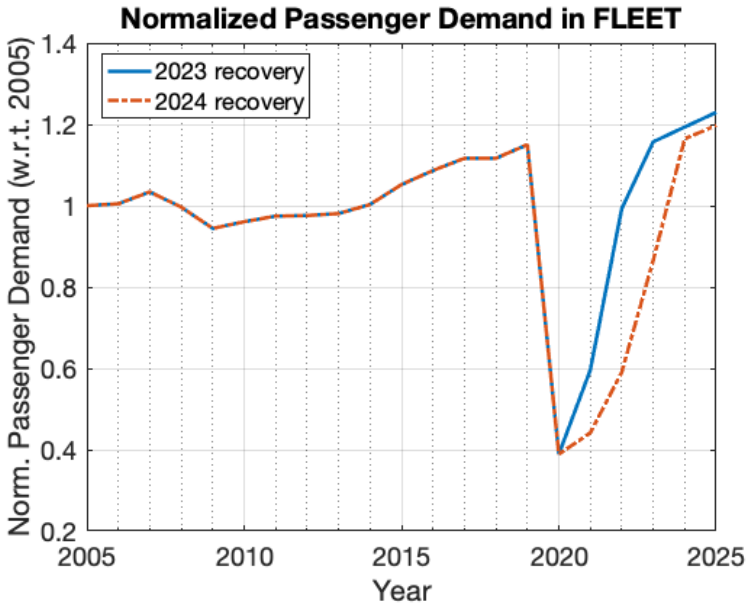

Figure 4.2. Projected demand recovery to pre-COVID-19 (2019) levels in FLEET

4.3 Introducing Hybrid-Electric Aircraft in FLEET

The single-aisle hybrid-electric aircraft is introduced in FLEET in 2035 as a future-in-class 3 aircraft with a range capability of 900 nmi. The hybrid-electric aircraft replaces the similar size (single-aisle) "magic wand" future-in-class 3 aircraft with a higher range capability of 3,260 nmi (refer to Section 4.1 for details on aircraft classification in FLEET based on size and technology age). The reduced range capability of the hybrid-electric aircraft makes it eligible for operation on only 1,082 routes out of the 1,975 routes available in the FLEET network.

4.3.1 Hybrid-Electric Aircraft Performance Coefficients

The energy management tool (refer to Section 3.3) provides the aircraft performance coefficients, i.e., optimal block fuel, to FLEET. The energy management tool is run for all four 8 MW hybrid-electric aircraft, considering seven route lengths, from 300 nmi to 900 nmi at 100 nmi intervals, and a load factor of 80%, i.e., (185∗0.8 =) 148 passengers. Figure 4.3 shows the block fuel characteristics of the four hybrid-electric aircraft in consideration

at 80% load factor. As expected, the block fuel savings increase as we move from case 1 (least technologically advanced) to case 4 (most technologically advanced), and from a shorter route to a longer route. As visible in Figure 4.3, the block fuel for all cases varies almost linearly with route length, making it reasonable to use linear regression to calculate the block fuel values for all the eligible routes in FLEET. Current work uses the seven data points shown in Figure 4.3 for each hybrid-electric aircraft to calculate the block fuel values across the whole route network using linear regression; this approach leads to computational time savings as the energy management tool is run only for a limited number of route lengths.

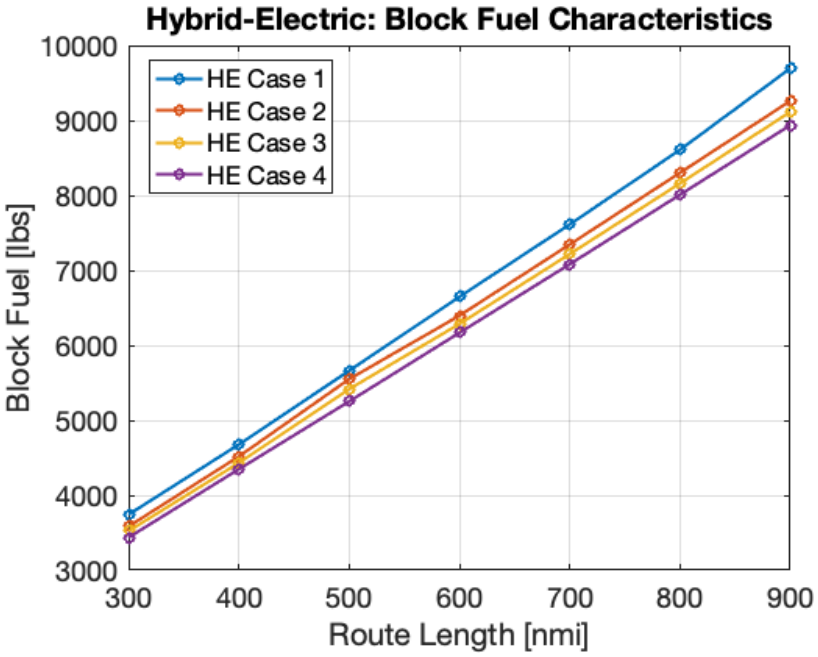

Figure 4.3. Hybrid-electric aircraft block fuel characteristics for all four aircraft technology cases in consideration (at 80% load factor)

4.3.2 Economic Factors

4.3.2.1 Aircraft Cost Modeling

This work uses the aircraft cost model discussed by Yang et al. [130] with updates to some cost components that reflect the acquisition and operating costs for a single-aisle hybrid-electric aircraft. The cost model estimates the acquisition cost and the operating

costs separately. The acquisition cost is based on the modified DAPCA (Development and Production Costs for Aircraft) model described by Raymer [91], and is calibrated using existing commercial aircraft cost data for different aircraft sizes. The operational costs – non-fuel direct operating costs (DOC) and indirect operating costs (IOC) – are based on the cost estimation equations from the Air Transportation Association of America (ATA) model [131], a DOC + Interest estimation developed by Liebeck [132], and a non-fuel DOC + IOC cost model developed for FLOPS by Johnson [133].

The acquisition cost for a hybrid-electric aircraft is expected to be higher compared to a conventional (all fuel-burning) aircraft of the same size because of the addition of a hybrid-electric propulsion system. The hybrid-electric propulsion system is expected to be costlier than a conventional propulsion system (gas turbine engine) because of the development costs associated with high-power-density electric motors, power electronics, thermal systems, and batteries – all of which are expected to accrue in the acquisition cost of the hybrid-electric aircraft. Since no direct methods or tools exist to estimate the exact development costs for electric motors and batteries, this work assumes that these costs will cause a 10% increase in the total acquisition cost compared to a conventional aircraft of the same size. For reference, gas turbine engine development cost for a conventional aircraft accounts for approximately 10% of the total acquisition cost.

4.3.2.2 Energy Cost Modeling

The fuel cost in FLEET is based on the predictions by EIA up to 2050, with some adjustments discussed in Ref. [117]. This work considers three fuel price cases – 'reference', 'low', and 'high'. The fuel prices are linearly extrapolated to 2055 based on the case-wise fuel price growth percentages provided in the 2022 EIA database [134]. Figure 4.4 shows the three sets of the adjusted fuel prices based on the 2012 EIA [135] reference fuel price case and the matching of the ASCENT Project 10 [117] survey respondents' estimates of 2050 prices. In the 'reference' fuel price scenario, the fuel prices grow according to the 2012 EIA reference fuel price case with a slight adjustment so that the fuel price in 2050 reaches \$77.08/bbl price, followed by a 1% annual growth in price until 2055. In the 'low' fuel

price scenario, the fuel prices grow according to the 2012 EIA reference fuel price case with adjustments to reach $41.00/bbl price in 2050, followed by a 0.8% annual growth in price until 2055. In the 'high' fuel price scenario, the fuel prices grow according to the 2012 EIA reference fuel price case with adjustments to reach $180.81/bbl price in 2050, followed by a 1.2% annual growth in price until 2055.

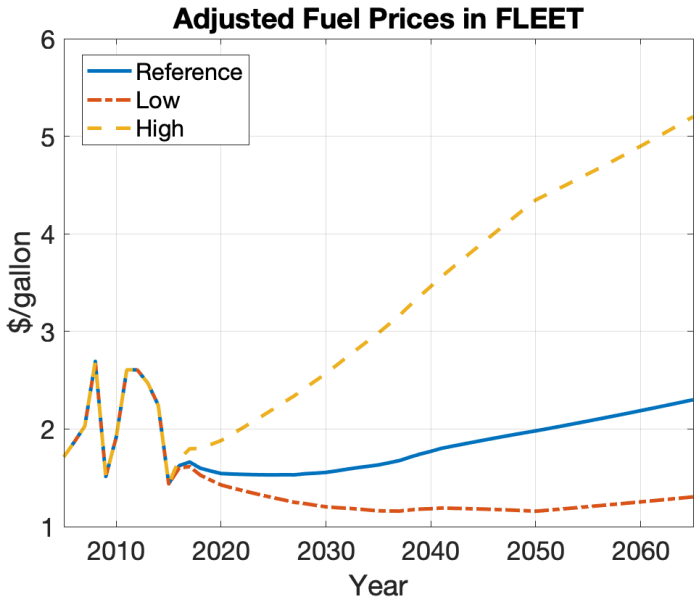

Figure 4.4. Adjusted fuel prices in FLEET

The electricity cost in FLEET is based on the 2022 EIA [134] electricity cost predictions. This work considers three electricity price cases – 'reference', 'low', and 'high'. The electricity cost employed is EIA's average price to all users until 2050, followed by linear extrapolation to 2055 based on case-wise electricity price growth percentages provided in the 2022 EIA database [134]. In the 'reference' electricity price scenario, the electricity prices follow the 2022 EIA reference electricity price trend, followed by a 0.3% annual reduction in price until 2055. In the 'low' electricity price scenario, the electricity prices follow the 2022 EIA low economy electricity price trend, followed by a 0.3% annual reduction in price until 2055. Similarly, in the 'high' electricity price scenario, the electricity prices follow the 2022 EIA high economy electricity price trend, followed by a 0.2% annual reduction in price until 2055. Figure 4.6 shows the three sets of electricity prices in FLEET.

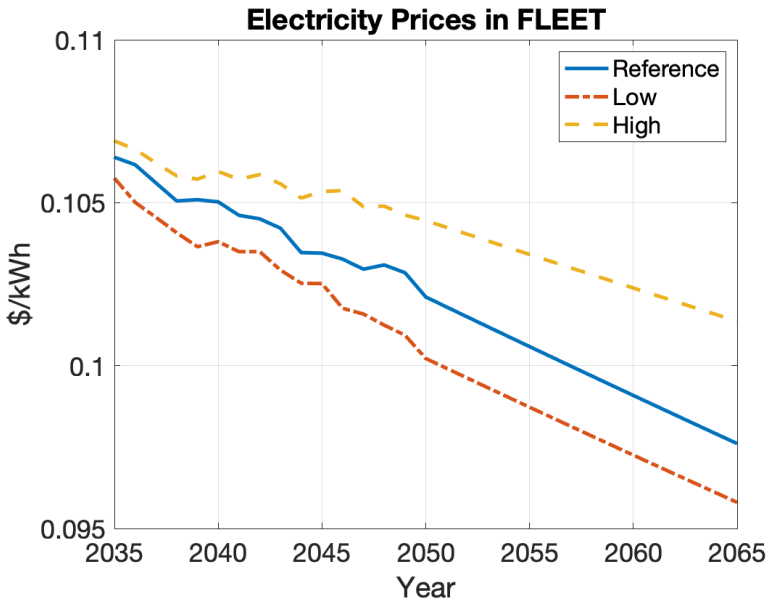

Figure 4.5. Electricity prices in FLEET

4.3.2.3 Total Operating Cost for Hybrid-Electric Aircraft

In FLEET, the non-fuel DOC consists of maintenance cost, crew cost, insurance, servicing cost, IOC, and acquisition cost. The total DOC for conventional aircraft is the sum of the non-fuel DOC and the fuel cost. For hybrid-electric aircraft, the total DOC also considers the electricity cost, i.e., the cost incurred to charge the hybrid-electric aircraft batteries before every flight. Hence, the total DOC for a hybrid-electric aircraft is the sum of the non-fuel DOC, fuel cost, and electricity cost. Table 4.4 compares the total DOC (for year 2036 on sample route – LGA-ORD) for all four hybrid-electric aircraft with the "business-as-usual" conventional future-in-class 3 aircraft they replace in FLEET.

The total DOC of the hybrid-electric aircraft (future-in-class 3) in FLEET is higher than that of a corresponding class conventional aircraft (future-in-class 3), mainly due to an increase in the maintenance and servicing cost of the hybrid-electric aircraft. Although the fuel cost for the hybrid-electric aircraft is lower than future-in-class 3 conventional aircraft (an outcome of partial electrification), the total energy cost (sum of fuel cost and electricity cost) for all four hybrid-electric aircraft is higher than the fuel cost for the future-in-class 3

Table 4.4. Total Direct Operating Cost (DOC) for hybrid-electric and "business-as-usual" conventional future-in-class 3 aircraft in FLEET (for year 2036 on sample route – LGA-ORD)

Costs [$]	HE Case 1	HE Case 2	HE Case 3	HE Case 4	Future-in-class 3 (non-HE)
Non-fuel DOC	13,206.30	13,085.97	13,079.91	13,040.33	9,883.59
Fuel Cost	1,689.90	1,625.64	1,598.20	1,569.37	1,721.70
Electricity Cost	185.64	180.68	180.25	161.03	0.00
Total DOC	15,081.84	14,892.28	14,858.36	14,770.72	11,605.29

conventional aircraft. The increase in total DOC also leads to a visible increase in the fares charged for flying on routes with hybrid-electric aircraft operations in FLEET.

4.3.3 Life-cycle CO_2 Emission Intensity

In FLEET, the CO_2 emission intensity of Jet-A fuel is assumed to be 3.67 lb-CO_2/lb-fuel, considering all life-cycle emissions. The CO_2 emission intensity of electricity considering life-cycle emissions is not a constant number, rather it changes every year based on the changes in the sources of electricity production, with renewable sources (like solar or wind) leading to lower emission intensities compared to non-renewable sources (like coal or natural gas). The 2022 EIA database [134] provides source-wise electricity production predictions until 2050. The database considers five main sources for electricity production – coal, petroleum / oil, natural gas, nuclear power, and renewable sources. This work estimates the overall life-cycle emission intensity from electricity production for a given year by calculating the weighted average of the emissions intensities from all five electricity production sources. After 2050, the electricity production trend follows the source-wise electricity production growth percentages available in the EIA database [134]. Equation 4.6 depicts the expression used to calculate the overall life-cycle emission intensity.

$$EI = \frac{\sum_k ElecProd_k * EI_k}{ElecProd_{total}} \tag{4.6}$$

where, k refers to electricity sources – coal, oil, natural gas, nuclear power, and renewables, $ElecProd_k$ refers to the electricity produced (in kWh) by source k in a year, EI_k refers to the emission intensity from source k, and $ElecProd_{total}$ refers to the total electricity produced (in kWh) in a year.

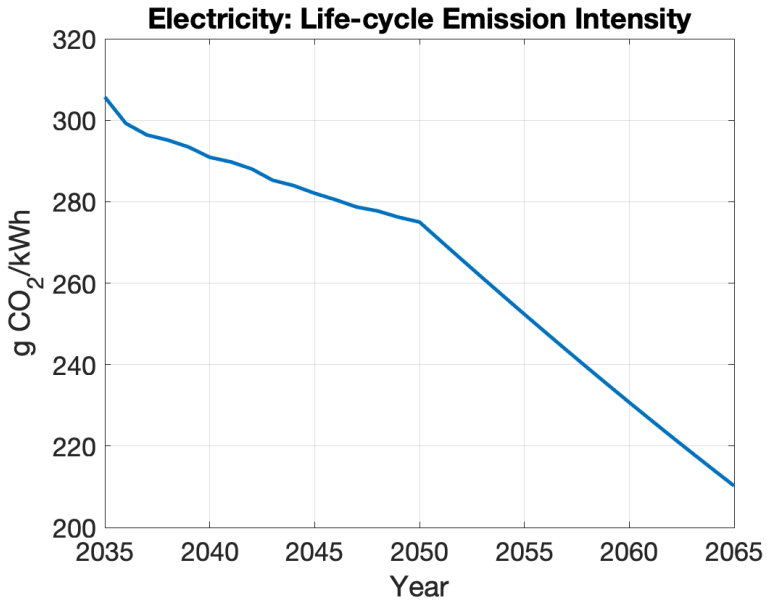

Figure 4.6. Life-cycle CO_2 emission intensity of electricity in FLEET

The life-cycle emission intensities for the different sources, EI_k, are adapted from the values published by NREL [136]. The life-cycle emission intensity value for renewables is determined using the weighted average of the emission intensities from different renewable sources (wind, hydropower, solar, biomass, and geothermal) and their contributions (in kWh) to total electricity production [137]. Figure 4.6 shows the life-cycle CO_2 emission intensity of electricity; the yearly CO_2 emissions from electricity are calculated as a product of the emission intensity for a given year and the electricity used to charge hybrid-electric aircraft (proportional to the number of trips flown) over a whole year.

5. MODELING THE IMPACT OF HYBRID-ELECTRIC AIRCRAFT ON FUTURE FLEET-LEVEL EMISSIONS

The FLEET simulation is run from years 2005 to 2055 with single-aisle parallel hybrid-electric aircraft introduced as future-in-class 3 aircraft in 2035. Year 2055 is chosen as the final year of the simulation because of two reasons. First, the typical gap in EIS date between two consecutive aircraft generations in FLEET is 15-20 years, and the latest aircraft in FLEET has an EIS date of 2040 (refer to Table 4.1). Following the "business-as-usual" aircraft EIS trend in FLEET, a new advanced technology aircraft needs to be introduced in FLEET in the late-2050s. Running the FLEET simulation until 2055 allows us to prevent an overlap with a new technology aircraft of the 2050s. Second, year 2055 is far enough from the EIS date of the hybrid-electric aircraft (2035) to allow us to analyze a majority of the impact that the induction of single-aisle hybrid-electric aircraft might have at a fleet-level.

In FLEET simulations, the aircraft are available to the airline to use one year after its EIS date (i.e., the aircraft was first available during the EIS year, but the representative day when that aircraft was part of regular service is the year following the EIS). Hence, the hybrid-electric aircraft becomes available for allocation by the airline for a representative day in 2036. The FLEET results only include CO_2 emissions due to aircraft operations; other carbon emissions related to updating current infrastructure are beyond the scope of this work.

5.1 Fleet-level Simulation Results

This work investigates the possible changes in future fleet-level CO_2 emissions with the introduction of single-aisle hybrid-electric aircraft by exploring several simulation scenarios; the scenarios include variation in hybrid-electric aircraft technology, cost of energy (for both aviation fuel and electricity), and future demand projections. The aircraft technology is varied as per the four hybrid-electric propulsion technology cases discussed in Section 3.2.1, with case 1 using the most conservative technology and case 4 using the most optimistic technology. The energy cost (including both aviation fuel and electricity) is varied from a

'low' to a 'high' value, as discussed in Section 4.3.2.2. The passenger demand projections take into account the impact of the COVID-19 pandemic on air travel demand and consider demand recovery to pre-COVID-19 (2019) levels by 2023 or 2024 as the two variations. This leads to a total of 24 scenarios using all possible aircraft technology, energy cost, and demand projection combinations. Table 5.1 lists all these combinations, with the red colored text signifying the primary scenario.

Table 5.1. FLEET simulation scenarios considering hybrid-electric aircraft technology, energy price, and future demand projections

		Hybrid-Electric Aircraft Technology			
2023 Recovery (*2023r*)		**Case 1**	**Case 2**	**Case 3**	**Case 4**
Energy Price	**Low**	*2023r + Case 1 + Low*	*2023r + Case 2 + Low*	*2023r + Case 3 + Low*	*2023r + Case 4 + Low*
	Reference	*2023r + Case 1 + Reference*	*2023r + Case 2 + Reference*	*2023r + Case 3 + Reference*	*2023r + Case 4 + Reference*
	High	*2023r + Case 1 + High*	*2023r + Case 2 + High*	*2023r + Case 3 + High*	*2023r + Case 4 + High*
2024 Recovery (*2024r*)		**Case 1**	**Case 2**	**Case 3**	**Case 4**
Energy Price	**Low**	*2024r + Case 1 + Low*	*2024r + Case 2 + Low*	*2024r + Case 3 + Low*	*2024r + Case 4 + Low*
	Reference	*2024r + Case 1 + Reference*	*2024r + Case 2 + Reference*	*2024r + Case 3 + Reference*	*2024r + Case 4 + Reference*
	High	*2024r + Case 1 + High*	*2024r + Case 2 + High*	*2024r + Case 3 + High*	*2024r + Case 4 + High*

5.1.1 Primary Scenario

With the current modeling, the 2055 fleet-level CO_2 emissions with the introduction of single-aisle parallel hybrid-electric aircraft in 2035 are 1.21% lower than the baseline "business-as-usual" case (with no hybrid-electric aircraft). Figure 5.1 shows the normalized CO_2 emissions for both the cases. The hybrid-electric aircraft considered in this scenario is 'case 1 - 8MW', i.e., the one with the most conservative hybrid-electric propulsion technology (refer to Section 3.2.1). The fleet-level CO_2 emissions for the case with hybrid-electric aircraft are slightly higher than the baseline "business-as-usual" case until year 2049 (with a maximum increase of 0.74% compared to the baseline case), followed by a continuous reduction in emissions up to year 2055. The difference in CO_2 emissions for the two cases

from years 2036 to 2052 is not large enough to be clearly visible in Figure 5.1. Figure 5.2 shows the passenger demand and the trips flown for both the cases.

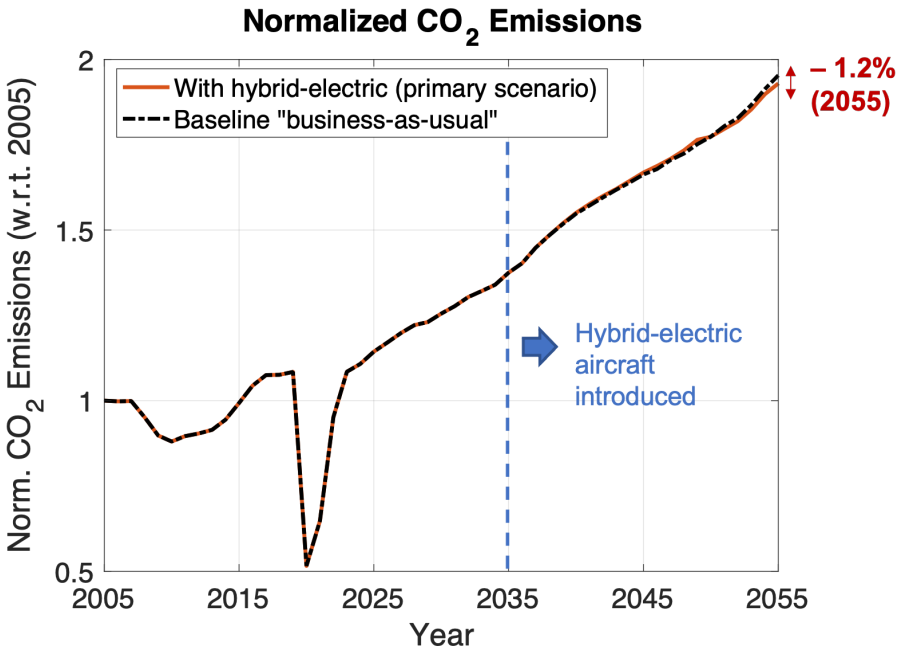

Figure 5.1. Normalized fleet-level CO_2 emissions for primary scenario from FLEET simulation

The reduction in fleet-level CO_2 emissions with the induction of single-aisle hybrid-electric aircraft in the airline fleet does not seem to be proportional to the aircraft-level fuel consumption benefit seen in the previous chapters. There are two main reasons for this behavior – 1) limited range of the hybrid-electric aircraft compared to a conventional aircraft of the same passenger capacity, and 2) higher operational cost of the hybrid-electric aircraft compared to the conventional future-in-class 3 aircraft it replaces.

The introduction and allocation of the range-limited hybrid-electric aircraft in FLEET causes the airline to change the usage, retirement and acquisition of its conventional aircraft. Essentially, the airline modifies its conventional aircraft allocation for classes 4, 5 and 6 after year 2035 to accommodate the new reduced-range class of single-aisle hybrid-electric aircraft. The change in the utilization of the conventional aircraft fleet when hybrid-electric aircraft are introduced is visible by comparing the two charts in Figure 5.3. In the figure, each layer (represented by a different color) in both charts indicates the class-wise CO_2 emissions from

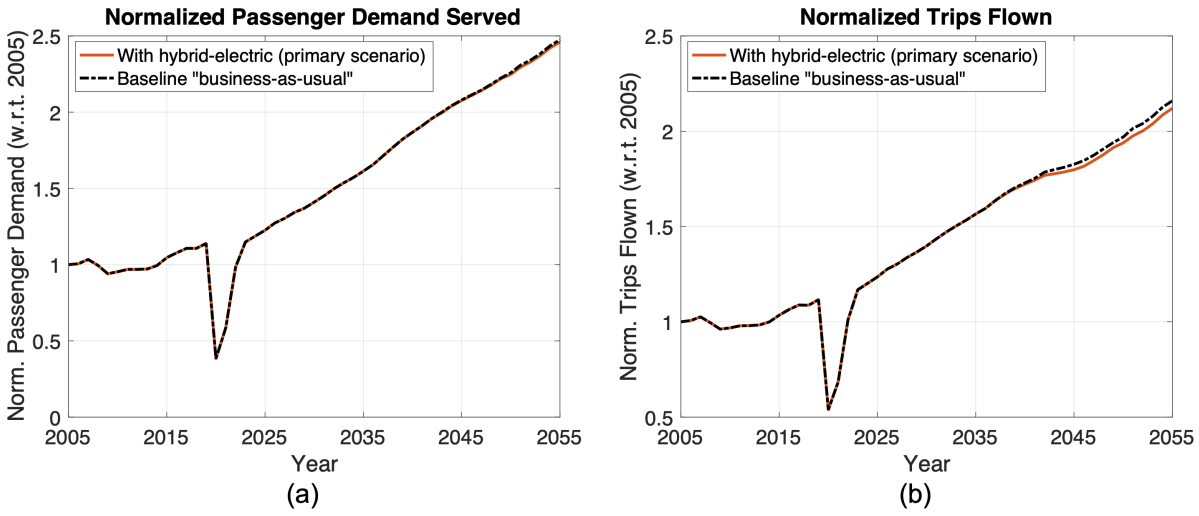

Figure 5.2. Primary scenario – (a) passenger demand served, (b) number of trips flown

each of the six classes of subsonic aircraft in FLEET, with overall CO_2 emissions from class 1 aircraft appearing at the bottom and the overall CO_2 emissions from class 6 stacked at the top. Comparing the two charts, the pattern differs significantly after 2035, indicating a drastic change in the CO_2 emissions (and the allocation) of the conventional aircraft fleet after the introduction of hybrid-electric aircraft in 2035.

As expected, the contribution of class 3 aircraft to overall CO_2 emissions visibly reduces after 2035 (yellow layer in Figure 5.3a) due to the introduction of the future-in-class 3 hybrid-electric aircraft. However, as these future-in-class 3 hybrid-electric aircraft are limited to a much shorter mission range of 900 nmi (compared to the 3,260 nmi range of the conventional – all Jet-A fuel burning – class 3 aircraft that they replaced), aircraft from classes 4 and 5 need to be utilized to serve the passenger demand on routes with route lengths greater than 900 nmi, i.e., routes that were predominantly served by the conventional class 3 aircraft in airline fleet until year 2035 in the simulation. Subsequently, this leads to an increase in the contribution of classes 4 and 5 to the fleet-level CO_2 emissions (compare the purple and green layers in Figures 5.3a and 5.3b) because they are now utilized less efficiently on routes much shorter than their design ranges to satisfy the passenger demand, offsetting the reduction in CO_2 emissions from future-in-class 3 hybrid-electric aircraft after 2035.

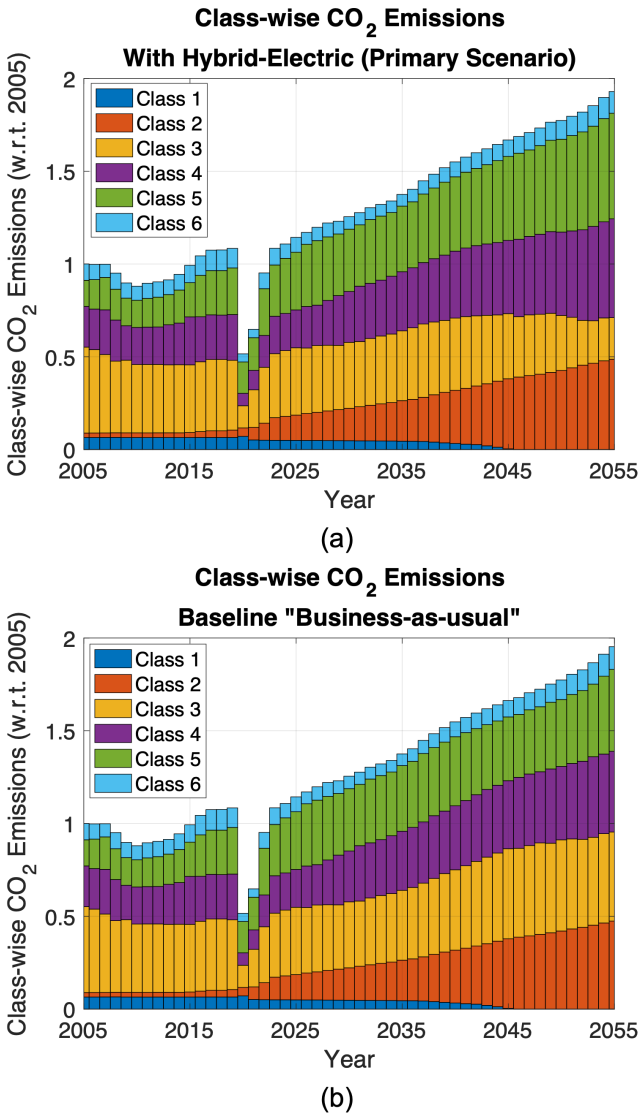

Figure 5.3. Class-wise CO_2 emissions – (a) primary scenario with hybrid-electric aircraft, (b) baseline "business-as-usual" scenario

Additionally, the higher cost of operation associated with the hybrid-electric aircraft (Table 4.4 shows the sample operating cost) pushes the airline further to allocate aircraft from other classes – mainly classes 4 and 5 – on routes previously served by class 3 aircraft to maintain overall profitability. By 2053, the airline's class 3 aircraft fleet consists only of hybrid-electric aircraft, but still, the future-in-class 3 hybrid-electric aircraft only serve 404 routes out of the 1,182 eligible routes in FLEET in 2055 (with only 2,917 daily round-trips). In contrast, the conventional future-in-class 3 aircraft for the baseline "business-as-usual"

case serve 772 routes with 3,740 daily round-trips, indicating that the limited range and higher operation costs of the hybrid-electric aircraft hinder their widespread allocation in FLEET.

5.1.2 Additional Scenarios

5.1.2.1 Variation in Hybrid-Electric Aircraft Technology

The scenarios presented in this section explore the impact of hybrid-electric aircraft technology on future fleet-level CO_2 emissions. The hybrid-electric aircraft considered here are 'case 1 - 8MW', 'case 2 - 8MW', 'case 3 - 8MW', and 'case 4 - 8MW', and are summarized in Table 3.3 (Section 3.2.2). To properly capture the impact of the hybrid-electric aircraft technology, the energy cost and passenger demand projection are held constant and set to 'reference' cost and '2023 recovery' values, respectively.

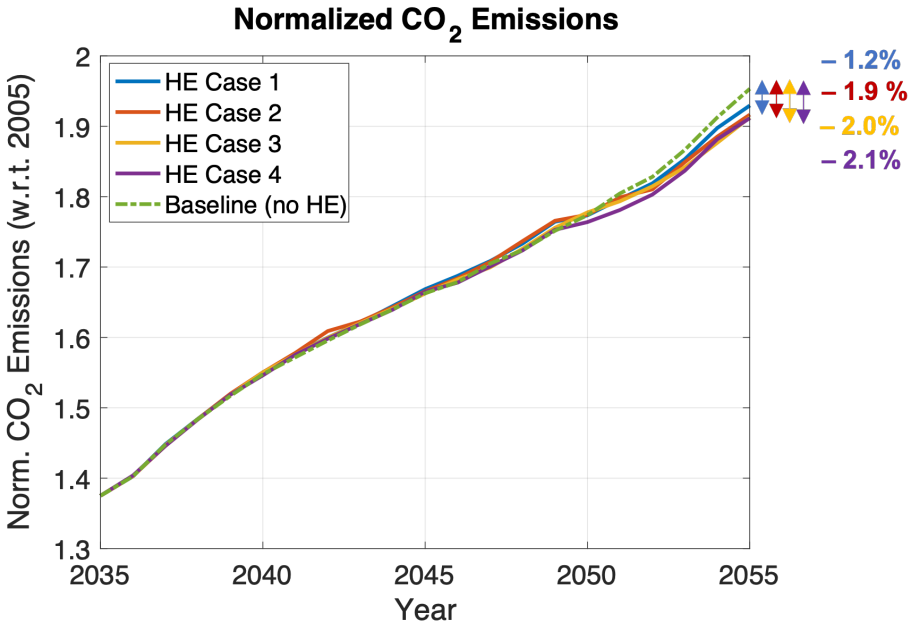

Figure 5.4. Fleet-level CO_2 emissions considering variations in hybrid-electric aircraft technology; based on the *'2023r + Reference'* scenario

Figure 5.4 shows the changes in future fleet-level CO_2 emissions with the introduction of the four different technology hybrid-electric aircraft (separately) in FLEET. As expected, we see a maximum reduction in 2055 emissions when we introduce the most fuel-efficient case 4

hybrid-electric aircraft (one with the most advanced hybrid-electric technology), compared to the baseline "business-as-usual" case. The 2055 CO_2 emissions reduce by 2.1% for case 4, 2.0% for case 3, 1.9% for case 2, and 1.2% for case 1 (one with most conservative hybrid-electric technology). The case 4 hybrid-electric aircraft leads to early fleet-level emission reduction benefits compared to all other cases, starting from year 2049 (depicted by the purple solid line in Figure 5.4).

Analyzing the class-wise CO_2 emission charts shown in Figure 5.5, the introduction of hybrid-electric aircraft causes significant changes in the contribution of different classes to fleet-wide emissions. As expected, the class 3 emissions for all four cases are lower than the baseline case; however, the emissions from classes 2, 4, and 5 are higher for all four cases (except for class 2 emissions for case 3). Because all the charts in Figure 5.5 are scaled similarly, the significant reduction in emissions from the class 3 fleet is clearly off-set by the classes 2, 4, and 5 fleets. For example, considering year 2055 for case 3 (depicted by solid yellow line in all charts in Figure 5.5), even with reduced emissions from class 2 fleet (Figure 5.5a), class 3 fleet (emissions are minutely lower than case 4 – Figure 5.5d), and class 5 fleet (Figure 5.5d), the overall emissions are slightly higher than case 4 due to much higher emissions from class 4 (signifying that the airline finds it more profitable in this case to operate class 4 instead of class 2 aircraft on routes that are not profitable for class 3 hybrid-electric aircraft – Figure 5.5c). The CO_2 emission trends due to the introduction of case 3 and case 4 hybrid-electric aircraft are very close after year 2052, with a maximum difference of 0.32% in fleet-level emissions. This indicates that the based on the current modeling, fleet-level benefits possible from the introduction of highly advanced case 4 aircraft are negligible compared to the additional research and development costs and effort involved in developing the highly advanced case 4 hybrid-electric technology over the technology present in case 3, which might make technology advancement for single-aisle hybrid-electric aircraft economically infeasible after a particular stage (that stage is case 3 hybrid-electric technology for the current discussion).

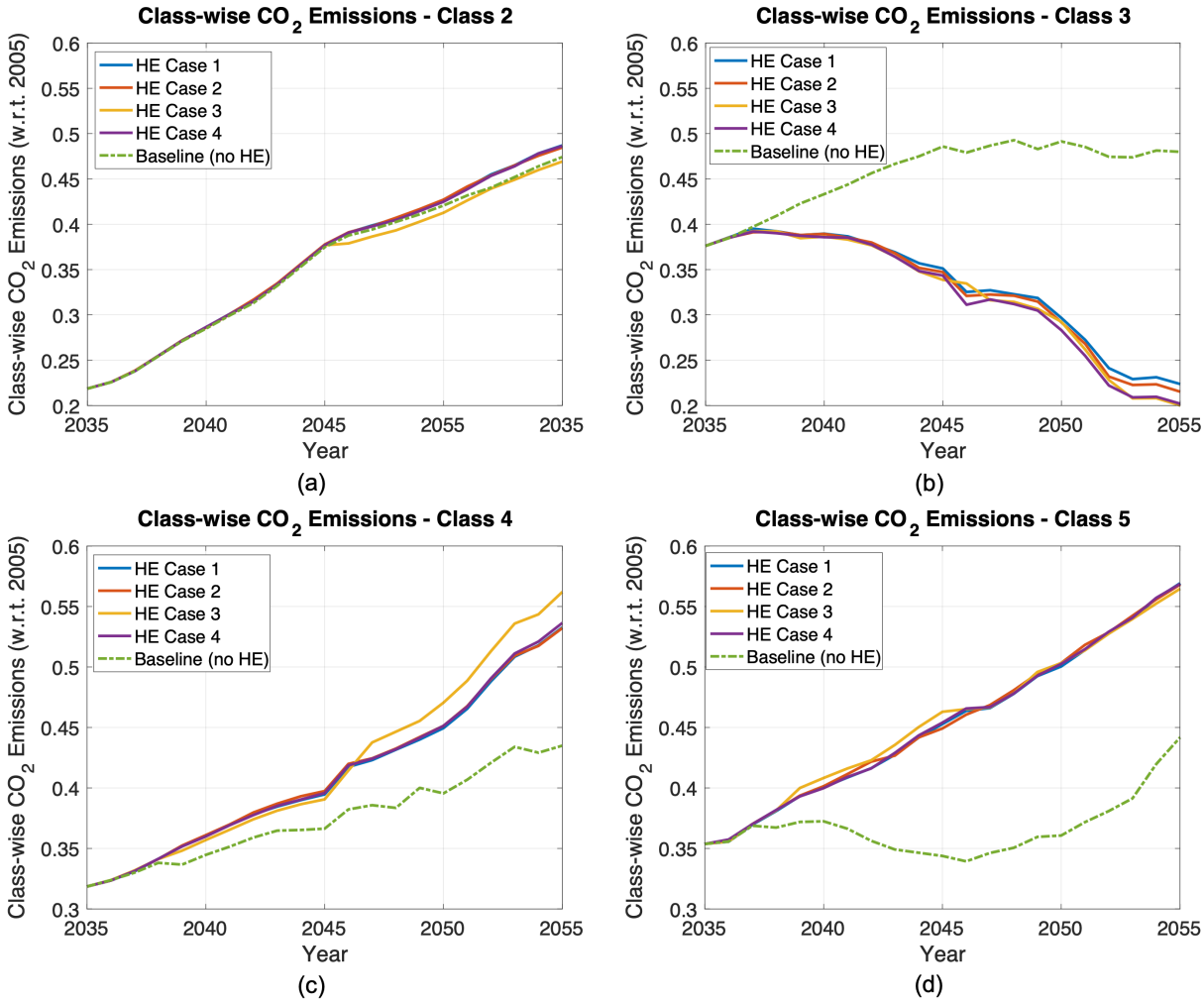

Figure 5.5. Class-wise CO_2 emissions considering variations in hybrid-electric aircraft technology – (a) class 2, (b) class 3, (c) class 4, and (d) class 5; based on the *'2023r + Reference'* scenario

5.1.2.2 Variation in Energy Cost

The FLEET simulation runs conducted here explore the impact of fuel cost and electricity cost on future fleet-level CO_2 emissions; the energy costs (fuel and electricity) considered here are 'reference', 'low', and 'high' (Section 4.3.2.2 provides a detailed description of the cost modeling in FLEET). This study could help to directly influence future policy making decisions regarding levying higher carbon taxes, or regulating aviation fuel price, to either mold passenger demand or airlines' environment-friendly growth strategies. To solely capture

the impact of energy cost on emissions at a fleet-level, the hybrid-electric aircraft technology and passenger demand projection are held constant and set to 'case 1' hybrid-electric aircraft and '2023 recovery' value, respectively. Figure 5.6 shows the changes in future fleet-level CO_2 emissions with variations in the energy cost in FLEET, along with their respective baseline "business-as-usual" (without hybrid-electric aircraft) emissions.

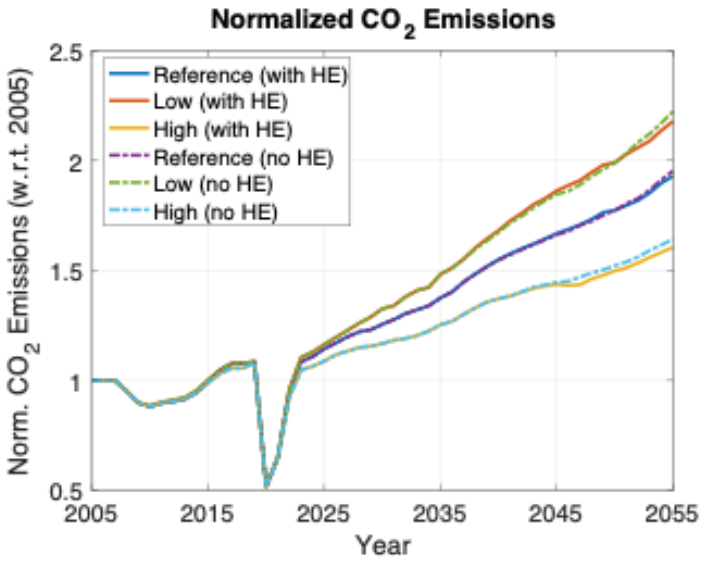

Figure 5.6. Fleet-level CO_2 emissions considering variations in energy cost; based on the *'2023r + HE case 1'* scenario

As expected, the scenario with 'high' energy costs leads to the lowest fleet-level emissions after 2022 for both with hybrid-electric and baseline (without hybrid-electric) cases. The introduction of case 1 hybrid-electric aircraft leads to a 2.25% reduction in CO_2 emissions in 2055 compared to the 'high' baseline case. Comparing with the scenarios with 'low' and 'reference' energy costs, the 'high' energy cost scenario leads to 26.17% and 15.92% reduction in 2055 emissions for the baseline (no hybrid-electric) cases, and 26.34% and 16.80% reduction in 2055 emissions for the cases with hybrid-electric aircraft.

One of the reasons for the lower emissions from the 'high' energy cost scenario is that the high energy price (for both aviation fuel and electricity) directly impacts the operating cost of the aircraft, causing the airline to charge higher ticket fares, which subsequently lowers passenger demand and airline operations, ultimately leading to lower fleet-level CO_2 emissions in the simulation. Figure 5.7 shows the passenger demand and trips flown in

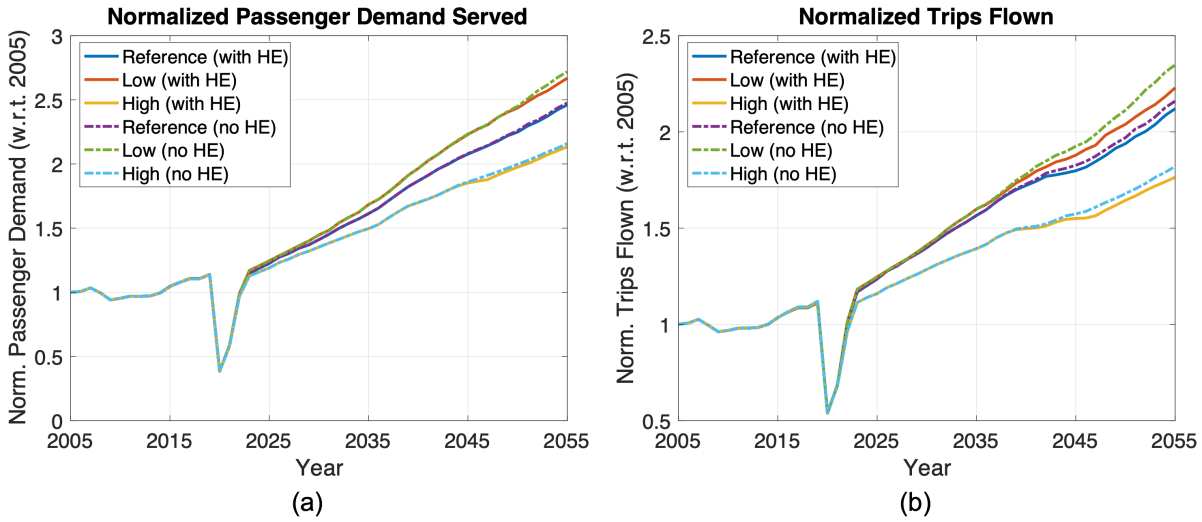

Figure 5.7. Variation in energy cost – (a) passenger demand served, (b) number of trips flown, all normalized with respect to the 2005 values; based on the *'2023r + HE case 1'* scenario

FLEET for the different energy costs in consideration; it is clearly visible from the figure that 'high' energy cost leads to lower passenger demand, and subsequently, lower number of trips flown. Another reason for the lower emissions from the 'high' energy cost scenario is a change in the airline's usage, retirement and acquisition of its aircraft when the fuel cost is high. Figure 5.8 shows the class-wise contribution to fleet-level emissions for all the cases. Analyzing Figure 5.8b, the airline tends to use more class 5 aircraft than class 4 aircraft, which is very different compared to the other two energy price cases (5.8a and 5.8c).

Similarly, the scenario with 'low' energy costs leads to the highest fleet-level emissions for both with hybrid-electric and baseline (without hybrid-electric) cases, which is an attribute of the higher passenger demand (and subsequently higher number of trips flown) seen for the case. The introduction of case 1 hybrid-electric aircraft leads to a 2.02% reduction in CO_2 emissions in 2055 compared to the baseline case. The 'reference' energy cost scenario lies almost in the middle in terms of the future fleet-level CO_2 emission predictions (see Figure 5.6).

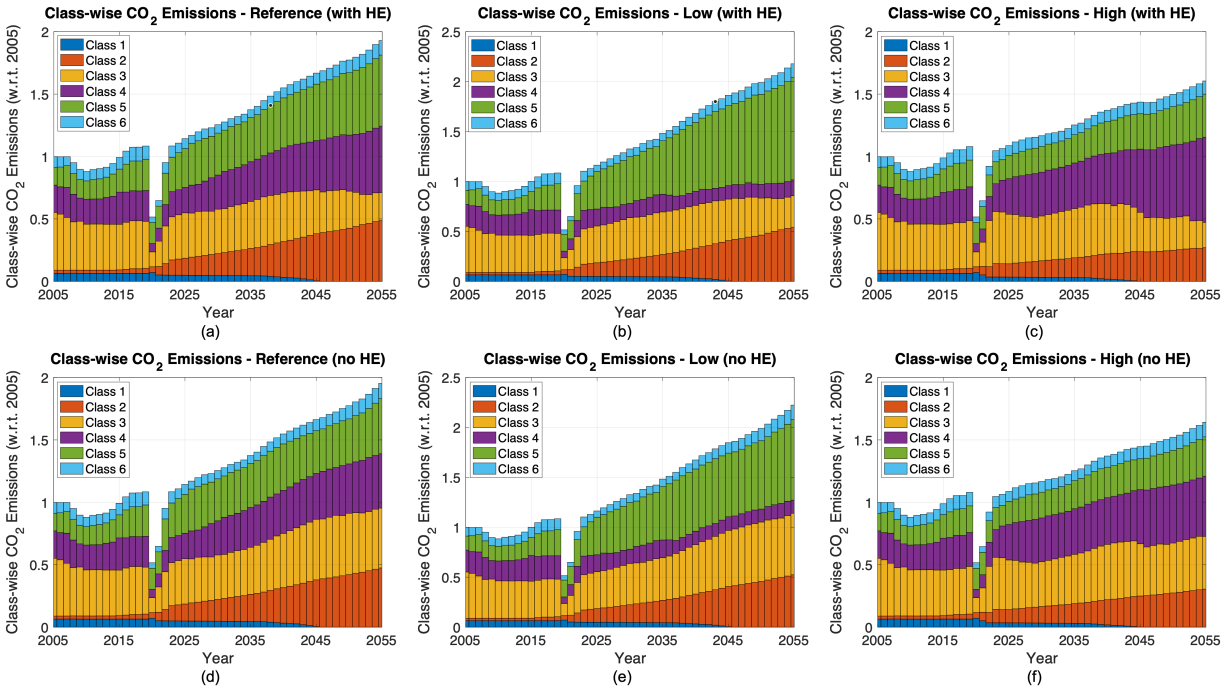

Figure 5.8. Class-wise CO_2 emissions considering variations in energy cost – (a) reference cost (with hybrid-electric), (b) low cost (with hybrid-electric), (c) high cost (with hybrid-electric), (d) reference cost (without hybrid-electric), (e) low cost (without hybrid-electric), (f) high cost (without hybrid-electric); based on the *'2023r + HE case 1'* scenario

5.1.2.3 Variation in Future Passenger Demand Projections

The FLEET simulation runs conducted in this section explore the impact of future passenger demand projections (related to recovery from COVID-19-related demand slump) on future fleet-level CO_2 emissions. This work considers the '2023 recovery' scenario (demand recovery to pre-COVID-19 levels by 2023) and '2024 recovery' scenario (demand recovery to pre-COVID-19 levels by 2024); Section 4.2 provides a detailed description of COVID-19-related demand modeling in FLEET. To capture the impact of future passenger demand projections on emissions at a fleet-level, the hybrid-electric aircraft technology and energy cost are held constant and set to 'case 1' hybrid-electric aircraft and 'reference' value, respectively. Figure 5.9 shows the changes in future fleet-level CO_2 emissions with variations in the future passenger demand projections in FLEET, along with their respective baseline "business-as-usual" (without hybrid-electric aircraft) emissions.

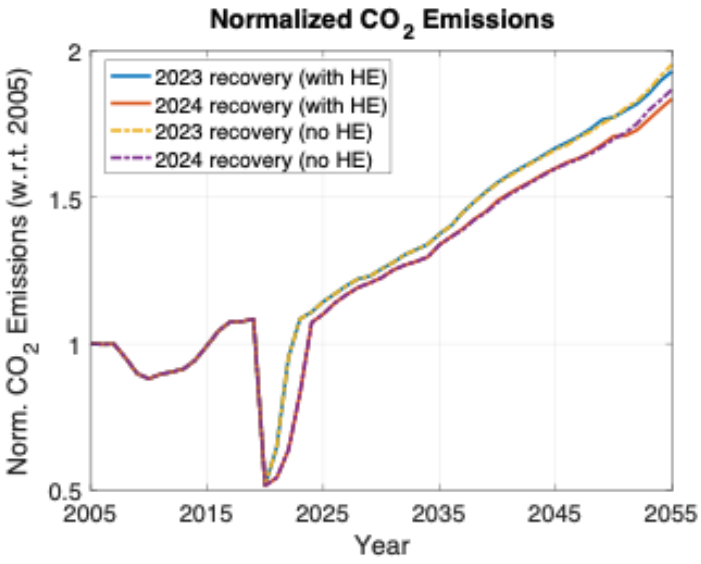

Figure 5.9. Fleet-level CO_2 emissions considering variations in future passenger demand projections; based on the *'HE case 1 + Reference'* scenario

The '2024 recovery' scenario leads to lower fleet-level emissions compared to the '2023 recovery' scenario for all years after 2020; there is a reduction of 4.35% for the baseline (no hybrid-electric) case and 4.87% for the case with hybrid-electric aircraft. This behavior is an attribute of the slower passenger demand recovery for the '2024 recovery' case, which leads to a lower overall passenger demand after the demand slump in 2020 due to COVID-19 pandemic. The lower passenger demand leads to a lower number of trips, ultimately leading to lower CO_2 emissions. Figure 5.10 shows the passenger demand and trips flown for the two passenger demand recovery scenarios in FLEET. With the introduction of hybrid-electric aircraft, the 2055 CO_2 emissions reduce by 1.23% for the '2023 recovery' case and 1.77% for the '2024 recovery' case. These results re-emphasize the fact that passenger demand can drive future fleet-level emissions and will always remain in important factor whenever we are predicting the future impact of commercial aviation.

5.1.3 Future Emission Trends

This section explores the changes in future fleet-level emissions considering all 24 scenarios with hybrid-electric (summarized in Table 5.1). The CO_2 emissions from all 24 scenarios

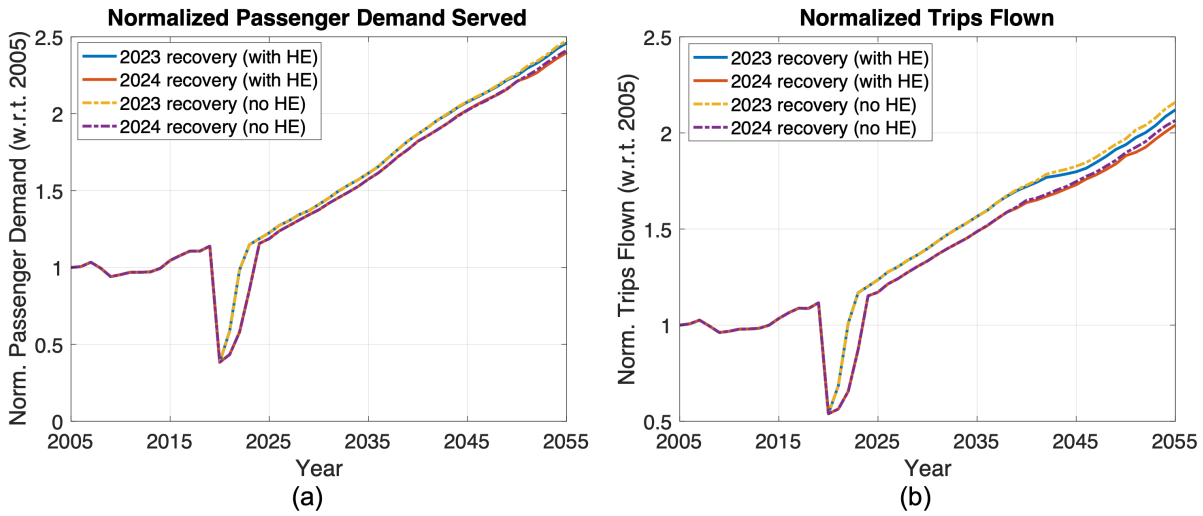

Figure 5.10. Variation in future passenger demand projections – (a) passenger demand served, (b) number of trips flown, all normalized with respect to the 2005 values; based on the *'HE case 1 + Reference'* scenario

and the six baseline scenarios ('*2023 recovery+reference cost*','*2023 recovery+low cost*', '*2023 recovery+high cost*', '*2024 recovery+reference cost*', '*2024 recovery+low cost*', '*2024 recovery+high cost*') are plotted using a box plot. Figure 5.11 shows the range of CO_2 emissions possible with the use of hybrid-electric aircraft (shown in green color) and without them ("baseline business-as-usual" – shown in black color), considering all 24 scenarios. The central round mark in the figure indicates the median, and the bottom and top edges of the box indicate the 25^{th} and 75^{th} percentiles; the whiskers extend to the most extreme data points. Following the central round marks in the figure, we can clearly see that the median value for the CO_2 emissions with the introduction of hybrid-electric aircraft starts to reduce after 2050; the degree of reduction possible in the CO_2 emissions is dependent on the scenario at hand. Based on the current modeling, the fleet-level emissions seem to reduce with more advanced hybrid-electric aircraft technology, higher energy cost, and slower demand recovery.

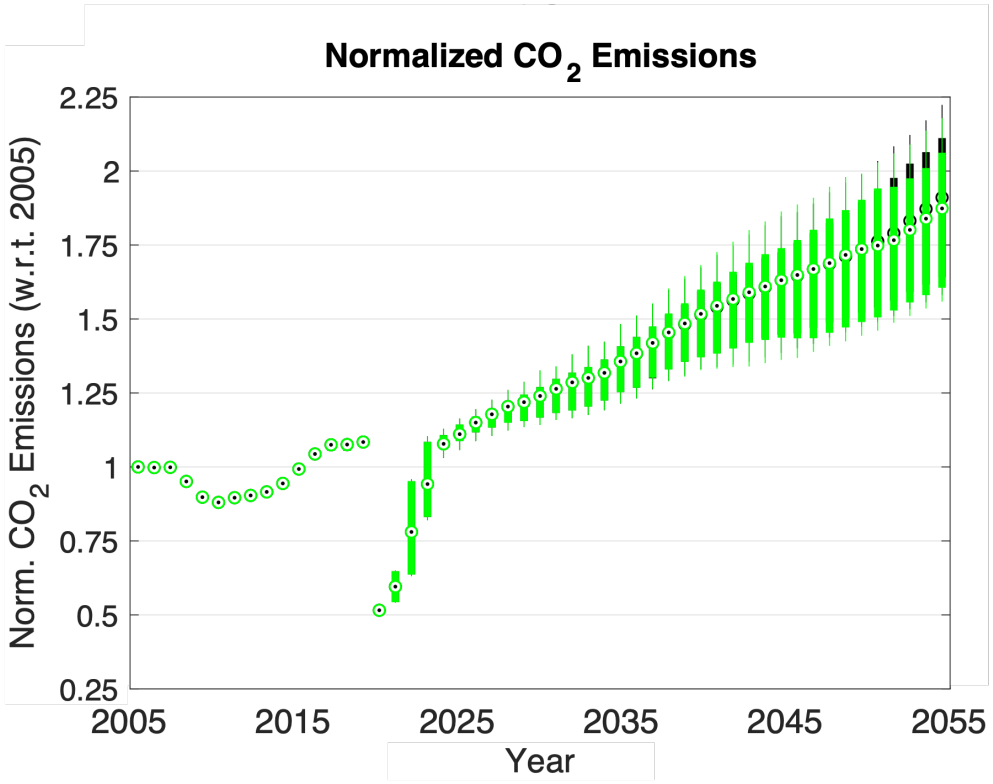

Figure 5.11. Normalized fleet-level CO_2 emissions considering all scenarios; box plot shows the median, the 25^{th} and 75^{th} percentile, and the most extreme data points, to signify the possible range of future emissions

5.2 Additional Studies

5.2.1 Impact of Hybrid-Electric Aircraft Range Capability

This study explores the impact on fleet-level emissions when a hybrid-electric aircraft with an increased design range is introduced in an airline fleet. The design range of the hybrid-electric aircraft is increased to 1,200 nmi and only the 'case 1 - 8MW' and 'case 4 - 8MW' technology cases are taken into consideration. To accomplish this study, the author sized two new hybrid-electric aircraft (case 1 and case 4, without fuselage resizing) with the increased design range of 1,200 nmi using the hybrid-electric aircraft sizing tool, followed by generating their performance coefficients using the energy management tool (using the same approach explained for all other hybrid-electric aircraft). To properly capture the fleet-

level impact of increasing the hybrid-electric aircraft range capability, the energy cost and passenger demand projection values in FLEET are held constant and set to 'reference' cost and '2023 recovery', respectively.

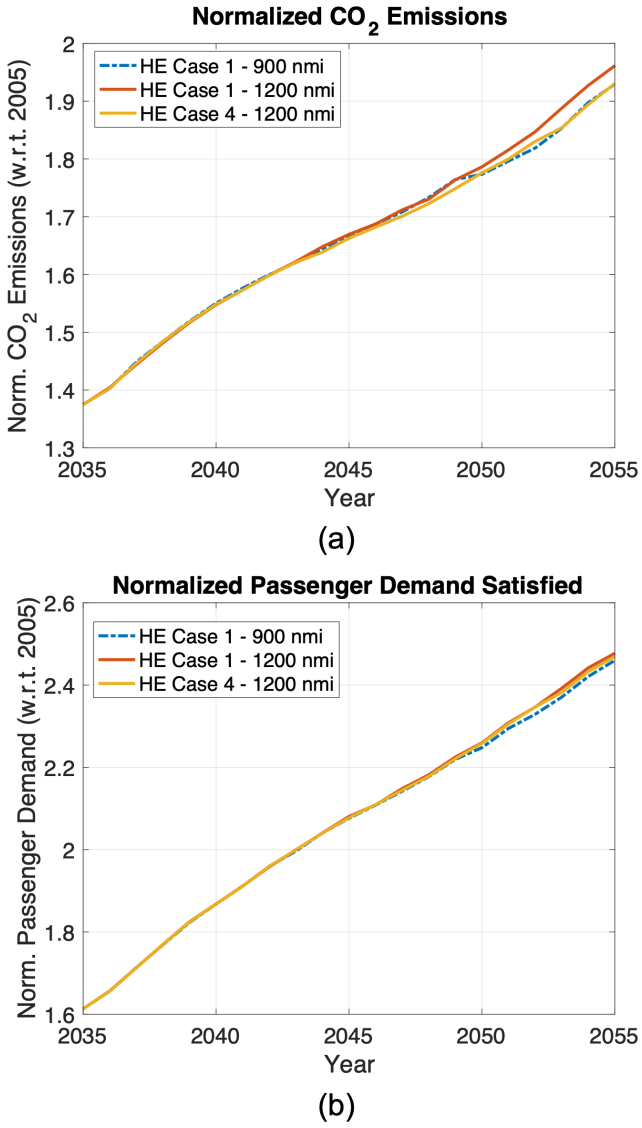

Figure 5.12. Increase in hybrid-electric aircraft range capability – (a) fleet-level CO_2 emissions, (b) passenger demand served, all normalized with respect to the 2005 values; based on the *'2023r + Reference'* scenario

Figure 5.12a shows the changes in future fleet-level CO_2 emissions with the introduction of longer range hybrid-electric aircraft in FLEET. Interestingly, we see that the overall CO_2 emissions increase by approximately 1.5% when the case 1 hybrid-electric aircraft with 1,200

nmi range are made available to the airline (denoted by red solid line in Figure 5.12a). The reason for this behavior is that the airline is now able to allocate these longer range hybrid-electric aircraft on a larger number of routes. These increased allocations increases the passenger demand served by the airline, which is accompanied by an increase in the number of trips, leading to higher fleet-level CO_2 emissions. However, when we introduce a 1,200 nmi range hybrid-electric aircraft with the most advanced technology case considered in this work, i.e., case 4 ('case 4 - 1200 nmi'), we see that the fleet-level CO_2 emissions are visibly lower compared to 'case 1 - 1200 nmi' (shown by red and yellow solid lines in Figure 5.12a). When compared to one of the 900 nmi range cases ('case 1 - 900 nmi'), 'case 4 - 1200 nmi' scenario leads to lower emissions for all years (except 2050 to 2053) even while serving a higher passenger demand; Figure 5.12b depicts the normalized passenger demand for the cases in consideration.

5.2.2 Impact of Hybrid-Electric Aircraft Non-Fuel Direct Operating Cost

As explained in Section 4.3.2.1, the total aircraft operating cost is the sum of the non-fuel DOC and the energy cost (fuel cost and electricity cost). Since the energy costs are governed by the energy cost scenarios ('reference', 'low', and 'high'), this study explores the fleet-level emission impact of changes in the future hybrid-electric aircraft non-fuel DOC. Two aircraft cost scenarios are taken into consideration – 1) the hybrid-electric aircraft non-fuel DOC is same as that of a conventional (non hybrid-electric) future-in-class 3 aircraft in FLEET (referred to as 'HE cost 1'), and 2) the hybrid-electric aircraft non-fuel DOC is only 85% of the non-fuel DOC of a conventional (non hybrid-electric) future-in-class 3 aircraft in FLEET (referred to as 'HE cost 2'). The hybrid-electric aircraft non-fuel DOCs for both the scenarios presented here are lower than the non-fuel DOC used in all the previous scenarios – as discussed in Section 4.3.2.1 (referred to as 'Reference HE cost'). To solely capture the impact of aircraft cost on emissions at a fleet-level, the hybrid-electric aircraft technology, energy cost, and passenger demand projection are held constant and set to 'case 1' hybrid-electric aircraft, 'reference' cost, and '2023 recovery' values, respectively.

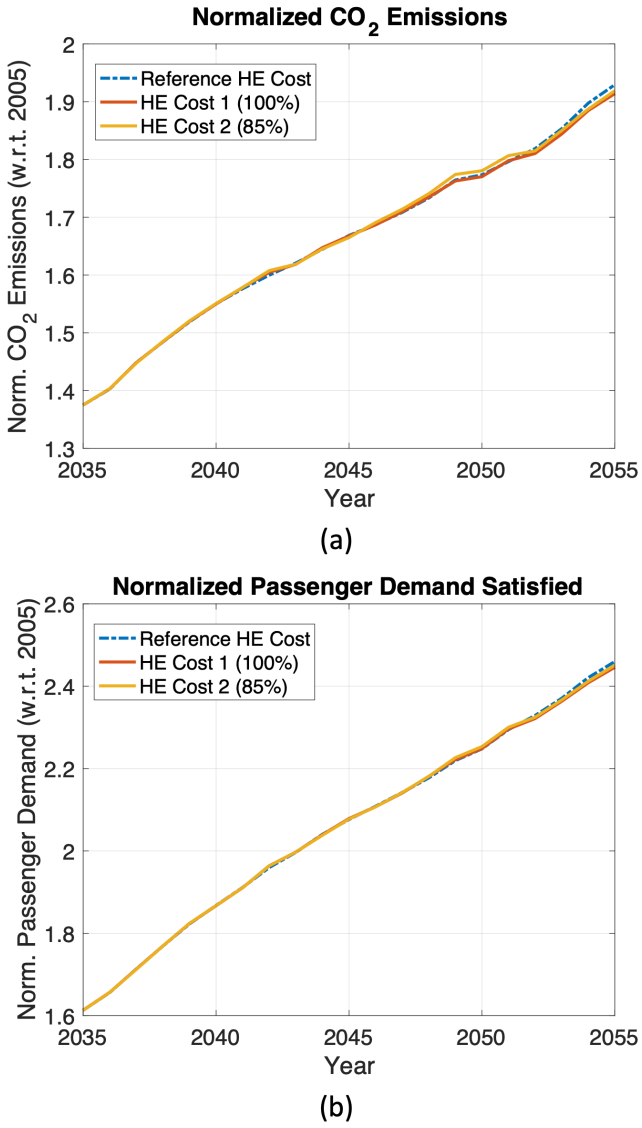

Figure 5.13. Change in hybrid-electric aircraft non-fuel DOC – (a) fleet-level CO_2 emissions, (b) passenger demand served, all normalized with respect to the 2005 values; based on the *'2023r + Reference'* scenario

Figure 5.13 shows the changes in future fleet-level CO_2 emissions with variations in the hybrid-electric aircraft cost in FLEET. As visible from Figure 5.13a, the fleet-level emissions are slightly lower after 2053 for 'HE cost 1' and 'HE cost 2' scenarios (denoted by red and yellow solid lines, respectively), with 'HE cost 1' leading to the lowest emissions in 2055. Before 2053, the fleet-level emissions for 'HE cost 1' and 'HE cost 2' scenarios are slightly higher than the 'Reference HE cost' case, with the 'HE cost 2' scenario leading to

the highest emissions. This behavior is an attribute of the fact that, as the hybrid-electric non-fuel DOC gets lower (which means that the aircraft becomes cheaper to operate), the airline increases the hybrid-electric aircraft allocations, which in turn causes a ripple effect across the allocations of all other aircraft classes. From Figure 5.13b, we can see that the airline ends up serving a slightly higher demand before 2053 for 'HE cost 1' and 'HE cost 2' scenarios, which is accompanied by higher number of trips, leading to higher emissions.

5.3 Conclusion

The results presented in this work conclude that the introduction of a single-aisle hybrid-electric aircraft in 2035 could potentially lead to reduced fleet-level CO_2 emissions compared to the baseline "business-as-usual" case with only conventional aircraft. The maximum reduction in 2055 fleet-level emissions is seen with the introduction of case 4 hybrid-electric aircraft, along with 'high' energy cost scenario and '2024 recovery' scenario. The introduction and allocation of the reduced range capability hybrid-electric aircraft changes the airline's usage, retirement and acquisition of its conventional aircraft fleet. Even though the emissions from the class 3 hybrid-electric are lower compared to the baseline case, their introduction creates a ripple effect, causing an increase in the emissions from classes 2, 4, and 5 aircraft as they need to satisfy a larger segment of the passenger demand compared to the baseline case (a combined effect of the hybrid-electric aircraft's lower range and higher operating cost).

The 2055 fleet-level CO_2 emissions vary with variations in hybrid-electric aircraft technology, energy cost, and future demand projections. As expected, more advanced hybrid-electric aircraft technology leads to lower fleet-level CO_2 emissions, as does lower future demand projection. Higher energy costs also lead to lower emissions due to a reduction in passenger demand (as the higher fuel and electricity prices get transferred to the passengers through higher ticket fares, discouraging air travel demand growth).

The additional studies provide further information about the sensitivity of the future fleet-level CO_2 emission predictions with respect to hybrid-electric aircraft range-capability and operating cost. Looking at the impact of an increase in the hybrid-electric aircraft range capability, even a 300 nmi increase in the design range of the hybrid-electric aircraft (from 900

nmi to 1,200 nmi) leads to noticeable changes in the future fleet-level emissions. Analyzing the impact of changes in the hybrid-electric aircraft operating cost (non-fuel DOC), even for a 36% reduction in the non-fuel DOC of the hybrid-electric aircraft (for 'HE cost 2' scenario compared to the reference hybrid-electric aircraft cost – discussed in Section 4.3.2.1), the changes in future fleet-level emissions are not significant. Hence, based on the current modeling, the future fleet-level CO_2 emissions could be less sensitive to the operating cost of the hybrid-electric aircraft than its range capability.

6. LIMITATIONS AND FUTURE WORK

The current work develops and validates a "flight-mechanics-based" hybrid-electric aircraft sizing tool, and then uses the tool to size multiple hybrid-electric aircraft. The sizing tool so developed uses low-fidelity approaches for propulsion modeling, aerodynamics, and weight estimation, and medium-fidelity approaches for mission analysis and geometry modeling. On the propulsion side, the current approach uses rubber engine sizing based on a baseline gas turbine engine modeled in NPSS; there is no continuous integration of the NPSS engine model with the sizing optimizer. Future work could include continuously linking the gas turbine engine model in NPSS with the sizing tool to avoid rubber engine sizing, and to provide better estimates for the electric motor and battery sizing. This approach would also allow us to model the hybrid-electric system components (motors, inverters, etc.) in NPSS, allowing for a higher fidelity. On the geometry side, current work first models the aircraft using CAD and then stretches the fuselage based on the required battery volume to accommodate the battery packs. Future work could include setting up a continuous integration of the CAD model with the sizing optimizer to allow the optimizer to explore different aircraft configurations, including unconventional configurations, while sizing the hybrid-electric aircraft.

Once the aircraft is optimally sized, the energy management tool identifies the optimal power split between the gas turbine engines and the electric motors to allow the aircraft to fly an off-design mission with minimal fuel consumption. Current work uses a traditional optimization approach to find the optimal power split that minimizes off-design mission fuel burn. This approach involves dividing the mission into smaller segments and finding a constant power split value for every segment. A continuous optimization of the power split between the two propulsion sources onboard the aircraft could lead to even lower fuel burn for a given off-design mission. Future work could include using a reinforcement learning-based (RL-based) problem setup to solve for optimal fuel consumption for an off-design mission. Such an approach will remove the mission range-based sub-segments in the cruise segment and provide a more uniform / realistic approach for controlling the gas turbine engine and

electric motor throttles. A RL-based approach will also allow us to include uncertainties, like winds-aloft, in the optimal power split solution, making it applicable in the real world.

Although the current work sheds light on the possible fleet-level impacts of introducing hybrid-electric aircraft in an airline fleet using FLEET, the results are based on FLEET's current point-to-point route network. The route network in FLEET is based on the BTS T-100 Segment data, limiting the route network to US-touching routes only, in addition to the point-to-point nature. Given the reduced range capability of the hybrid-electric aircraft, the author suspects that airlines might move to a hub-and-spoke model when the hybrid-electric aircraft are introduced in the mid-2030s. This is because the hybrid-electric aircraft could serve shorter routes to and from smaller airports (with lower passenger demand) to the hub, while the bigger (longer-range) aircraft can be used to connect different hubs. This could lead to high load factors for both hybrid-electric aircraft connecting the spokes to the hubs, and the longer-range aircraft making other busier and longer connections, potentially increasing the overall profit for airlines. Implementing such a hub-and-spoke airline model in FLEET would require a network and airline model update, which would require updating the current resource allocation problem to an assignment problem. Additionally, expanding FLEET's route network to a global network could be helpful to see the global impact of the introduction of hybrid-electric aircraft.

Future work could also include incorporating additional aircraft with electrified propulsion in the FLEET simulation to closely mimic the current (and future) aviation industry trends, leading to better estimates of future fleet-level CO_2 emissions. These additional aircraft could include a regional parallel hybrid-electric aircraft (would replace the conventional future-in-class 2 aircraft in FLEET with an EIS of 2025), a large (twin-aisle) series hybrid-electric aircraft with clean-sheet design using unconventional configurations like boundary layer ingestion, distributed electric propulsion, blended-wing-body, etc. (would replace the conventional future-in-class 4 or 5 aircraft in FLEET with an EIS of mid-2040s), and a very large turbo-electric aircraft (would replace the conventional future-in-class 6 aircraft in FLEET with an EIS of early 2050s).

7. CONCLUSION

This dissertation describes an attempt to simulate a profit-seeking "U.S.-flag carrier" airline's behavior when hybrid-electric aircraft are made available to its fleet in 2035, and to predict the subsequent total fleet carbon emissions. Since hybrid-electric aircraft modeling (sizing and performance analysis) has its own challenges as traditional sizing approaches and legacy sizing tools do not work directly for these aircraft, this work presents a sizing tool and a performance analysis tool (energy management) to enable the sizing and analysis of hybrid-electric aircraft. The fleet-level results assess the possible contribution of single-aisle hybrid-electric aircraft in driving down future fleet-level CO_2 emissions.

To appropriately model hybrid-electric aircraft, the author presents a "flight-mechanics-based" sizing tool, with an optimization problem at its core to minimize fuel consumption while meeting multiple performance and simultaneous-design-and-analysis (SAND) approach constraints. Some of the distinct features of the sizing tool include the capability to size the electric motors in conjunction with downsizing the gas turbine engines while satisfying the one-engine-inoperative and top-of-climb constraints, and the capability to re-size / stretch the aircraft fuselage to meet the volumetric constraints associated with accommodating the required battery packs. Current work considers that electric power is available only during the takeoff and climb segments, but the tool can be easily adapted to include other flight segments. Four hybrid-electric propulsion technology cases related to future battery and electric motor technology predictions are considered, with case 1 serving as the most conservative case (with low uncertainty) and case 4 serving as the most optimistic case (with very high uncertainty). This work conducts conceptual design for only a single-aisle parallel hybrid-electric aircraft with 185 seats and a design range of 900 nmi; other size hybrid-electric aircraft can be sized using the presented tool with minimal modifications.

Considering fuselage re-sizing options (with fuselage re-sizing ($wFuse$) and without fuselage re-sizing ($woFuse$)) and maximum electric motor power available to the sizing optimizer (8 MW and 20 MW), 16 hybrid-electric aircraft designs are presented, with $woFuse$ aircraft saving more fuel than the $wFuse$ aircraft, and the 20 MW aircraft saving more fuel than the 8 MW aircraft. The sized hybrid-electric aircraft showcase a minimum fuel savings of

15.6% (case 1 – $wFuse$ – 8MW) and a maximum fuel savings of 22.5% (case 4 – $woFuse$ – 20MW) compared to a Boeing 737-800 aircraft. These fuel savings reduce to 1.7% and 10.3%, respectively, when compared to a same-generation conventional aircraft sized for a design range of 900 nmi.

The sized hybrid-electric aircraft will rarely be flown for its design range of 900 nmi at a 100% load factor as a part of airline operations. To identify the aircraft's performance characteristics for an off-design mission (characterized by lower payload, or lower mission range, or both), an optimal energy management scheme that minimizes mission fuel burn while optimally using the onboard battery energy is developed. The energy management tool identifies the optimal power split between the two energy sources to minimize the fuel burn for the payload-range combination in consideration; the tool can also concurrently optimize the flight path. Current work explores two approaches for energy management with differences in cruise segment implementation – "rule-based" cruise and "variable throttle" cruise. For a standard mission (with no flight path optimization) of 637 nmi mission (LGA-ORD route) at a 80% load factor, the "rule-based" cruise energy management scheme saves about 142.1 lbs of fuel per flight compared to when there is no energy management. The "variable throttle" cruise energy management scheme saves slightly more fuel 146.1 lbs compared to when there is no energy management, but given the computational time required to obtain a solution is very high for this scheme, the "rule-based" scheme seems like the more feasible approach. When the flight path is concurrently optimized with the power split between the two energy sources, the fuel savings increase to 276.1 lbs of fuel per flight (for the same payload-range combination).

With the hybrid-electric aircraft performance coefficients generated using the "rule-based" energy management scheme, this work predicts the possible changes in future fleet-level emissions and aircraft operations using the Fleet-Level Environmental Evaluation Tool (FLEET). The fleet-level results assess the contribution of single-aisle parallel hybrid-electric aircraft in driving down future fleet-level CO_2 emissions. With the current modeling, the future fleet-level CO_2 emissions do reduce proportional to the fuel burn reductions observed for the hybrid-electric aircraft at an aircraft-level. This behavior can be majorly attributed to the limited design range and the higher operating costs associated with the hybrid-electric

aircraft compared to the single-aisle conventional aircraft they replace. The short range and higher cost of the hybrid-electric aircraft forces the airline to allocate other classes of aircraft on routes that were predominantly served by single-aisle aircraft to meet the passenger demand and maintain profitability. Although there is a reduction in emissions from the single-aisle aircraft class (due to operation of hybrid-electric aircraft), the emissions from other classes of aircraft (particularly twin-aisle and large twin-aisle) increase due to their increased number of trips (twin-aisle and large twin-aisle burn more fuel per seat-nmi, leading to more emissions), dwarfing the benefits seen by the operation of the hybrid-electric aircraft.

The 2050 fleet-level emissions vary with variations in hybrid-electric aircraft technology, energy cost, and future demand projections. As expected, more advanced hybrid-electric aircraft technology leads to lower fleet-level CO_2 emissions, as does lower future demand projection. Higher energy costs also lead to lower emissions due to a reduction in passenger demand (as the higher fuel and electricity prices get transferred to the passengers through higher ticket fares, discouraging air travel demand growth).

With the current modeling, the 2050 fleet-level CO_2 emissions with the introduction of single-aisle hybrid-electric aircraft are much higher than the 2005 CO_2 emissions levels. This clearly indicates that the 2050 CO_2 emissions goals set forth by organizations such as IATA and ICAO cannot be met just by introducing single-aisle parallel hybrid-electric aircraft to airline fleets. Although a reduction in passenger demand could get us closer to the 2005 levels, this is not a feasible solution to reducing the carbon footprint of commercial aviation.

The author firmly believes that no single aircraft technology or approach could be a solution to the carbon emission problem at hand. Rather, a combination of technologies and policy are required to reduce the overall fleet-level CO_2 emissions from commercial aviation. Sustainable aviation fuels show potential to bring some respite in fleet-level CO_2 emissions [82], given that their penetration-levels and production levels meet the required targets. Similarly, hydrogen aircraft could be a part of the solution, given that we can produce and supply hydrogen sustainably, along with figuring out some aircraft design challenges associated with propulsion and hydrogen storage onboard the aircraft. On the other hand, introducing all-electric smaller aircraft like small regional jets and regional jets could help

to further bring down emissions, when used in conjunction with other technologies. The single-aisle parallel hybrid-electric aircraft could also contribute to bringing down fleet-level emission when introduced with other technology aircraft and some policy changes to lower down their operating costs. Until then, the aviation community working on different aircraft technologies, fuels, and policy-making need to work together to ensure that all of them complement each other, rather than competing with each other.

REFERENCES

[1] B. Graver, D. Rutherford, and S. Zheng, *Co2 emissions from commercial aviation: 2013, 2018, and 2019. icct report*, 2020.

[2] *IATA - CORSIA*, Available at http://www.iata.org/policy/environment/Pages/corsia.aspx. [Online]. Available: http://www.iata.org/policy/environment/Pages/corsia.aspx.

[3] P. Steele, *A Global Framework For Addressing Aviation CO 2 Emissions*, Available at https://sustainabledevelopment.un.org/content/documents/PaulSteele.pdf. [Online]. Available: https://sustainabledevelopment.un.org/content/documents/PaulSteele.pdf.

[4] F. Collier, *Nasa concepts and technologies for green aviation*, Green Engineering Masters Forum, 2009, Retrieved March, 2020. [Online]. Available: https://www.nasa.gov/pdf/395949main_collier.pdf.

[5] W. Haller and M. Guynn, *Technical challenges to systems analysis and mdao for advanced subsonic transport aircraft*, AIAA Aerospace Sciences Meeting, 2012, Retrieved March, 2020. [Online]. Available: https://ntrs.nasa.gov/archive/nasa/casi.ntrs.nasa.gov/20150010336.pdf.

[6] R. Wahls, *Nasa n+3 technologies and concepts*, Green Aviation Summit, NASA Ames Research Center, 2010, Retrieved March, 2020. [Online]. Available: https://www.hq.nasa.gov/office/aero/pdf/wahls_2_green_aviation_summit.pdf.

[7] K. A. Moolchandani, P. Govindaraju, S. Roy, W. A. Crossley, and D. A. DeLaurentis, "Assessing Effects of Aircraft and Fuel Technology Advancement on Select Aviation Environmental Impacts," *Journal of Aircraft*, vol. 54, no. 3, pp. 857–869, May 2017, ISSN: 00218669. DOI: 10.2514/1.C033861. [Online]. Available: https://arc.aiaa.org/doi/10.2514/1.C033861.

[8] *That's how fast the carbon clock is ticking*, Mercator Research Institute on Global Commons and Climate Change, December 2018, Retrieved March, 2020. [Online]. Available: https://www.mcc-berlin.net/en/research/co2-budget.html.

[9] *According to new ipcc report, the world is on track to exceed its "carbon budget" in 12 years*, World Resources Institute, October 2018, Retrieved March, 2020. [Online]. Available: https://www.wri.org/blog/2018/10/according-new-ipcc-report-world-track-exceed-its-carbon-budget-12-years.

[10] *Ipcc, 2018: Global warming of 1.5°c. an ipcc special report on the impacts of global warming of 1.5°c above pre-industrial levels and related global greenhouse gas emission pathways, in the context of strengthening the global response to the threat of climate change, sustainable development, and efforts to eradicate poverty.* IPCC, April 2018, Retrieved March, 2020. [Online]. Available: https://www.ipcc.ch/sr15/.

[11] *Analysis: How much 'carbon budget' is left to limit global warming to 1.5c?* Carbon Budgets, Carbon Brief - Clear on Climate, April 2018, Retrieved March, 2020. [Online]. Available: https://www.carbonbrief.org/analysis-how-much-carbon-budget-is-left-to-limit-global-warming-to-1-5c.

[12] B. Graver, K. Zhang, and D. Rutherford, "Co2 emissions from commercial aviation, 2018. working paper," 2019.

[13] *Facts & figures*, ATAG - Air Transport Action Group, January 2020, Retrieved March, 2020. [Online]. Available: https://www.atag.org/facts-figures.html.

[14] *Fact sheet: The growth in greenhouse gas emissions from commercial aviation - part 1 of a series on airlines and climate change*, EESI - Environmental and Energy Study Institute, October 2019, Retrieved March, 2020. [Online]. Available: https://www.eesi.org/papers/view/fact-sheet-the-growth-in-greenhouse-gas-emissions-from-commercial-aviation.

[15] *Up in the air: How airplane carbon pollution jeopardizes global climate goals*, Center for Biological Diversity, December 2015, Retrieved October, 2019. [Online]. Available: https://www.biologicaldiversity.org/programs/climate_law_institute/transportation_and_global_warming/%20airplane_emissions/pdfs/Airplane_Pollution_Report_December2015.pdf.

[16] *Analysis: Aviation could consume a quarter of 1.5c carbon budget by 2050.* International Policy, Carbon Brief - Clear on Climate, August 2016, Retrieved October, 2019. [Online]. Available: https://www.carbonbrief.org/aviation-consume-quarter-carbon-budget.

[17] *Climate concerns could reignite commercial aerospace, or burn it*, Aviation Week Space Technology, June 2019, Retrieved October, 2019. [Online]. Available: https://aviationweek.com/commercial-aviation/climate-concerns-could-reignite-commercial-aerospace-or-burn-it.

[18] *Opinion: How the airline industry can wage war on climate change*, Aviation Week Space Technology, August 2019, Retrieved October, 2019. [Online]. Available: https://aviationweek.com/commercial-aviation/opinion-how-airline-industry-can-wage-war-climate-change.

[19] *'worse than anyone expected': Air travel emissions vastly outpace predictions*, The New York Times, September 2019, Retrieved October, 2019. [Online]. Available: https://www.nytimes.com/2019/09/19/climate/air-travel-emissions.html.

[20] *Air travel is surging. that's a huge problem for the climate.* Vox - Energy and Environment, January 2019, Retrieved October, 2019. [Online]. Available: https://www.vox.com/energy-and-environment/2019/1/11/18177118/airlines-climate-change-emissions-travel.

[21] D. Lee, L. L. Lim, and B. Owen, *Bridging the aviation co_2 emissions gap: Why emissions trading is needed*, 2013. [Online]. Available: http://www.cate.mmu.ac.uk/wp-content/uploads/Bridging_the_aviation_emissions_gap_010313.pdf.

[22] *New ipcc report shows 1.5c° is still possible, but more needed from aviation and shipping*, Carbon Market Watch, October 2018, Retrieved March, 2020. [Online]. Available: https://carbonmarketwatch.org/2018/10/08/new-ipcc-report-shows-1-5c-is-still-possible-but-more-needed-from-aviation-and-shipping/.

[23] J. L. Felder, *Nasa electric propulsion system studies*, 2015. [Online]. Available: https://ntrs.nasa.gov/archive/nasa/casi.ntrs.nasa.gov/20160009274.pdf.

[24] R. H. Jansen, C. Bowman, A. Jankovsky, R. Dyson, and J. L. Felder, *Overview of nasa electrified aircraft propulsion research for large subsonic transports*, 2017. [Online]. Available: https://ntrs.nasa.gov/archive/nasa/casi.ntrs.nasa.gov/20170012222.pdf.

[25] M. K. Bradley and C. K. Droney, "Subsonic ultra green aircraft research: Phase i final report, nasa/cr–2011-216847," Tech. Rep., 2011. [Online]. Available: https://ntrs.nasa.gov/archive/nasa/casi.ntrs.nasa.gov/20110011321.pdf.

[26] M. K. Bradley and C. K. Droney, "Subsonic ultra green aircraft research: Phase ii - volume ii - hybrid electric design exploration, nasa/cr–2015-218704/volume ii," Tech. Rep., 2015. [Online]. Available: https://ntrs.nasa.gov/archive/nasa/casi.ntrs.nasa.gov/20150017039.pdf.

[27] C. E. Lents and L. W. Hardin, "Fuel burn and energy consumption reductions of a single-aisle class parallel hybrid propulsion system," 2019. DOI: 10.2514/6.2019-4396. [Online]. Available: https://arc.aiaa.org/doi/abs/10.2514/6.2019-4396.

[28] C. Pornet, C. Gologan, P. C. Vratny, A. Seitz, O. Schmitz, A. T. Isikveren, and M. Hornung, "Methodology for sizing and performance assessment of hybrid energy aircraft," *Journal of Aircraft*, vol. 52, no. 1, pp. 341–352, 2015. DOI: 10.2514/1.C032716. [Online]. Available: https://doi.org/10.2514/1.C032716.

[29] B. T. Schiltgen and J. Freeman, "Eco-150-300 design and performance: A tube-and-wing distributed electric propulsion airliner," 2019. DOI: 10.2514/6.2019-1808. [Online]. Available: https://arc.aiaa.org/doi/abs/10.2514/6.2019-1808.

[30] B. T. Schiltgen and J. Freeman, "Aeropropulsive interaction and thermal system integration within the eco-150: A turboelectric distributed propulsion airliner with conventional electric machines," in *16th AIAA Aviation Technology, Integration, and Operations Conference*. 2016. DOI: 10.2514/6.2016-4064. [Online]. Available: https://arc.aiaa.org/doi/abs/10.2514/6.2016-4064.

[31] A. Gibson, D. Hall, M. Waters, P. Masson, B. Schiltgen, T. Foster, and J. Keith, "The potential and challenge of turboelectric propulsion for subsonic transport aircraft," 2010. DOI: 10.2514/6.2010-276. [Online]. Available: https://arc.aiaa.org/doi/abs/10.2514/6.2010-276.

[32] J. Welstead and J. L. Felder, "Conceptual design of a single-aisle turboelectric commercial transport with fuselage boundary layer ingestion," 2016. DOI: 10.2514/6.2016-1027. [Online]. Available: https://arc.aiaa.org/doi/abs/10.2514/6.2016-1027.

[33] J. Welstead, J. Felder, M. Guynn, W. Haller, M. Tong, S. Jones, I. Ordaz, J. Quinlan, and B. Mason, "Overview of the nasa starc-abl (rev. b) advanced concept," Tech. Rep., 2017. [Online]. Available: https://ntrs.nasa.gov/archive/nasa/casi.ntrs.nasa.gov/20170005612.pdf.

[34] B. J. Brelje and J. R. Martins, "Electric, hybrid, and turboelectric fixed-wing aircraft: A review of concepts, models, and design approaches," *Progress in Aerospace Sciences*, vol. 104, pp. 1–19, 2019, ISSN: 0376-0421. DOI: https://doi.org/10.1016/j.paerosci.2018.06.004. [Online]. Available: https://www.sciencedirect.com/science/article/pii/S0376042118300356.

[35] C. L. Bowman, J. L. Felder, and T. Marien, "Turbo- and hybrid-electrified aircraft propulsion concepts for commercial transport," in *2018 AIAA/IEEE Electric Aircraft Technologies Symposium (EATS)*, 2018, pp. 1–8.

[36] M. K. Bradley and C. K. Droney, "Subsonic ultra green aircraft research phase ii: N+4 advanced concept development, nasa/cr-2012-217556," Tech. Rep., 2012. [Online]. Available: https://ntrs.nasa.gov/archive/nasa/casi.ntrs.nasa.gov/20120009038.pdf.

[37] D. F. Finger, C. Bil, and C. Braun, "Initial sizing methodology for hybrid-electric general aviation aircraft," *Journal of Aircraft*, vol. 57, no. 2, pp. 245–255, 2020. DOI: 10.2514/1.C035428. eprint: https://doi.org/10.2514/1.C035428. [Online]. Available: https://doi.org/10.2514/1.C035428.

[38] D. F. Finger, C. Braun, and C. Bil, "Comparative assessment of parallel-hybrid-electric propulsion systems for four different aircraft," *Journal of Aircraft*, vol. 57, no. 5, pp. 843–853, 2020. DOI: 10.2514/1.C035897. eprint: https://doi.org/10.2514/1.C035897. [Online]. Available: https://doi.org/10.2514/1.C035897.

[39] R. de Vries, M. Brown, and R. Vos, "Preliminary sizing method for hybrid-electric distributed-propulsion aircraft," *Journal of Aircraft*, vol. 56, no. 6, pp. 2172–2188, 2019. DOI: 10.2514/1.C035388. eprint: https://doi.org/10.2514/1.C035388. [Online]. Available: https://doi.org/10.2514/1.C035388.

[40] R. de Vries, M. F. M. Hoogreef, and R. Vos, "Range equation for hybrid-electric aircraft with constant power split," *Journal of Aircraft*, vol. 57, no. 3, pp. 552–557, 2020. DOI: 10.2514/1.C035734. eprint: https://doi.org/10.2514/1.C035734. [Online]. Available: https://doi.org/10.2514/1.C035734.

[41] C. Pornet, C. Gologan, P. C. Vratny, A. Seitz, O. Schmitz, A. T. Isikveren, and M. Hornung, "Methodology for sizing and performance assessment of hybrid energy aircraft," *Journal of Aircraft*, vol. 52, no. 1, pp. 341–352, 2015. DOI: 10.2514/1.C032716. eprint: https://doi.org/10.2514/1.C032716. [Online]. Available: https://doi.org/10.2514/1.C032716.

[42] B. J. Brelje and J. R. Martins, "Development of a conceptual design model for aircraft electric propulsion with efficient gradients," in *2018 AIAA/IEEE Electric Aircraft Technologies Symposium*. DOI: 10.2514/6.2018-4979. eprint: https://arc.aiaa.org/doi/pdf/10.2514/6.2018-4979. [Online]. Available: https://arc.aiaa.org/doi/abs/10.2514/6.2018-4979.

[43] I. Chakraborty and A. A. Mishra, "Generalized energy-based flight vehicle sizing and performance analysis methodology," *Journal of Aircraft*, vol. 58, no. 4, pp. 762–780, 2021. DOI: 10.2514/1.C036101. eprint: https://doi.org/10.2514/1.C036101. [Online]. Available: https://doi.org/10.2514/1.C036101.

[44] J. Zamboni, R. Vos, M. Emeneth, and A. Schneegans, "A method for the conceptual design of hybrid electric aircraft," in *AIAA Scitech 2019 Forum*. DOI: 10.2514/6.2019-1587. eprint: https://arc.aiaa.org/doi/pdf/10.2514/6.2019-1587. [Online]. Available: https://arc.aiaa.org/doi/abs/10.2514/6.2019-1587.

[45] J. R. Welstead, D. Caldwell, R. Condotta, and N. Monroe, "An overview of the layered and extensible aircraft performance system (leaps) development," in *2018 AIAA Aerospace Sciences Meeting*. DOI: 10.2514/6.2018-1754. eprint: https://arc.aiaa.org/doi/pdf/10.2514/6.2018-1754. [Online]. Available: https://arc.aiaa.org/doi/abs/10.2514/6.2018-1754.

[46] L. A. McCullers, "FLOPS, software package, ver. 8.12," NASA Langley Research Center, 2010.

[47] F. M. Capristan and J. R. Welstead, "An energy-based low-order approach for mission analysis of air vehicles in leaps," in *2018 AIAA Aerospace Sciences Meeting*. DOI: 10.2514/6.2018-1755. eprint: https://arc.aiaa.org/doi/pdf/10.2514/6.2018-1755. [Online]. Available: https://arc.aiaa.org/doi/abs/10.2514/6.2018-1755.

[48] T. Marien, N. J. Blaesser, Z. J. Frederick, M. D. Guynn, J. Kirk, K. Fisher, S. Schneider, R. P. Thacker, and P. Frederic, "Methodology used for an electrified aircraft propulsion design exploration," in *AIAA AVIATION 2021 FORUM*. DOI: 10.2514/6.2021-3191. eprint: https://arc.aiaa.org/doi/pdf/10.2514/6.2021-3191. [Online]. Available: https://arc.aiaa.org/doi/abs/10.2514/6.2021-3191.

[49] T. Marien, N. J. Blaesser, Z. J. Frederick, M. D. Guynn, J. Kirk, K. Fisher, S. Schneider, R. P. Thacker, and P. Frederic, "Results for an electrified aircraft propulsion design exploration," in *AIAA Propulsion and Energy 2021 Forum*. DOI: 10.2514/6.2021-3280. eprint: https://arc.aiaa.org/doi/pdf/10.2514/6.2021-3280. [Online]. Available: https://arc.aiaa.org/doi/abs/10.2514/6.2021-3280.

[50] C. Perullo and D. Mavris, "A review of hybrid-electric energy management and its inclusion in vehicle sizing," *Aircraft Engineering and Aerospace Technology: An International Journal, Emerald Group Publishing Limited*, vol. 86, pp. 1–19, 2014, ISSN: 0002-2667. DOI: https://doi.org/10.1108/AEAT-04-2014-0041.

[51] D. Trawick, K. Milios, J. C. Gladin, and D. N. Mavris, "A method for determining optimal power management schedules for hybrid electric airplanes," in *2019 AIAA/IEEE Electric Aircraft Technologies Symposium (EATS)*, 2019, pp. 1–21. DOI: 10.2514/6.2019-4500.

[52] H. Lee, C. M. Harris, J. C. Gladin, and D. N. Mavris, "A method for simultaneous optimization of power split and flight path trajectories for hybrid electric aircraft," in *AIAA Scitech 2021 Forum*. DOI: 10.2514/6.2021-1010. eprint: https://arc.aiaa.org/doi/pdf/10.2514/6.2021-1010. [Online]. Available: https://arc.aiaa.org/doi/abs/10.2514/6.2021-1010.

[53] M. Wang and M. Mesbahi, "Power allocation for hybrid electric aircraft via optimal control during climb, cruise, and descent," in *AIAA Scitech 2021 Forum*. DOI: 10.2514/6.2021-0640. eprint: https://arc.aiaa.org/doi/pdf/10.2514/6.2021-0640. [Online]. Available: https://arc.aiaa.org/doi/abs/10.2514/6.2021-0640.

[54] J. Abara, "Applying integer linear programming to the fleet assignment problem," *Interfaces*, vol. 19, no. 4, pp. 20–28, 1989, ISSN: 00922102, 1526551X. [Online]. Available: http://www.jstor.org/stable/25061245.

[55] C. A. Hane, C. Barnhart, E. L. Johnson, R. E. Marsten, G. L. Nemhauser, and G. Sigismondi, "The fleet assignment problem: Solving a large-scale integer program," *Mathematical Programming*, vol. 70, no. 1, pp. 211–232, Oct. 1995, ISSN: 1436-4646. DOI: 10.1007/BF01585938. [Online]. Available: https://doi.org/10.1007/BF01585938.

[56] B. Smith and E. Johnson, "Robust airline fleet assignment: Imposing station purity using station decomposition," *Transportation Science*, vol. 40, pp. 497–516, Nov. 2006. DOI: 10.1287/trsc.1060.0153.

[57] T. L. Jacobs, B. C. Smith, and E. L. Johnson, "Incorporating network flow effects into the airline fleet assignment process," *Transportation Science*, vol. 42, no. 4, pp. 514–529, 2008. DOI: 10.1287/trsc.1080.0242. [Online]. Available: https://doi.org/10.1287/trsc.1080.0242.

[58] C. Barnhart, T. Kniker, and M. Lohatepanont, "Itinerary-based airline fleet assignment," *Transportation Science*, vol. 36, no. 2, pp. 199–217, May 2002. DOI: 10.1287/trsc.36.2.199.566.

[59] C. Barnhart, A. Farahat, and M. Lohatepanont, "Airline fleet assignment with enhanced revenue modeling," *Operations Research*, vol. 57, no. 1, pp. 231–244, 2009. DOI: 10.1287/opre.1070.0503.

[60] M. E. Berge and C. A. Hopperstad, "Demand driven dispatch: A method for dynamic aircraft capacity assignment, models and algorithms," *Operations Research*, vol. 41, no. 1, pp. 153–168, 1993. DOI: 10.1287/opre.41.1.153.

[61] R. A. RUSHMEIER and S. A. KONTOGIORGIS, "Advances in the optimization of airline fleet assignment," *Transportation Science*, vol. 31, no. 2, pp. 159–169, 1997, ISSN: 00411655, 15265447. [Online]. Available: http://www.jstor.org/stable/25768765.

[62] N. Antoine, S. Bieniawski, I. Kroo, and D. Wolpert, "Fleet assignment using collective intelligence," Feb. 2004. DOI: 10.2514/6.2004-622.

[63] M. Grönkvist, "The tail assignment problem," Ph.D. dissertation, 2005.

[64] H. D. Sherali, E. K. Bish, and X. Zhu, "Airline fleet assignment concepts, models, and algorithms," *Eur. J. Oper. Res.*, vol. 172, pp. 1–30, 2006.

[65] Y. Li and N. Tan, "Study on fleet assignment problem model and algorithm," *Mathematical Problems in Engineering*, vol. 2013, Mar. 2013. DOI: 10.1155/2013/581586.

[66] C. Barnhart, N. L. Boland, L. W. Clarke, E. L. Johnson, G. L. Nemhauser, and R. G. Shenoi, "Flight string models for aircraft fleeting and routing," *Transportation Science*, vol. 32, no. 3, pp. 208–220, 1998. DOI: 10.1287/trsc.32.3.208.

[67] L. W. Clarke, C. A. Hane, E. L. Johnson, and G. L. Nemhauser, "Maintenance and crew considerations in fleet assignment," *Transportation Science*, vol. 30, no. 3, pp. 249–260, 1996. DOI: 10.1287/trsc.30.3.249.

[68] G. Desaulniers, J. Desrosiers, Y. Dumas, M. M. Solomon, and F. Soumis, "Daily aircraft routing and scheduling," *Management Science*, vol. 43, no. 6, pp. 841–855, 1997, ISSN: 00251909, 15265501. [Online]. Available: http://www.jstor.org/stable/2634626.

[69] B. Rexing, C. Barnhart, T. Kniker, A. Jarrah, and N. Krishnamurthy, "Airline fleet assignment with time windows," *Transportation Science*, vol. 34, no. 1, pp. 1–20, 2000. DOI: 10.1287/trsc.34.1.1.12277.

[70] M. Lohatepanont and C. Barnhart, "Airline schedule planning: Integrated models and algorithms for schedule design and fleet assignment," *Transportation Science*, vol. 38, no. 1, pp. 19–32, 2004. DOI: 10.1287/trsc.1030.0026.

[71] H. D. Sherali, K.-H. Bae, and M. Haouari, "Integrated airline schedule design and fleet assignment: Polyhedral analysis and benders' decomposition approach," *INFORMS Journal on Computing*, vol. 22, no. 4, pp. 500–513, 2010. DOI: 10.1287/ijoc.1090.0368.

[72] D. Caetano and N. Gualda, "Solving the integrated schedule generation and fleet assignment problem: An acobased metaheuristic approach," *Journal of Transport Literature*, vol. 9, pp. 30–34, Sep. 2015. DOI: 10.1590/2238-1031.jtl.v9n3a6.

[73] N. Kenan, A. Jebali, and A. Diabat, "An integrated flight scheduling and fleet assignment problem under uncertainty," *Computers Operations Research*, Sep. 2017. DOI: 10.1016/j.cor.2017.08.014.

[74] K. Wei, V. Vaze, and A. Jacquillat, "Airline timetable development and fleet assignment incorporating passenger choice," *SSRN Electronic Journal*, Jan. 2018. DOI: 10.2139/ssrn.3198882.

[75] I. J. Tetzloff, "An allocation approach to investigate new aircraft concepts and technologies on fleet-level metrics," Ph.D. dissertation, 2010, p. 129, ISBN: 978-1-124-15932-4. [Online]. Available: https://search-proquest-com.ezproxy.lib.purdue.edu/docview/749921962?accountid=13360.

[76] I. Tetzloff and W. Crossley, "An allocation approach to investigate new aircraft concepts and technologies on fleet-level metrics," Sep. 2009, ISBN: 978-1-60086-977-8. DOI: 10.2514/6.2009-6979.

[77] P. Nolte, A. Apffelstaedt, V. Gollnick, and T. Rötger, "Quantitative assessment of technology impact on aviation fuel efficiency," in *Air Transport and Operations. Third International Air Transport and Operations Symposium*, 2012, pp. 514–531.

[78] S. Sgouridis, P. A. Bonnefoy, and R. J. Hansman, "Air transportation in a carbon constrained world: Long-term dynamics of policies and strategies for mitigating the carbon footprint of commercial aviation," *Transportation Research Part A: Policy and Practice*, vol. 45, no. 10, pp. 1077–1091, 2011, ISSN: 0965-8564. DOI: https://doi.org/10.1016/j.tra.2010.03.019. [Online]. Available: http://www.sciencedirect.com/science/article/pii/S0965856410000583.

[79] S. Sgouridis, "Symbiotic strategies in enterprise ecology: Modeling commercial aviation as an enterprise of enterprises, chapter 9," *Doctoral Thesis, Massachusetts Institute of Technology*, 2007. [Online]. Available: http://dspace.mit.edu/handle/1721.1/43859?show=full.

[80] J. I. Hileman, E. D. l. R. Blanco, P. A. Bonnefoy, and N. A. Carter, "The carbon dioxide challenge facing aviation," *Progress in Aerospace Sciences*, vol. 63, pp. 84–95, 2013, ISSN: 0376-0421. DOI: https://doi.org/10.1016/j.paerosci.2013.07.003. [Online]. Available: http://www.sciencedirect.com/science/article/pii/S0376042113000663.

[81] M. Hassan, H. Pfaender, and D. Mavris, "Probabilistic assessment of aviation co2 emission targets," *Transportation Research Part D: Transport and Environment*, vol. 63, pp. 362–376, 2018, ISSN: 1361-9209. DOI: https://doi.org/10.1016/j.trd.2018.06.006. [Online]. Available: http://www.sciencedirect.com/science/article/pii/S1361920917300548.

[82] S. Jain, H. Chao, M. Mane, W. A. Crossley, and D. A. DeLaurentis, "Estimating the reduction in future fleet-level co2 emissions from sustainable aviation fuel," *Frontiers in Energy Research*, vol. 9, 2021, ISSN: 2296-598X. DOI: 10.3389/fenrg.2021.771705. [Online]. Available: https://www.frontiersin.org/article/10.3389/fenrg.2021.771705.

[83] H. Chao, *Fleet Level Environmental Evaluation of Emission Taxing Scheme and Biofuel: A Combined Optimization and Multi-Actor Approach (MS Thesis)*. 2016, p. 76.

[84] H. Chao, D. DeLaurentis, and B. Agusdinata, "Sensitivity analysis of fleet-level life cycle carbon emissions to biofuel options and emission policy schemes for the U.S. commercial airlines," in *17th AIAA Aviation Technology, Integration, and Operations Conference*, 2017, ISBN: 9781624105081. [Online]. Available: https://arc.aiaa.org/doi/abs/10.2514/6.2017-3768.

[85] H. Chao, D. B. Agusdinata, and D. A. DeLaurentis, "The potential impacts of emissions trading scheme and biofuel options to carbon emissions of u.s. airlines," *Energy Policy*, vol. 134, p. 110 993, 2019, ISSN: 0301-4215. DOI: https://doi.org/10.1016/j.enpol.2019.110993. [Online]. Available: http://www.sciencedirect.com/science/article/pii/S0301421519305804.

[86] MathWorks, "Documentation – optimization toolbox – fmincon.," 2022. [Online]. Available: https://www.mathworks.com/help/optim/ug/fmincon.html.

[87] MathWorks, "Documentation – optimization toolbox – fminsearch.," [Online]. Available: https://www.mathworks.com/help/matlab/ref/fminsearch.html.

[88] *Nordisk akh (ld3-45)*, Nordisk Aviation Products, Retrieved May, 2021. [Online]. Available: https://www.nordisk-aviation.com/en/ld-containers/akh-ld3-45/nordisk-akh-/.

[89] J. D. Mattingly, W. H. Heiser, and D. T. Pratt, *Aircraft Engine Design, Second Edition*, ser. AIAA education series. American Institute of Aeronautics and Astronautics, 2002, ISBN: 978-1-56347-538-2. [Online]. Available: https://doi.org/10.2514/4.861444.

[90] *Numerical propulsion system simulation (npss)*, Southwest Research Institute, Retrieved May, 2021. [Online]. Available: https://www.swri.org/consortia/numerical-propulsion-system-simulation-npss.

[91] D. Raymer, *Aircraft Design: A Conceptual Approach, Sixth Edition*, ser. AIAA education series. American Institute of Aeronautics and Astronautics, 2018, ISBN: 978-1-62410-490-9. [Online]. Available: https://doi.org/10.2514/4.104909.

[92] R. D. Finck, *Usaf (united states air force) stability and control datcom (data compendium)*, McDonnell Aircraft Co., April 1974, Retrieved Jan, 2019. [Online]. Available: http://www.dept.aoe.vt.edu/~mason/Mason_f/B737.pdf.

[93] "Aircraft drag polar estimation based on a stochastic hierarchical model," in *Eighth SESAR Innovation Days, 3rd – 7th December 2018, Salzburg, Austria*, Green Open Access added to TU Delft Institutional Repository, 2018.

[94] W. Lammen and J. Vankan, "Energy optimization of single aisle aircraft with hybrid electric propulsion," in *AIAA Scitech 2020 Forum*. DOI: 10.2514/6.2020-0505. [Online]. Available: https://arc.aiaa.org/doi/abs/10.2514/6.2020-0505.

[95] *International civil aviation organization (icao), annex 6 operation of aircraft – part 1: International commercial air transport – aeroplanes*, ICAO, 2010, Retrieved May, 2020.

[96] M. Lukic, A. Hebala, P. Giangrande, C. Klumpner, S. Nuzzo, G. Chen, C. Gerada, C. Eastwick, and M. Galea, "State of the art of electric taxiing systems," in *2018 IEEE International Conference on Electrical Systems for Aircraft, Railway, Ship Propulsion and Road Vehicles International Transportation Electrification Conference (ESARS-ITEC)*, 2018. DOI: 10.1109/ESARS-ITEC.2018.8607786.

[97] D. P. Wells, B. L. Horvath, and L. A. McCullers, "The flight optimization system weights estimation method," NASA Technical Reports Server (NTRS), NASA/TM–2017–219627/Volume I, 2017. [Online]. Available: https://ntrs.nasa.gov/citations/20170005851.

[98] P. Lolis, "Development of a preliminary weight estimation method for advanced turbofan engines," Ph.D. dissertation, 2014. [Online]. Available: http://dspace.lib.cranfield.ac.uk/handle/1826/9244.

[99] *Pratt whitney's geared turbofan engine: Changing the course of avaition*, Design Engine, April 2013, Retrieved May, 2022. [Online]. Available: https://design-engine.com/pratt-whitneys-geared-turbofan-engine-changing-the-course-of-avaition/.

[100] *737 airplane characteristics for airport planning*, Boeing Commercial Airplanes, October 2005, Retrieved May, 2020. [Online]. Available: http://www.dept.aoe.vt.edu/~mason/Mason_f/B737.pdf.

[101] P. Liu and S. Meng, "Battery500 consortium: Development of high capacity cathodes and robust solid electrolytes," Jan. 2022. DOI: 10.2172/1838452. [Online]. Available: https://www.osti.gov/biblio/1838452.

[102] C. E. Lents, L. W. Hardin, J. Rheaume, and L. Kohlman, "Parallel hybrid gas-electric geared turbofan engine conceptual design and benefits analysis," in *52nd AIAA/SAE/ASEE Joint Propulsion Conference*. DOI: 10.2514/6.2016-4610. eprint: https://arc.aiaa.org/doi/pdf/10.2514/6.2016-4610. [Online]. Available: https://arc.aiaa.org/doi/abs/10.2514/6.2016-4610.

[103] J. Zamboni, "A method for the conceptual design of hybrid electric aircraft," *MS Thesis*, 2018. [Online]. Available: http://repository.tudelft.nl/.

[104] J. D'Errico, *Fminsearchbnd, fminsearchcon*, MATLAB Central File Exchange, Retrieved June, 2022. [Online]. Available: https://www.mathworks.com/matlabcentral/fileexchange/8277-fminsearchbnd-fminsearchcon.

[105] E. Botero, A. Wendorff, T. Macdonald, A. Variyar, J. Vegh, T. Lukaczyk, J. Alonso, T. Orra, and C. Silva, "Suave: An open-source environment for conceptual vehicle design and optimization," Jan. 2016. DOI: 10.2514/6.2016-1275.

[106] P. E. Gill, W. Murray, and M. A. Saunders, *User's guide for snopt version 7: Software for large-scale nonlinear programming*.

[107] *Pass, program for aircraft synthesis studies, software package, ver1.7*, 2005.

[108] S. Choi, J. J. Alonso, I. M. Kroo, and M. Wintzer, "Multifidelity design optimization of low-boom supersonic jets," *Journal of Aircraft*, vol. 45, no. 1, pp. 106–118, 2008. DOI: 10.2514/1.28948. eprint: https://doi.org/10.2514/1.28948. [Online]. Available: https://doi.org/10.2514/1.28948.

[109] S. Choi, J. J. Alonso, and I. M. Kroo, "Two-level multifidelity design optimization studies for supersonic jets," *Journal of Aircraft*, vol. 46, no. 3, pp. 776–790, 2009. DOI: 10.2514/1.34362. eprint: https://doi.org/10.2514/1.34362. [Online]. Available: https://doi.org/10.2514/1.34362.

[110] MathWorks, "Documentation – optimization toolbox – ga.," [Online]. Available: https://www.mathworks.com/help/gads/ga.html.

[111] J. Hao, "Comparison of derivative free algorithms in optimization high dimension problems," *MS Thesis*, 2015. [Online]. Available: http://hdl.handle.net/10415/4914.

[112] K. A. Moolchandani, D. B. Agusdinata, M. Mane, W. A. Crossley, and D. A. DeLaurentis, "Impact of Development Rates of Future Aircraft Technologies on Fleet-Wide Environmental Emissions," in *11th AIAA Aviation Technology, Integration, and Operations (ATIO) Conference*, 2011, pp. 1–13, ISBN: 9781600869419 (ISBN). DOI: 10.2514/6.2011-6843. [Online]. Available: https://arc.aiaa.org/doi/abs/10.2514/6.2011-6843.

[113] K. A. Moolchandani, D. B. Agusdinata, D. A. DeLaurentis, and W. A. Crossley, "Airline Competition in Duopoly Market and its Impact on Environmental Emissions," in *12th AIAA Aviation Technology, Integration, and Operations (ATIO) Conference*, 2012, pp. 1–11, ISBN: 9781600869303. DOI: 10.2514/6.2012-5466. [Online]. Available: https://arc.aiaa.org/doi/abs/10.2514/6.2012-5466.

[114] K. A. Moolchandani, D. B. Agusdinata, M. Mane, D. A. DeLaurentis, and W. A. Crossley, "Assessment of the Effect of Aircraft Technological Advancement on Aviation Environmental Impacts," in *51st AIAA Aerospace Sciences Meeting including the New Horizons Forum and Aerospace Exposition*, Reston, Virigina: American Institute of Aeronautics and Astronautics, Jan. 2013, p. 13, ISBN: 978-1-62410-181-6. DOI: 10.2514/6.2013-652. [Online]. Available: http://arc.aiaa.org/doi/10.2514/6.2013-652.

[115] H. Chao, K. E. Ogunsina, K. A. Moolchandani, D. A. DeLaurentis, and W. A. Crossley, "Airline Competition in Duopoly Market and its Impact on Environmental Emissions: A Game Theory Approach," in *16th AIAA Aviation Technology, Integration, and Operations Conference*, Reston, Virginia: American Institute of Aeronautics and Astronautics, Jun. 2016, ISBN: 978-1-62410-440-4. DOI: 10.2514/6.2016-3759. [Online]. Available: http://arc.aiaa.org/doi/10.2514/6.2016-3759.

[116] K. E. Ogunsina, H. Chao, N. Kolencherry, K. A. Moolchandani, W. A. Crossley, and D. A. DeLaurentis, "A Model of Aircraft Retirement and Acquisition Decisions Based On Net Present Value Calculations," in *17th AIAA Aviation Technology, Integration, and Operations Conference*, 2017, ISBN: 978-1-62410-508-1. DOI: 10.2514/6.2017-3600. [Online]. Available: https://arc.aiaa.org/doi/10.2514/6.2017-3600.

[117] D. Mavris, D. Delaurentis, W. Crossley, and J. J. Alonso, "Project 10 Aircraft Technology Modeling and Assessment: Phase I Report," 2017. [Online]. Available: https://s3.wp.wsu.edu/uploads/sites/192/2017/10/ASCENT_P10_2017_PhaseI_Final_Report.pdf.

[118] K. Ogunsina, H. Chao, N. Kolencherry, S. Jain, K. Moolchandani, W. A. Crossley, and D. A. DeLaurentis, "Fleet-level environmental assessments for feasibility of aviation emission reduction goals," in *Proceedings of CESUN Global Conference, Tokyo, Japan*, 2018.

[119] S. Jain, K. E. Ogunsina, H. Chao, W. A. Crossley, and D. A. DeLaurentis, "Predicting routes for, number of operations of, and fleet-level impacts of future commercial supersonic aircraft on routes touching the united states," in *AIAA AVIATION 2020 FORUM*. 2020. DOI: 10.2514/6.2020-2878. [Online]. Available: https://arc.aiaa.org/doi/abs/10.2514/6.2020-2878.

[120] S. Jain, M. Mane, W. A. Crossley, and D. A. DeLaurentis, "Investigating how commercial supersonic aircraft operations might impact subsonic operations and total co_2 emissions," in *21st AIAA Aviation Technology, Integration, and Operations Conference, AIAA AVIATION*, 2021.

[121] M. Mane, S. Jain, W. A. Crossley, and D. A. DeLaurentis, "Speed and cost impact on market success of supersonic passenger transport aircraft," in *21st AIAA Aviation Technology, Integration, and Operations Conference, AIAA AVIATION*, 2021.

[122] W. A. Crossley and D. A. DeLaurentis, *System-of-systems approach for assessing new technologies in ngats*, Purdue University, West Lafayette, IN, 2013.

[123] *Airline origin and destination survey (db1b) [online database], u.s. dept. of transportation, bureau of transportation statistics*, Retrieved Dec. 2017. [Online]. Available: http://www.transtats.bts.gov/DatabaseInfo.asp?DB_ID=125&Link=0.

[124] S. Jain, M. Mane, H. Chao, W. A. Crossley, and D. A. DeLaurentis, "Estimating the impact of novel coronavirus (covid-19) on future fleet-level co_2 emissions and airline operations," in *21st AIAA Aviation Technology, Integration, and Operations Conference, AIAA AVIATION*, 2021.

[125] Airbus, *Flying on Demand, Global Market Forecast Booklet 2014*, Available at http://www.airbus.com/content/dam/corporate-topics/strategy/global-market-forecast/GMF-2019-2038-Airbus-Commercial-Aircraft-book.pdf, 2014.

[126] "Population reference bureau, world population data sheet 2013," 2013, Available at http://www.prb.org/wp-content/uploads/2015/01/2013-population-data-sheet_eng.pdf. [Online]. Available: https://www.prb.org/2013-world-population-data-sheet/.

[127] S. Vlek and M. Vogels, "Aero - aviation emissions and evaluation of reduction options," *Air Space Europe*, vol. 2, no. 3, pp. 41–44, 2000, ISSN: 1290-0958. DOI: https://doi.org/10.1016/S1290-0958(00)80062-3. [Online]. Available: http://www.sciencedirect.com/science/article/pii/S1290095800800623.

[128] *Optimism when borders reopen*, IATA Press Release No: 33, May 2021, Retrieved Jun, 2021. [Online]. Available: https://www.iata.org/en/pressroom/pr/2021-05-26-01/.

[129] *2020 worst year in history for air travel demand*, IATA Press Release, February 2021, Retrieved Jun, 2021. [Online]. Available: https://www.iata.org/en/pressroom/pr/2021-02-03-02/.

[130] B. Yang, M. Mane, and W. A. Crossley, "An approach to evaluate fleet level co2 impact of introducing liquid-hydrogen aircraft to a world-wide network," in *AIAA Aviation 2022 Forum*. DOI: 10.2514/6.2022-3313. eprint: https://arc.aiaa.org/doi/pdf/10.2514/6.2022-3313. [Online]. Available: https://arc.aiaa.org/doi/abs/10.2514/6.2022-3313.

[131] *Standard method of estimating comparative direct operating costs of turbine powered transport airplanes*, Air Transport Association of America, 1967.

[132] R. H. Liebeck, D. A. Andrastek, J. Chau, R. Girvin, R. Lyon, B. K. Rawdon, P. W. Scott, and R. A. Wright, "Advanced subsonic airplane design and economic studies," 1995.

[133] V. S. Johnson, "Life cycle cost in the conceptual design of subsonic commercial aircraft," Ph.D. dissertation, 1989.

[134] *Annual energy outlook 2022*, U.S. Energy Information Administration, January 2022, Retrieved May, 2022. [Online]. Available: https://www.eia.gov/outlooks/aeo/.

[135] *Annual energy outlook 2012*, U.S. Energy Information Administration, January 2012, Retrieved August, 2015. [Online]. Available: https://www.eia.gov/outlooks/aeo/.

[136] *Life cycle greenhouse gas emissions from electricity generation: Update*, National Renewable Energy Laboratory (NREL), 2021, Retrieved May, 2022. [Online]. Available: https://www.nrel.gov/docs/fy21osti/80580.pdf.

[137] *What is u.s. electricity generation by energy source?* U.S. Energy Information Administration, FAQs, 2022, Retrieved May, 2022. [Online]. Available: https://www.eia.gov/outlooks/aeo/.

VITA

Samarth Jain earned his Bachelor's in Mechanical and Automotive Engineering from Delhi Technological University (formerly Delhi College of Engineering), India, and his Master's in Aeronautics & Astronautics from Purdue University, USA. His research interests include sizing and performance analysis of advanced technology aircraft, multidisciplinary design optimization (MDO), data-driven modeling and simulation of complex transportation systems, and environmental modeling.

During his PhD at Purdue, Samarth developed a "flight-mechanics-based" hybrid-electric aircraft sizing MDO tool along with a battery energy management tool to model hybrid-electric aircraft and their off-design performance characteristics. This computational model of the aircraft formed the basis for the fleet-level studies he conducted to predict the future environmental impact of introducing hybrid-electric aircraft in airline fleets in the mid-2030s (conducted using an airline decision modeling tool named FLEET). Concurrently, he supported the FAA ASCENT Project 10 to assess the impact of future commercial supersonic aircraft on airline operations and fleet-level emissions. As a part of his Master's thesis, he developed a multi-fidelity MDO framework to solve expensive multi-objective mixed-discrete nonlinear programming problems, with application to greener aircraft design.